Trajectory Optimisation for a Rail-based Track Surveying System

Msc. Thesis

Frederik A.G. Collot d'Escury

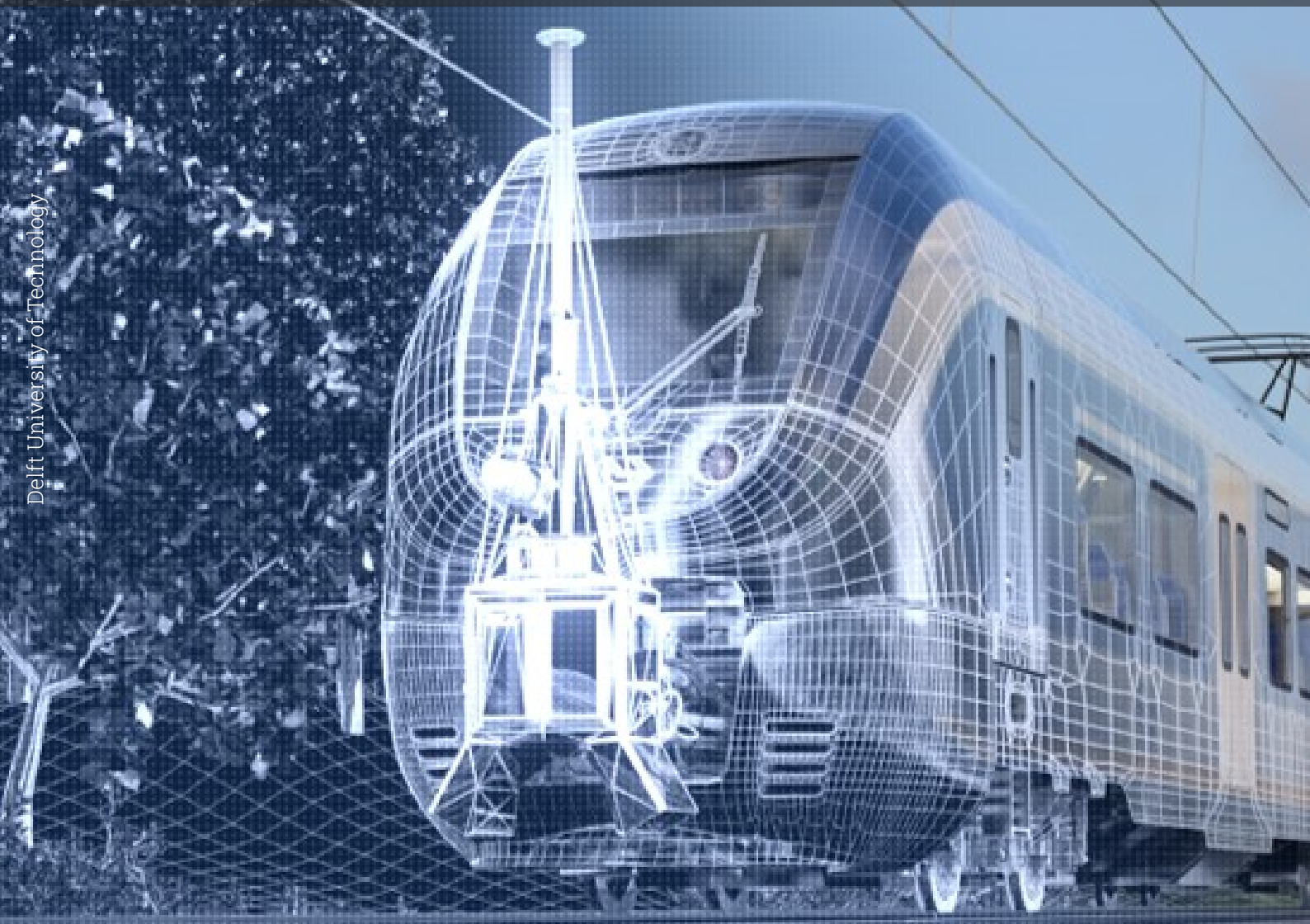

Delft University of Technology

TU Delft

FUGRO

Page intentionally left blank

Trajectory Optimisation for a Rail-based Track Surveying System

Msc. Thesis

by

Frederik A.G. Collot d'Escury

to obtain the degree of Master of Science
at the Delft University of Technology,
to be defended publicly on F June 8, 2023 at 15:00 PM.

Student number:	4668928	
Project duration:	December 12, 2022 - June 8, 2023	
Company:	Fugro	
Department:	Rail Service Line	
Thesis committee:	Dr. ir. E. Schrama,	TU Delft, Chair
	Dr. ir. W. van der Wal,	TU Delft, Supervisor
	Dr. ir. C. Tiberius,	TU Delft, Examiner
	ir. L. Amoureus,	Fugro, Supervisor

Cover: Fugro RILA system visualisation (Source: Fugro)

TU Delft FUGRO

This page was intentionally left blank.

Preface

The completion of this report marks not only the end of the thesis research but also the end of my studies, a very exciting and insightful period of my life. It makes me feel incredibly lucky and privileged to have been able to perform my studies among such a driven group of students and teaching staff, at the cutting edge of aerospace technology. For that, I'm thankful to everyone who has contributed to my academic and personal development at the faculty of Aerospace Engineering. This is especially true for my thesis supervisor Wouter van der Wal. Thank you very much for your motivation, insights and ability to put things in context. Your support has been essential and very valuable for the successful completion of this research.

The past few months, in which this thesis research has been performed, have been a whole new and very valuable experience for me. Apart from the many things I've learned regarding (academic) research, it has opened my eyes to the vast extent of practical applications of aerospace knowledge. The opportunity to contribute to the RILA system, a unique and demanding application of trajectory determination, has been very motivating and valuable. I'm grateful for this opportunity to Fugro and the entire Raildata engineering team. However, I'd like to express special thanks to my supervisor Luc Amoureus. You have provided me with a lot of help and guidance, especially in situations where I thought I was stuck or going in the wrong direction.

Finally, I'd like to thank family, friends and everyone close to me for their unconditional support and motivation during my thesis research, and my entire studies. Thanks for your friendship.

Frederik A.G. Collot d'Escury
Delft, May 2023

This page was intentionally left blank.

Abstract

Railway transportation is crucial to reducing greenhouse gas emissions and meeting increasing global demand for passenger and freight transport. To maintain a reliable, high-capacity railway infrastructure, regular and accurate maintenance is necessary. The recent development of a Rail-based Track Surveying System that can be mounted on any operational train, presents a comprehensive solution to acquire track geometry measurements while limiting track unavailability. The system is able to simultaneously acquire measurements of both the absolute- and relative track geometry using a combination of a GNSS / INS integrated navigation system and a laser ranging sensor. The measurement unit is able to obtain consistently accurate absolute track geometry measurements ($\sigma_{2D} = 8$ [mm] (Wang et al. 2019)) in areas with good GNSS signal reception. However, in areas with limited GNSS coverage, the accuracy of these measurements can fall below the requirements for rapid track inventory acquisition (3 [cm], $p = 0.95$ (Specht et al. 2016)). This thesis, developed and conducted in close collaboration with Fugro, aims to improve the accuracy of the trajectory solution for rail-based track surveying systems in such limited GNSS environments.

At the time this research was performed, there was no ground truth or reference trajectory available to assess the accuracy of a trajectory solution. Therefore, the research first establishes quality metrics to provide a measure of the accuracy and certainty of the integrated GNSS/INS estimated trajectory solution. By nature of the data acquisition process of the RTSS, multiple runs, or trajectory estimates, are available of an arbitrary track segment. The observed cross-track trajectory spread (precision) provides a qualitative metric to assess the level of accuracy of multiple passes over the same track segment, given that the individual measurements are unbiased. To quantify the cross-track trajectory spread, the standard deviation and smallest circle radius are selected as statistical and absolute metrics.

Next, the research identifies the existence of unreliable or inaccurate GNSS positioning updates in the integrated trajectory solution by linking the cross-track trajectory spread to the Quality Control metrics of individual runs. The level of accuracy of the GNSS / IMU integrated trajectory solution was found to be decreased at track segments where one (or multiple) runs showed sustained periods of high (> 5) PDOP values. A decreased accuracy in the order of 10 [cm] was observed for the high PDOP GNSS positioning updates. Furthermore, these inaccurate position updates were weighted too heavily in the Loosely Coupled integration scheme, reducing the accuracy of the integrated GNSS/IMU trajectory solution. To improve the accuracy and certainty of the integrated trajectory solution, the GNSS positioning updates in segments with sustained high PDOP values can be inactivated. Inactivating these high PDOP GNSS positioning updates, reduced the observed cross-track trajectory spread by as much as c.50%.

The thesis provides valuable results for the improvement of the accuracy and certainty of GNSS/IMU trajectory determination in rail-based applications. Furthermore, the framework and data-analysis algorithm developed and presented in this thesis research could be used to quantify the effect of different quality parameters and processing thresholds on the accuracy of the trajectory solution. The main conclusion and recommendation of this report - processing the trajectory against a tight PDOP constraint - leads to a trajectory estimate for a rail-based surveying application with improved accuracy and certainty. Moreover, recommendations for research implementation, further trajectory accuracy gains and continuation of this research are also presented in this report.

This page was intentionally left blank.

Contents

Nomenclature

Abbreviations

Abbreviation	Definition
AL	Alert Limit
COM	Centre Off Mass
DCPP	Differential Carrier Phase Positioning
DFD	Discrete Fréchet Distance
DOP	Dilution Of Precision
DTW	Dynamic Time Warping
ECEF	Earth Centred Earth Fixed [reference frame]
FD	Fréchet Distance
GNSS	Global Navigation Satellite System
GPS	Global Positioning System
IAL	Immediate Action Limit
IGS	International GNSS Service
IL	Intervention Limit
INS	Inertial Navigation Unit
IMU	Inertial Measurement Unit
ISO	International Organization for Standardization
LiDAR	Light Detection And Ranging
LSED	Lock-Step Euclidean Distance
LC	Loosely Coupled [Integration]
ML	Machine Learning
MMS	Mobile Mapping System
NS	Number of Satellites used in the trajectory solution
OLE	Overhead Line Equipment
ORB-SLAM	Oriented fast and Rotated Brief Simultaneous Localisation And Mapping
PBR	Parity Bit Resolved
PCD	Point Cloud Data
PDOP	Position Dilution Of Precision
PP	Post Processing
PPK	Post-Processed Kinematic [mode]
QC	Quality Control
RILA	Rail Infrastructure aLignment Acquisition [system]
RMS	Root Mean Square
RPi	ReProcessing i [of the trajectory solution]
RTK	Real Time Kinematic
RTSS	Rail-based Track Surveying System
SBET	Smoothed Best Estimate Trajectory
SLAM	Simultaneous Localisation And Mapping
STD	STandard Deviation
SVM	Support Vector Machine
TCL	Track Centre Line
TGMT	Track Geometry Measuring Trolley
UERE	User Equivalent Range Error
VO	Visual Odometry
VRS	Virtual Reference Station

Symbols

Symbol	Definition	Unit
$\mathbf{A}$	design matrix	[-]
h	cross track interpolation error	[m]
$\mathbf{I}$	identity matrix	[-]
p	probability	[-]
$\mathbf{Q}$	covariance matrix	[-]
R	radius of the interpolation curve	[m]
t	time	[s]
$\mathbf{W}$	weighting matrix	[-]
θ	arc segment angle	[°]
ρ	pseudorange	[m]
λ	Longitude	[rad]
φ	Latitude	[rad]
σ	standard deviation (std)	[m]
σ_{ct}	std of the cross-track trajectory spread	[m]
σ^2	(co)variance	[m]

List of Figures

List of Tables

This page was intentionally left blank.

1 Introduction

Railway transportation plays a key role in global plans for reducing greenhouse gas emissions. The transportation of both passengers[1] and freight[2] by rail, is reported to emit up to 80% fewer greenhouse gasses compared to available alternatives such as cars, planes and trucks. Due to the increased demand for sustainable, rail-based transportation capacity, the amount of passengers and freight transported by trains is expected to more than double by 2050 (IEA 2019).

With the increased demand for railway transportation volume, there is a strong need for reliable, high-capacity railway infrastructure. As railway tracks degrade with every Gross-Tonne of train movement, regular, accurate and efficient maintenance is required to limit unavailability. To map railway degradation and efficiently schedule maintenance operations, systematic and accurate updates of the track geometry measurements are required. Traditionally, these measurements were obtained by surveying crews and Track Recording Vehicles. However, recent developments of a rail-based track surveying system (RILA[3]), that can be mounted on any train during the regular service schedule, have significantly streamlined the track geometry measurement acquisition process.

Such a rail-based track surveying system uses an integrated GNSS/IMU trajectory solution from which the track geometry measurements are derived. However, it is found that in areas with limited GNSS coverage, the accuracy of the obtained measurements can decrease below the required accuracy levels for track geometry measurements (Specht et al. 2022). In this thesis report, research has been conducted in close collaboration with Fugro, a world-leading geo-data and surveying company, with the aim of improving the accuracy of the trajectory solution of such a rail-based track surveying system.

First of all, in chapter 2 additional background information is provided on the need and requirements for railway track surveying, followed by a literature review and description of the problem and research questions. In chapter 3, the research framework and methodology for integrated trajectory estimation improvement are provided and discussed together with the relevant information on the accuracy of trajectory processing. Next, the results of a case study are presented in chapter 4 with supporting research in chapter 5 and chapter 6. Finally, chapter 7 presents the conclusions together with recommendations for implementation and further research.

[1] https://ourworldindata.org/travel-carbon-footprint#:~:text=Using%20a%20bike%20instead%20of,your%20emissions%20by%20-84%25.

[2] https://dhl-freight-connections.com/en/trends/the-future-of-rail-freight-in-europe/

[3] https://www.fugro.com/our-services/asset-integrity/raildata

This page was intentionally left blank.

2

Background & Problem Description

The purpose of this chapter is to provide background information on the relevance and need for railway track maintenance surveying. Furthermore, current methods and requirements for rail-based track surveying systems are discussed together with their performance and limitations and subsequent difficulties experienced by operators. First of all, in section 2.1, general railway track maintenance practices are discussed together with the accompanying requirements. Secondly, in section 2.2, a brief overview of the developments in railway surveying is given together with an introduction to the RILA system. This system is an example of a state-of-the-art railway surveying of which the data will be investigated in this research. In section 2.3, the limitations to the accuracy of a Rail-based Track Surveying System (RTSS) will be presented after which alternative trajectory solutions are discussed in section 2.4. Finally, this chapter will be concluded with a problem statement and scope in section 2.5 followed by the research questions in section 2.6.

2.1. Railway Track Maintenance

A railway track is a complicated infrastructure consisting of many elements such as tracks, track switches, Overhead-Line-Equipment (OLE), signalling systems and telecommunication equipment. Within railway infrastructure, railway track tamping is especially important and consumes a significant amount of resources from railway asset management companies.

Railway Tamping

In general, railway tracks are founded on loose ballast (crushed stones). Apart from providing stable support for railway tracks, the ballast is able to absorb slight deformation of the tracks due to heat absorption and train passage (Guo et al. 2022). However, because of the loose nature of the ballast, regular use of the tracks by trains will cause them to change in position and geometry, away from their intended alignment. This process, called railway track degradation, can seriously affect train passengers' comfort and even impact railway operations' safety. In the most extreme case, sufficiently degraded railway tracks can lead to train derailment (Elkhoury et al. 2018). To prevent or repair degraded tracks, railway maintenance companies are making use of a process called *tamping*. Railway tamping re-aligns and levels the railway track and compacts the loose ballast underneath using a track tamping machine as seen in Figure 2.1. This process is crucial for the comfortable and safe usage of railway networks.

The frequency at which a track segment needs to be re-aligned and tamped depends on the rate at which the track geometry degrades. Track geometry degradation is in turn dependent on the frequency of use, railbed soil and operated train types - i.e. heavy cargo trains or light passenger trains. Furthermore, curved track segments or connections between solid- and loose trackbeds (for example at bridges) can also impact the speed of degradation. Tamping frequency can range from several years on good track sections with low usage, to 3-4 months on track sections with high usage and low-quality foundation soil (Clinnick 2013). There are no specific rules for the exact frequency at which a track is tamped. However, when certain track geometry thresholds are exceeded, tamping is required.

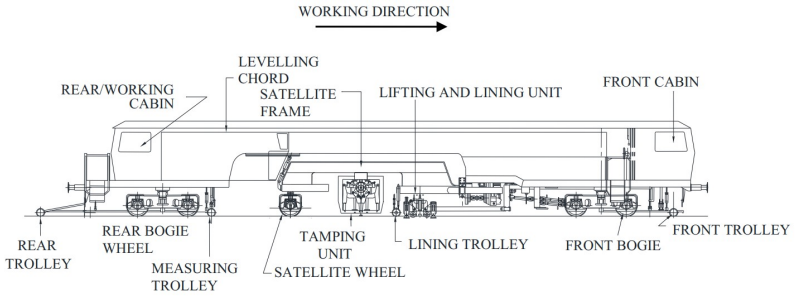

Figure 2.1: Schematic overview of a typical railway tamping machine (Chaube et al. 2019)

Track Geometry Accuracy Requirements

In Europe, the requirements for the track geometry have been defined in the European standard EN 13848-1 (CEN 2019). In practice, railway maintenance companies enforce certain track geometry thresholds to timely perform maintenance works and make sure that the track does not exceed the regulatory tolerances. The maintenance actions are guided by the Alert Limit (AL), Intervention Limit (IL) and Immediate Action Limit (IAL) thresholds, depicted in Figure 2.2 (Kraft et al. 2016).

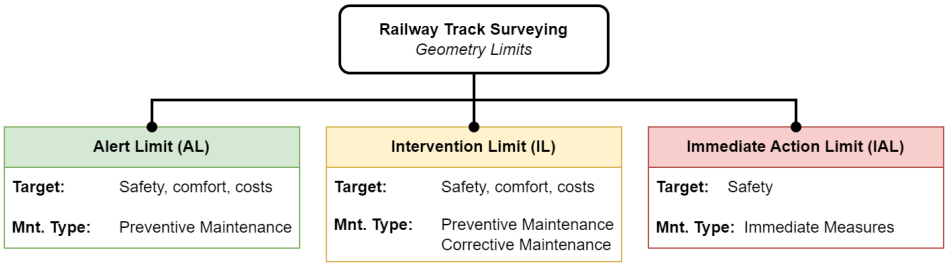

Figure 2.2: Schematic overview of the track geometry limits (Tamparas 2016)

Measurements taken during railway inspections can be broadly put into two categories: *Absolute Geometry* and *Relative Geometry* measurements. The absolute geometry measurements, defined by a 3D string (trajectory) of geospatial coordinates, determine the true position of the railway Track Centre Line (TCL). Apart from the absolute track position, absolute geometry measurements are used as track design parameters such as the track curvature and slope.

The relative geometry measurements determine the position of the two railway tracks (railheads) relative to each other and the track centre line. Relative track geometry metrics can be important track design parameters. However, the relative track geometry is important for the assessment of the current quality state of the track. An extensive overview of the different track geometry parameters can be found in Appendix A, however, the most relevant relative track geometry metrics are presented in Table 2.1. Research by Khajehei et al. (2019) has shown that to minimise the annual maintenance cost of a railway network, the Alert Limit for the relative track geometry should be in the range of 1.5 to 1.6 [mm].

Table 2.1: Definitions of the most relevant relative track geometries

Geometry	Type	Definition
Gauge	Relative	Distance between the inner sides of both rail heads perpendicular to the track centre
Longitudinal Level	Relative	Deviations in the vertical position between the topside of both rail heads from the ideal running plane
Cant (Cross Level)	Relative	Elevation difference between the topside of both rail heads perpendicular to the track centre line

Requirements for the accuracy of the absolute geometry measurements follow from either railway asset manager (client) demands, or general track geometry maintenance thresholds. A study by Specht et al. (2016) identifies three distinct absolute track geometry measurement accuracy levels required for different geodetic tasks in railway engineering. The accuracy levels for the absolute track geometry (trajectory) measurements are presented in Table 2.2.

Table 2.2: Track absolute geometry (trajectory) accuracy requirements by railway engineering task (Specht et al. 2016)

Railway Engineering Task	Absolute Traj. Accuracy Req. [cm]	Confidence Level
Monitoring track deformations	1.0	$p = 0.95$
Rapid (high speed) track inventory acquisition	3.0	$p = 0.95$
Design & construction works	10.0	$p = 0.95$

Surveying Frequency

Degradation of the track quality is dependent on a lot of hard-to-predict parameters such as the age of rails, carriage axle load, speed, traffic density, Million Gross Tonnes (MGTs) and foundation stability. Even if two track sections are situated in similar conditions, track degradation can still occur at different rates. Therefore, maintenance companies need frequent absolute- and relative track geometry measurements to monitor the track geometry change (Liao et al. 2022). These measurements are crucial to guide any maintenance work (Wang et al. 2019). Therefore, it is in the best interest of railway asset managers to acquire the track geometry measurements as often as possible.

However, there are three main factors limiting the railway track surveying frequency. First of all, especially in Europe (IEA 2019), the current growth in railway traffic, caused by the demand for sustainable transport alternatives, is increasingly limiting the track availability for surveying (Fontul et al. 2018). Secondly, there is a need for increasingly accurate track geometry measurements (needing longer acquisition times), following stricter accuracy requirements imposed by governing bodies (Judek et al. 2022). The third and major limiting factor is the high acquisition cost of the measurements. This is because the acquisitions of absolute- and relative measurements are two separated, labour-intensive processes, handled by different departments within railway maintenance companies (Wang et al. 2019).

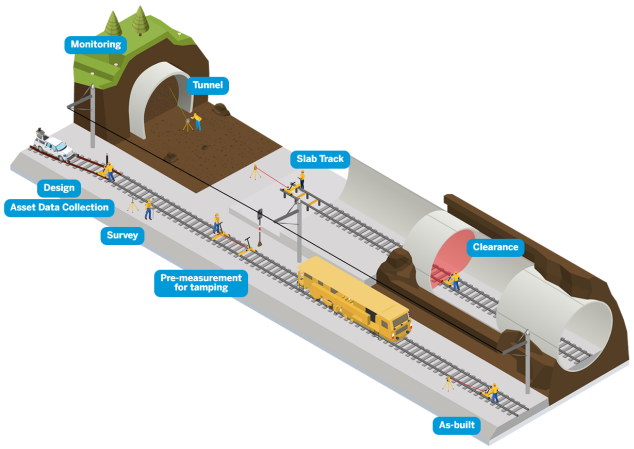

Figure 2.3: A schematic overview of traditional rail survey elements, methods and tools[1]

Traditionally, the absolute track geometry of railway segments is measured by geodetic surveying crews contracted by rail asset managers. This requires the surveying crew to be on and around the track segments to be measured. To ensure their safety, the track segment will be closed-off entirely to any railway traffic until all measurements have been acquired. The absolute geometry measurements are collected using a combination of hand-pushed trolleys (Chen et al. 2018), total station surveys and both stationary and moving (along-track) laser scanning surveys (Selig et al. 1994) (Wienia 2015).

[1] Source: https://gedo.trimble.com/en

Relative track geometry measurements are acquired using a track geometry car. Although a track geometry car can travel along a railway segment much faster than a surveying crew, it still requires the track segment to be closed off to other railway traffic during operations. A schematic overview of the entire traditional rail surveying process can be found in Figure 2.3.

The three limiting factors are generally true for global railway networks. However, they especially constrain the railway surveying frequency in regions with high railway network usage such as urban agglomerations - for example North-Western Europe, Eastern China, United States East Coast etc (Fontul et al. 2018). As a result, the measurement frequency of the track geometry parameters is low. In most European countries, the relative geometry measurements are only collected twice a year (Wang et al. 2021). Obtaining absolute track geometry measurements generally occurs at an even lower sampling rate, at once every five years (Wang et al. 2019).

All in all, monitoring the track quality and condition is a significant cost item for railway asset managers, operators and maintenance companies. An overview of the two track geometry types together with their respective requirements and considerations is presented in Table 2.3. Therefore, stakeholders involved with track surveying and maintenance are always looking for ways to improve and streamline the measurement acquisition process, to reduce cost.

Table 2.3: Overview of track geometry types

Surveying Parameter	**Absolute Track Geometry**	**Relative Track Geometry**
Surveying Technique	Surveying crews	Track Recording Vehicle
Current Surveying Interval [years]	5	0.5
Required Measurement Accuracy [mm]	10 - 100	1.5 - 1.6

2.2. Developments in Railway Track Surveying

With increasing computational resources available, an effort has been made to model and predict the track degradation process (Elkhoury et al. 2018). By doing so, researchers hope to limit the dependency of maintenance scheduling on up-to-date track geometry measurements. This could reduce the number of surveys needed for general maintenance processes and therefore reduce the overall cost. Recent developments of predictive track degradation models based on Machine Learning (ML) algorithms prove to show a performance increase compared to traditional models (Liao et al. 2022). For example, Support Vector Machine (SVM) based track degradation prediction models were shown to be able to predict track geometry defects with 70% accuracy (Hu et al. 2016). However, most predictive models are only tested on small track segments (5 - 200 [m]) and require large computational resources, limiting their use for entire railway networks (Liao et al. 2022). Furthermore, with the tight regulatory accuracy requirements and safety limits, these models still can't substitute survey data for track degradation identification. Hence, there remains a strong need for reliable and accurate track geometry measurements collected on a regular basis. To get the cost of up-to-date track geometry data down, alternative surveying solutions are being investigated.

Rail-based Track Surveying System

A solution developed to make the acquisition of railway geometry measurements more cost-efficient is an integrated Rail-based Track Surveying System (RTSS) (Bronsvoort et al. 2013). This system integrates both a high-quality GNSS receiver and Inertial Measurement Unit (IMU), together with a variety of sensors to gain accurate, simultaneous readings of the absolute- and relative track geometry measurements. A Track Geometry Measuring Trolley (TGMT) is an example of such an RTSS. There exist TGMTs designed to collect only absolute- or relative track geometry measurements, or both and are usually hand pushed (Chen et al. 2018). Although being able to collect all relevant measurements simultaneously, it still has the disadvantage of being relatively slow (± 5 km\h).

To speed up the measurement acquisition process even more, an integrated RTSS has been developed by Fugro[2] that can be mounted on any train in regular operation. This unique and patented system called RILA has two distinct advantages over the more traditional surveying methods. First of all, the system is able to collect the measurements at the regular, operational (line-) speed of the train, significantly reducing the data acquisition time of a certain track segment. Secondly, as the system can be mounted on any (passenger)train within two minutes, the regular railway service schedule does not have to be interrupted. Currently, such an implementation of an RTSS is unique in railway surveying and is estimated to acquire all the track geometry measurements at 25% of the cost of traditional railway surveying techniques.

RILA System

The first version of the Rail Infrastructure aLignmnet Acquisition system (RILA) was developed by Fugro in 2009. By combining an integrated GNSS/IMU navigation system, together with laser scanners called railstripers, a detailed geospatial model of the observed track can be made. The current version of RILA is able to collect relative geometry measurements with [mm] accuracy and absolute- geometry measurements with < 5 [cm] accuracy levels, given unobstructed and favourable conditions for GNSS reception. Furthermore, the system is able to collect the measurements at speeds up to 200 [km]\h (Wang et al. 2019). RILA also integrates a LiDAR scanner and video camera system to be able to produce various other products that can be relevant for railway maintenance companies. Integrating observations from all sensors allows for a detailed and accurate 3D model to be constructed of all objects in and around the railway track (railcorridor). An image of the RILA system together with all its sensors can be found in Figure 2.4. An extended overview of all sensors together with their intended use, contribution and sampling frequencies can be found in Appendix B.

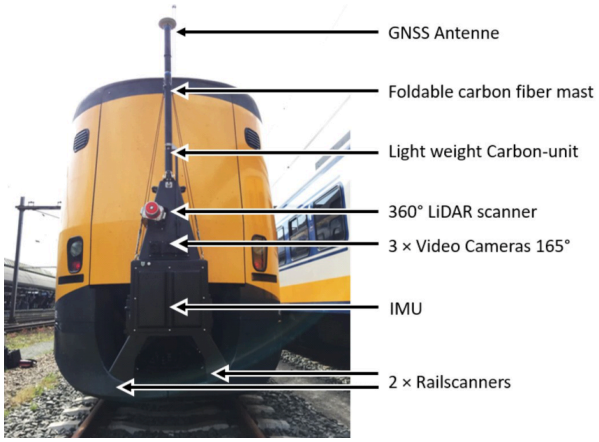

Figure 2.4: Overview of the RILA system with an overview of all navigation and data acquisition sensors (source: Fugro)

2.3. Performance & Limitations of an RTSS

Although railway surveying using an RTSS is a very efficient way of obtaining track geometry measurements, a system like RILA has limitations to the accuracy of the measurements that can be obtained. Relative track geometry parameters can be confidently measured to within the requirements of the European Standard (CEN 2011) as shown in Table 2.4 (Wang et al. 2019). To construct the requirements in Table 2.4, the European Committee for Standardization (CEN) takes the conventional track surveying method, a certified Track Recording Vehicle (TRV), as benchmark. The CEN requirements presented in the table, therefore, represent the allowed uncertainty (or reproducibility) in track geometry measurements compared to the conventional track surveying methods. It is important to note that other than the reproducibility requirement, the CEN does not constitute true accuracy requirements for the relative track geometry measurements of the TRV. The RILA uncertainty from Table 2.4 is, therefore, the discrepancy between the relative track geometry measurements of an RTSS like RILA and the benchmark conventional track-surveying methods at confidence level $p = 0.95$.

[2] https://www.fugro.com/our-services/asset-integrity/raildata

Table 2.4: Uncertainty of RTSS obtained relative track geometry parameters compared to classic track surveying methods (Wang et al. 2019)

Parameters	RILA Uncertainty [mm]	Uncertainty requirement (CEN 2011) [mm]
Gauge	0.85	1
Cant	0.94	5
Longitudinal Level D1	0.71 - 0.73	1
Longitudinal Level D2	2.02 - 2.06	3

The relative track geometry measurements are obtained using the Point Cloud Data (PCD) of the rail-stripers (and potentially LiDAR-scanner) only. Although relative track geometry measurements can be negatively impacted by sub-optimal surveying conditions such as rain or snowfall (Charron et al. 2018), they are not subject to situational or geographical changes in the measuring environment. In other words, when the laser-ranging sensors are able to obtain accurate measurements, the RTSS can provide accurate relative track geometry data irrespective of the environment the measurement unit travels through.

This is different for the absolute track geometry measurements. The absolute geometry measurements (or TCL trajectory) are dependent on the measurements obtained by the GNSS receiver and IMU sensor. Furthermore, the IMU is only able to provide position updates relative to a known location computed by integrating the acceleration measurements obtained by the sensor. Therefore, the GNSS receiver is the only sensor on the RTSS directly providing absolute position updates. Obtaining an accurate GNSS position estimate is dependent on the environment in which the receiver is situated. Obstacles along a railway track (such as trees, buildings, canyons or tunnels) can cause obstructions between the receiver and the different GNSS satellites, potentially decreasing the accuracy of the position estimate. Research by Specht et al. (2022) analyses the performance of a GNSS/IMU integrated navigation system for rail-based applications in three distinct environments with increasing GNSS challenges:

Environment 1 No terrain obstacles, resulting in high satellite visibility, good geometry and little disturbing influences

Environment 2 Numerous terrain obstacles such as high building density and trees with >10 [m] height, resulting in limited satellite visibility and high likelihood of multi-path disturbances

Environment 3 No access to GNSS signal, this situation can occur in a tunnel or a covered train station

Table 2.5: Overview of GNSS/IMU trajectory accuracy obtained with measurements in area's with different levels of GNSS coverage (Specht et al. 2022)

Environment	GNSS Coverage	Real Time Kinematic [cm]		Post Processing [cm]	
		2DRMS(2D)	R95(2D)	2DRMS(2D)	R95(2D)
1	Full / Unblocked	5.4	2.8	1.8	1.7
2	Limited / High Multipath	96.1	60	32.6	24.6
3	Signal Loss	482.9 - 586	488.1-588.6	54.3-85.9	32.8-64

The results of the research of a GNSS/IMU integrated system for rail-based applications can be found in Table 2.5. In this research, Twice the Distance Root Mean Square (2DRMS(2D)) and the radius of a circle centred at the true position, containing the position 2D estimate with a probability of 95% (R95(2D)) are used as the most important measures of the accuracy of the trajectory solution. These accuracy metrics are often used in the trajectory quality determination of rail-based GNSS positioning systems (Specht et al. 2020).

Furthermore, in all situations, Post-Processing (PP) provides more accurate positioning solutions than Real Time Kinetic (RTK) processing. In railway surveying, trajectory accuracy is more important than real-time applications. Hence, nearly all trajectory determination for the data acquisition in rail applications is done using post-processing. Post-processed trajectory solutions will therefore also be the focus of this thesis research.

As one can observe, the accuracy of the GNSS/IMU integrated trajectory solution decreases in environments with increasingly limited GNSS coverage. Another observation from Table 2.5 is that the positioning accuracy decrease in environment 3 (signal loss), is dependent on the signal loss time interval. Although the IMU can provide position updates - computed from the acceleration measurements - at epochs where insufficient GNSS observations are present, it is important to understand that the position error will accumulate. Short-term position errors resulting from the computed IMU position updates are generally very small, however, they degrade cumulatively over time and are unbounded (Angrisano et al. 2010). This is because IMU-derived state updates are computed from the accelerations measured by the Inertial Measurement Unit. In order to compute the position update, the accelerations measured by the IMU are integrated twice. Tiny measurement errors (uncertainties) of the acceleration have a profound effect on the uncertainty of the position update of the IMU due to the double integration step (Valtonen Ornhag et al. 2022). Furthermore, any uncertainties in the true position of the IMU sensor are propagated to the next epoch. When the GNSS/IMU integrated system does not receive any position updates from the GNSS - i.e. the IMU sensor is unaided - the uncertainty in the true position of the system accumulates with each IMU position update. This is called the IMU drift. In the integrated trajectory solution, the GNSS sensor and IMU complement each other where the IMU provides position updates at a high sample interval (300 [Hz]) between the GNSS position updates (1 [Hz]).

When looking at the accuracy requirements for the absolute geometry measurements (or TCL trajectory) defined in section 2.1 (see Table 2.2), another observation is relevant. Only in environment 1, the GNSS/IMU integrated system is able to meet the accuracy requirements for rapid track inventory acquisition (3 [cm], $p = 0.95$), relevant for the RTSS. In environments 2 and 3, the trajectory solution is not sufficiently accurate to comply with railway maintenance requirements. To further increase the accuracy of the absolute track geometry measurements acquired by the RILA system, a baseline survey is constructed where the measurements of at least four runs are combined. This allows the system to provide a TCL trajectory with a standard deviation of 8 [mm] in the horizontal plane (DRMS) and 12 [mm] in the vertical plane (Wang et al. 2019). The accuracy of the 4-run combined RILA trajectory, therefore, corresponds to a 1.6 [cm] 2DRMS(2D) and 1.4 [cm] R95(2D) in environment 1 in Table 2.5. An important note is that, according to the documentation on the RILA system, these accuracies can only be obtained under optimal GNSS conditions. Therefore, the trajectory accuracy of the four combined RILA runs corresponds to a When the GNSS conditions are sub-optimal (comparable to environment 2), the accuracy of the merged trajectory solution will also decrease, often below client expectations and/or railway maintenance thresholds[3].

These three types of environments are encountered along nearly all railway tracks around the world. For example, although there are no definitive statistics, railways through forested areas or with dense vegetation along the railway corridor are likely to experience similar GNSS reception to Environment 2. Underpasses, tunnels and covered train stations are also a regular occurrence along any railway track. Depending on the railway network and terrain in which an RTSS is used, the different environments can occur more or less often. It can be expected that it is generally more challenging to obtain consistent and reliable positioning estimates for a railway network in Switzerland, with its many mountains and tunnels than for the rail network in The Netherlands.

2.4. Sensor-based RTSS Trajectory Improvement

Due to the current performance limitations of a Rail-based Track Surveying System, the absolute track geometry measurements (TCL trajectory) obtained by the RTSS do not meet the imposed accuracy and confidence requirements in all encountered environments. Therefore, where the obtained standard

[3]There are no records kept of absolute geometry measurement inaccuracies in environments with sub-optimal GNSS coverage

deviations exceed the trajectory accuracy requirements, (manual) adjustment of the dataset is needed. In extreme cases, (parts of) measurement runs have to be discarded if their trajectory estimate proves to be too uncertain. To avoid this, methods have been developed to improve the accuracy of the absolute trajectory solution in both general- and railway-specific surveying applications.

One of these strategies is to implement a Distance Measurement Indicator such as a wheel odometer into the mobile surveying system (Puente et al. 2013) and (Zhang et al. 2021). This device could provide information on the position, velocity and acceleration of a train. Zhou et al. (2019) report that combined with the GNSS receiver and IMU, the system could maintain <5 [cm] accurate measurements in the horizontal and vertical plane with 700 seconds of GNSS outage. However, the odometer has to be mounted to the wheel of the train which has two issues. First of all, in the specific case of RILA, it voids the easy (de-)installation of the system when additional sensors have to be mounted to other parts of the train. Secondly, out of safety considerations, it is currently not allowed to attach anything to the running gear (wheels, drivetrain, etc) of the train for most railway networks where the RILA system is operational.

A second strategy to improve the measurement accuracy of an RTSS in case of limited GNSS reception is Simultaneous Localisation And Mapping (SLAM). Slam is a probabilistic method to generate a 2D or 3D map of unknown areas under imperfect localisation as defined by Birk et al. (2016). The algorithm uses the LiDAR measurements to build a map of an unknown area, while simultaneously using this map for localisation and updating the position of the sensor relative to this map (Durrant-Whyte et al. 2008). However, an ORB-SLAM3 method developed for an RTSS shows promising results for the limitation of IMU-drift when the system is at a standstill in a challenging GNSS environment (Habibzadeh 2023). However, it was found that for general trajectory optimisation of a survey, it is impossible to implement SLAM using the current, single LiDAR-scanner RILA setup (Secco 2022). At least two 3D-laser scanners are required for the successful implementation of SLAM along the entire survey. When considering the RTSS as a Mobile Mapping System (MMS), where the GNSS trajectory is combined with the visual measurement systems (cameras and lasers), one could also improve on the absolute trajectory accuracy by introducing control points (Kersting et al. 2016). These are physical 'targets' with known locations installed along the trajectory to serve as references for the calibration of the correction parameters to improve the estimation of the trajectory. The disadvantage of control points is that they have to be installed, measured and calibrated. Hence, their availability along all railway tracks is sparse.

Tie-points are proven to be an effective method to increase the accuracy of the trajectory of an MMS (Løvås 2017). Different to control points, the identification of tie-points is a SLAM-supported technique where individual features are found in overlapping parts of a (geo-referenced) pointcloud that can be used for calibration of correction parameters for the trajectory. Vector observations between the tie points and the trajectory can be implemented in the GNSS / IMU trajectory to improve its accuracy. A further strategy could be the implementation of Visual Odometry (VO) based on disparity changing (Fu et al. 2017). Disparity-based VO uses a camera system to compute and update the distances and angles to at least two tie points along the trajectory and updates the position of the MMS based on the differences between the different measurement epochs.

The problem with using MMS-based solutions for accuracy and certainty improvement of an RTSS trajectory such as SLAM, control points, tie-points and disparity-based VO, is that it requires extensive post-processing of the obtained point-cloud and video data. This consumes valuable resources such as operator time and computing power which could have been allotted towards other projects. For example, as can be seen in Figure 2.5 processing of the integrated GNSS / IMU trajectory solution takes c. 8.5 hours, half of which the responsible data engineer can work on other tasks. However, processing the RILA track data for only a 50 km segment, which contains the Point Cloud Data (PCD) of the railheads, integration of the multiple runs, modifying the data (patching) and quality control, can take up to three days as can be seen in Figure 2.6. Furthermore, as all steps in RILA track processing require input from an operator, it is much more labour-intensive than the processing of the trajectory. Although the process is not entirely the same as PCD processing for MMS-based trajectory accuracy improvement solutions, both procedures handle similar amounts of data. Therefore, the processing of RILA track data does give a good indication of the time and computational resources required for MMS-based trajectory solutions.

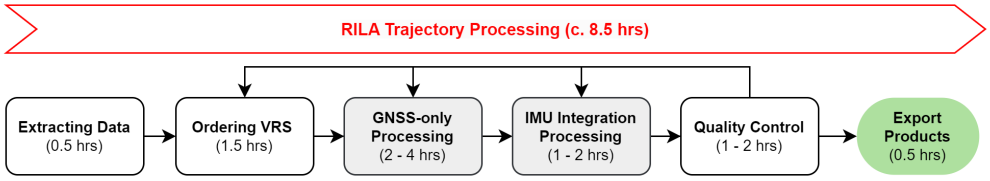

Figure 2.5: Flowchart with a time indication of the GNSS / IMU integrated trajectory solution of a RILA survey. Grey blocks indicate steps that a data engineer has to initiate but not monitor.

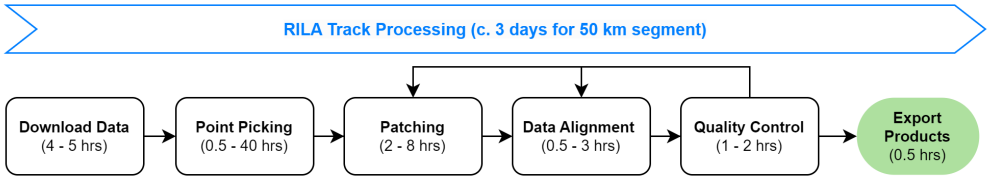

Figure 2.6: Flowchart with a time indication of a 50km track segment for RILA track data (integrated TCL)

Apart from strategies where additional sensors are used for improvement of the trajectory solution, one could also investigate the possibilities of imposing boundary conditions on the trajectory solution. A suggestion is to make use of one-dimensional constraints in trajectory estimation techniques for rail-based applications (Zhu 2014) (Czaplewski et al. 2020). The theory is that the trajectory of the train (RTSS) is fixed, by definition, to the railway tracks that it is running on. By making this assumption, the three-dimensional problem becomes a 1D one (along the track direction). However, enforcing these constraints on the trajectory solution defies the purpose of a rail-based surveying system. As the tracks move away from their intended position over time, for railway maintenance, data on this position change is required. The system, therefore, needs to be able to provide absolute, unconstrained three-dimensional geometry measurements for its user. One could also impose constraints on the relative position change moving from one measurement epoch to the next. As the train runs on the tracks, one can expect that the position change cannot exceed a certain predetermined threshold. However, in most trajectory processing software used to integrate GNSS and IMU measurements, extensive smoothing of the trajectory solution is performed. This eliminates most of the 'jumps' in the trajectory solution. Therefore, additional constraints on position change along the trajectory solution will likely not have a significant effect. All in all, in this research, imposing rail-based constraints is not further investigated.

2.5. Problem Statement and Scope

Considering the limitations of the RTSS and the alternative solutions explored in section 2.4, there is a strong need to improve the accuracy of the GNSS/IMU integrated trajectory solution of the RTSS. This would directly increase the performance and accuracy of the RTSS, and omit the need for extensive and costly post-processing alternative solutions. Furthermore, it would reduce the need for (manual) adjustment and/or deletion of parts of the dataset during the processing of the RTSS output products.

Current rail-based GNSS/IMU integrated trajectory estimation does not provide sufficiently accurate solutions in every encountered environment. Research by Specht et al. (2022) indicates that post-processed trajectory accuracies of 1.8 [cm] (2DRMS(2D)) can be obtained in areas with good GNSS coverage. However, in environments where the coverage is sub-optimal (environments 2 and 3 in Table 2.5), the accuracy of the integrated trajectory can go down to 30-50 [cm]. Absolute geometry accuracy requirements from Table 2.2, such as the requirements for rapid (high speed) track inventory acquisition (3 [cm]) and railway design & construction works (10 [cm]), far exceed the accuracies that an RTSS can currently obtain in challenging GNSS environments. Therefore, there is a need to increase the trajectory solution of a rail-based track surveying system in areas where the GNSS coverage is sub-optimal. In an ideal case, the accuracy of the integrated GNSS/IMU trajectory solution in challenging GNSS environments would be brought down to the rapid track inventory acquisition level (3

[cm] $p = 0.95$). As sufficiently accurate (1.8 [cm]) trajectory solutions can be obtained in environments with good GNSS coverage and under the assumption that the IMU performs normally (small constant drift), it can be stated that the degradation in trajectory quality originates from a decreased accuracy in GNSS positioning updates. Harsh GNSS environments usually occur in tunnels (signal loss) and cities where the effects of shadowing, multipath and inferior satellite geometry can be noticed. Also, segments along the railcorridor with dense and/or tall vegetation can have a negative impact on the receiver's sky-visibility, limiting the satellites in view and therefore the positioning accuracy.

The decision was made to predominantly analyse data from the *Environment 2* type from Table 2.5, as this is the area where most performance improvement is to be gained. Furthermore, *Environment 2* is often encountered at track segments of which the obtained measurements are especially important to the end users, such as railway stations, urban areas and shunting yards. The solution in *Environment 1* is currently considered to be sufficiently accurate, although a higher certainty is desired in certain cases. As Fugro is currently exploring other methods to increase the accuracy of the trajectory solution in environments with sustained complete GNSS signal loss, *Environment 3* has been kept outside of the scope of this research.

2.6. Research Questions

The main objective of the research described in this report is to provide a method to realise an improvement in the accuracy of the GNSS/IMU integrated trajectory solution obtained by a Rail-based Track Surveying System, in an area where the GNSS signal access is limited. To provide an academic framework and structure for this research, research questions have been defined. Answering the main research question, as presented below, will directly contribute to a solution to the problem described in section 2.5.

What would be a way to improve the accuracy of the GNSS/IMU integrated trajectory solution of a rail-based track surveying system, in environments with reduced GNSS signal access?

Sub-Questions

The research question is further divided into (sub-)sub-questions in order to dissect the problem into more easily solved parts. The 2D- and 3D trajectory accuracy metrics used in the literature discussed in section 2.3, quantify the trajectory accuracy based on a reference- or ground-truth trajectory. However, for nearly all of the railway tracks surveyed by the RILA system, there is no such reference trajectory available. The subject of the first sub-questions is, therefore, to develop good quality metrics with which the integrated trajectory solution obtained by the RTSS can be evaluated. The quality metrics should provide a qualitative indication of the accuracy of the trajectory solution of the RTSS.

Q1 *What would be a good quality metric to represent the accuracy of the integrated GNSS/IMU estimated trajectory solution?*

The second sub-question focuses on understanding the quality of the GNSS positioning updates in a GNSS-constrained environment along a track segment surveyed by the RILA system. Assuming that the degradation of the quality of the trajectory estimate originates from GNSS epochs with low accuracy, the first task is to quantify how much the position updates degrade and if they can be improved.

Q2 *In a GNSS signal-constrained environment, what is the magnitude of degradation in the accuracy of GNSS positioning updates, and what strategies can be employed to improve the accuracy of the GNSS positioning update?*

Finally, the third sub-question is tailored towards a potential solution for increasing the accuracy of the integrated trajectory estimate of a rail-based track surveying system. To do so, the effect of the inaccurate GNSS position updates on the integrated trajectory solution must be quantified. To improve on the accuracy of the integrated trajectory solution, a method is to be found that mitigates the effect of the inaccurate GNSS positioning updates.

Q3 *What is the effect of inaccurate GNSS position updates on the accuracy of the integrated trajectory solution of an RTSS, and what measures can be taken to mitigate these effects?*

3

RTSS Trajectory Solution

In this chapter, the definitions, estimation and analysis of the RTSS trajectory are discussed. The chapter begins with a brief description of the relevant reference frames in section 3.1 followed by the RILA data acquisition process in section 3.2. Next, the constructed trajectory accuracy metrics will be discussed in section 3.3. The chapter will be concluded with a discussion on the trajectory accuracy research methodology in section 3.4.

3.1. Reference Frames

In order to unambiguously describe the position and translation of any point or body along a trajectory, a point or system to reference the position and movement is needed. For that reason, reference frames are defined. All reference frames and coordinate systems discussed in this report follow the right-handed convention. For the analysis of the trajectory solution of the RILA system, there are three reference frames that are commonly used. These are the Earth Centred Earth Fixed (ECEF) frame, the Local Navigation Frame and the RILA body frame. Although the end product, the georeferenced track geometry measurements are given in a reference frame of choice for the end user, in this research, the ECEF frame will be used to describe the absolute RILA position and trajectory. The local navigation frame is used to describe the along-track and cross-track observations and the RILA body frame is used for the relative position determination of the different sensors mounted on the system.

Earth Centred Earth Fixed Frame

The Earth Centred Earth Fixed (ECEF) reference frame is a geocentric, rotating reference frame used to describe the position and motion of objects relative to the origin of Earth (Wakker 2015). The ECEF reference system is used to define the coordinates of the 3D trajectory of an RTSS, similar to research performed by Judek et al. (2022).

- The origin (O_e) is fixed at the centre of Earth
- $+Z_e$-axis points upwards towards the North-pole of Earth and aligned with its rotational axis
- $+X_e$-axis points towards the intersection of the prime meridian and the equator
- $+Y_e$-axis is aligned with the equatorial plane and completes the right-hand system

Local Navigation Frame

The navigation- or local-level frame, uses an East-North-Up-frame (ENU) convention and is a local reference frame of a plane that is tangent to the surface of the Earth at the origin. The North- and East-axes form the local tangent plane and the Z-axis points towards the centre of Earth (Kukko 2013). Furthermore, the origin of the local-level frame coincides with the origin of the body frame as reported by Shi et al. (2021a).

- The origin (O_n) coincides with centre-of-mass of the IMU sensor and the bodyframe (O_b)
- $+Z_n$-axis (U) points upwards along the direction of the ellipsoidal normal at the origin
- $+X_n$-axis (N) points towards the geodetic north of the ellipsoid, therefore, its direction is parallel to the tangent to the respective meridian (Kukko 2013)
- $+Y_n$-axis (E) completes the right-handed system and points towards the east

RILA Body Frame

The body frame is a local reference frame with its origin in a predefined point of the relevant body. For ease of implementation and georeferencing of the measurements installed on the RILA system, the origin of the body frame is at the centre of mass of the IMU sensor (Secco 2022). This local reference frame is used to relate the position and distances of different sensors mounted on the body to each other. A graphical representation of the body reference frame as defined for the RILA system can be found in Figure 3.1.

- The origin (O_b) is fixed at the centre of the IMU sensor of the RILA body
- $+Z_b$-axis points up at zenith (perpendicular to Earth's surface)
- $+X_b$-axis is aligned with the along-track (running) direction of the train
- $+Y_b$-axis completes the right-handed reference frame and is aligned cross-track

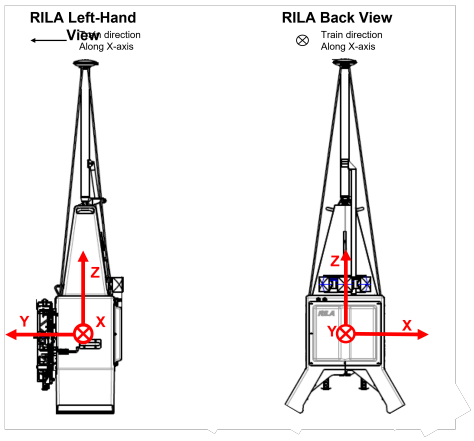

Figure 3.1: An overview of the body reference frame as defined for the RILA measurement system (source: adapted from Fugro internal documentation)

3.2. RILA Data Acquisition and Processing

A request from a client to measure a certain railway track segment is called the scope. When a scope is to be measured for the first time, a so-called baseline survey is conducted. A baseline survey consists of at least four runs (observations) over the scope. Having four independent measurements of the same track segment allows for the integration of the collected data improving the accuracy and confidence in the output data quality. Usually, these four runs are collected in a single day of surveying with the train travelling two times in one direction over the track (forward), and two times in the opposite direction over the track (backward). However, when the scope is very long, it can be the case that the individual observations for the baseline survey are collected over multiple days. Furthermore, to further improve the quality of the data, in some cases more observations are added to the baseline survey. It is important to clearly establish the different data acquisition definitions:

- **Run:** A run is a single observation by the measurement system, with an arbitrary direction, of the entire scope, at a given point in time. Therefore, when the RTSS exits the scope at its defined end, a run is terminated. A new run is started when the system again starts travelling over the scope, generally in opposite direction. However, the surveying system does not stop the data collection until the surveying day is concluded. The trajectories of multiple runs during a single day's worth of surveying are therefore ordered chronologically in a single data file.
- **Baseline survey:** The baseline survey is the total, integrated dataset of the scope consisting of at least four runs. The baseline survey can consist of multiple days worth of surveying and more than four runs. However, when additional runs are requested at a later point in time ($>$ 1 month) for an update of the measurements, the run is not counted towards the baseline survey.

The RILA measurement system collects a lot of data from a single measurement run. To explain how the data collection and processing process works, a (simplified) flowchart of the RILA measurement acquisition and processing process is given in Figure 3.2.

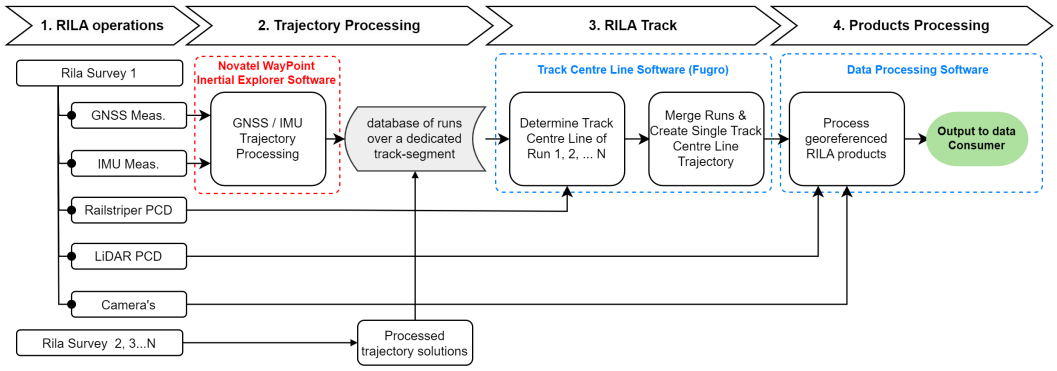

Figure 3.2: Simplified representation of the data collection and processing process for a certain track scope (PCD: Point Cloud Data)

3.2.1. RILA Operations

The first step in the surveying process is the operations, i.e. the actual acquisition of the track geometry measurements and data of the railcorridor with the RILA system mounted on a train. As previously discussed, a single day's worth of surveying usually consists of multiple runs over the same track segment. Furthermore, data can be collected over multiple days.

3.2.2. Trajectory Processing

After the data is collected, the next step is to integrate the GNSS and IMU measurements and process the trajectory solution of the data obtained during a single surveying day. This is done using third-party navigation software called Inertial Explorer[1], developed by Novatel. The processed trajectory is a continuous, GNSS time-stamped position for the entire duration of a day's worth of surveying. Therefore, multiple passes over the same track are not yet 'recognised' in this stage of data processing. Furthermore, any quality control of the trajectory solution is also performed using quality metrics on a time axis. The trajectory coordinates are given in the ECEF reference frame at the Centre-Off-Mass (COM) of the IMU sensor (see Figure 3.1).

To obtain an accurate trajectory solution, Differential Carrier Phase Positioning (DCPP) is used. DCPP works by combining the data of one or more reference stations with the measurements of the receiver, limiting inaccuracies introduced by satellite ephemeris errors (Tiberius et al. 2004). In addition, the trajectory accuracy is further improved by making use of Virtual Reference Stations (VRS). A VRS is constructed by integrating the correction signals of nearby fixed GNSS reference stations, to provide a correction signal from the VRS to the receiver (Odijk et al. 2017). Given good GNSS signal reception, *cm* level accurate GNSS positioning solutions are possible in Inertial Explorers Post-Processed Kinematic (PPK) mode using DCPP and VRS's, without the need for a local, physical base station to be present (Retscher 2002) (Ong Kim Sun et al. 2005). General practice in RILA trajectory processing is to place VRSs every 10 kilometres along the trajectory.

The basic trajectory processing flow is presented in Figure 3.3. The first step is to establish the Virtual Reference Station (VRS) data. The GNSS reference station data used to construct the VRSs in Inertial Explorer is provided by a regional GNSS network provider. Furthermore, apart from the observations obtained by the GNSS receiver and IMU sensor, the measurement system calibration parameters (lever arms etc) are required. Also, the rapid satellite ephemeris files (IGS Rapid clock- and orbit) for GPS are downloaded from the International GNSS Service (IGS) portal[2] and included in the processing input. Although, the effect is limited due to the differential positioning (DCPP), a slight performance increase has been recorded by El-Mohammedy Sabaa et al. (2019) for a similar system.

[1] https://novatel.com/products/waypoint-post-processing-software/inertial-explorer
[2] `https://igs.org/products/`

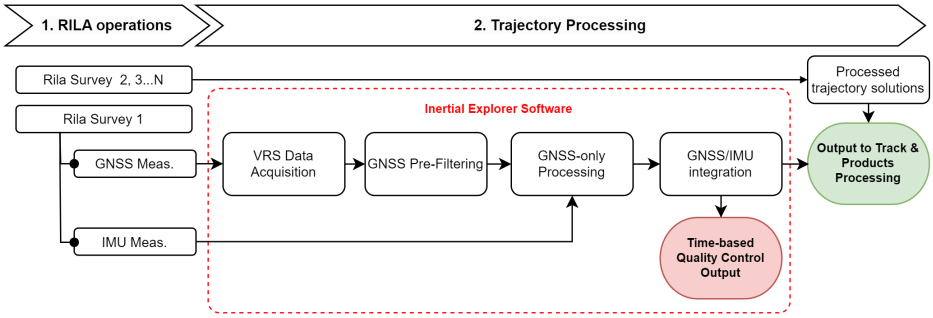

Figure 3.3: Trajectory processing flow for the RILA system

The next step is to process the trajectory using only the GNSS data. Currently, the GNSS trajectories are processed using only GPS and GLONASS (G2) observations[3]. Some relevant settings for the processing of the GNSS-only position solutions can be found in Table 3.1. A full overview of all the GNSS-only, and GNSS/IMU integration processing settings, together with their current values and respective descriptions can be found in Appendix B.

Table 3.1: Current RILA GNSS-only trajectory processing settings

Parameter	Unit	Current Setting
GNSS Constellations	n/a	*GPS + GLONASS*
Elevation Mask	deg	10
C/N0 rejection tolerance	dB-Hz	*disabled*
Maximum RMS	mm	3.00

The next step in the RILA trajectory processing is to integrate the GNSS-only processed trajectory solution with the IMU measurements, using a Loosely Coupled (LC) integration scheme (Falco et al. 2017). Again, a full list of settings for the integration scheme can be found in Appendix B. The LC trajectory solution is processed in both forward- and backward directions. The forward- and backward-processed trajectory solutions are then combined using inverse variance weighting, assigning more weight to the solution with the smaller estimated errors (Cosandier et al. 2018). Next, the IE software automatically performs backsmoothing of the trajectory solution with precise error modelling for the navigation sensors. Backsmoothing is a recursive process where the error filter states are updated along the trajectory to 'smoothen' the solution (Briers et al. 2009). The output result of RILA trajectory processing is a Smoothed Best Estimated Trajectory (SBET) solution in a given geodetic Cartesian reference frame (Mattheuwsen et al. 2019).

The RILA measurement unit is not always mounted on the same type of train, resulting in varying distances between the COM of the IMU and the true trajectory of the track. Furthermore, due to the suspension between the wheels of the train and the mounting point of the surveying system, the measurement unit should be considered to be 'floating' above the track. Therefore, one cannot directly compare the trajectories of different runs, centred at the IMU body frame origin as output of the trajectory processing software.

3.2.3. RILA Track

To obtain accurate measurements of the relative track geometry, the system collects accurate data on the position of the two tracks using the railstripers. In this stage of data processing, from the continuous time-based trajectory solution resulting from the trajectory processing, the different runs over the same track segment (scope) are identified. This is done using software developed by Fugro in a Matlab environment. Furthermore, every trajectory epoch is given a unique kilometre value, therefore defining the measured points at a distance along the track (mileage), with kilometre zero at the start of the scope indicated by the client.

[3]Although currently, a transition is being made to G4 GNSS processing (GPS + GLONASS + Galileo + Beidou)

For each of the measured epochs of the trajectory solution, the Track Centre Line (TCL) trajectory, defined in the ECEF coordinate system, is computed using data collected by the railstripers and the integrated GNSS/IMU trajectory solution. The TCL is an important concept as it is used by both Fugro and end-users of the data as a reference trajectory - i.e. all measurements collected by the RILA system are defined relative to the determined TCL trajectory. Furthermore, the computed TCL (in a local reference frame) is independent of the position of the RILA unit in relation to the tracks. Therefore, it is possible to compare the TCL trajectories of multiple runs to each other. The TCL defines the absolute railway track geometry measurements and can therefore also be used to determine track geometry change over time.

Computing the TCL works by using the measurements of the railheads by the rail-stripers, displayed in Figure 3.5. The software automatically identifies the uppermost data point as the top of the railway heads, $T1$ and $T2$ in Figure 3.4. Next, the software identifies the running edge[4] of the tracks by identifying the innermost point of the railhead, by definition 14 mm below the top of the railheads, points $R1$ and $R2$. The track centre line is then defined as the middle point between $R1$ and $R2$, Rc.

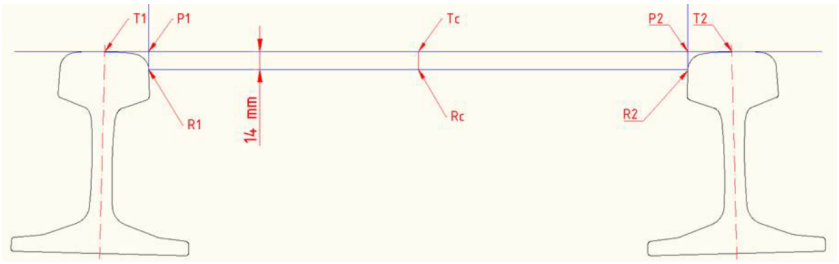

Figure 3.4: Deriving specific rail points from RILA rail-striper data. (source: Fugro)

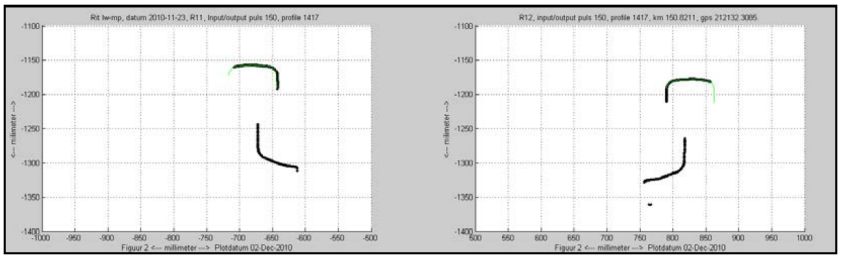

Figure 3.5: Rail-striper measurements of the railheads at an arbitrary cross-section of the track (source: Fugro)

In the computation of the TCL, there are several error sources affecting the accuracy of the trajectory solution. These errors include the measurement error and uncertainty in the measurements of the rail-striper (σ_s), error in the transformation of the rail-striper measurement to the IMU body frame (σ_s^b), error in the transformation of the IMU body frame to the Earth-Centred-Earth-Fixed (ECEF) reference frame (σ_b^e) and error in the processed GNSS/IMU position (σ_r). As these errors are assumed to be uncorrelated, to compute the total error variance (σ_{meas}) in the TCL trajectory, the simplified relation in Equation 3.1 can be used.

$$\sigma_{meas}^2 = \sigma_s^2 + (\sigma_s^b)^2 + (\sigma_b^e)^2 + \sigma_r^2 \tag{3.1}$$

Although all these error variances must be taken into account when comparing the TCLs of different trajectories to each other, it is expected that the errors introduced by the TCL algorithm, σ_s, σ_s^b and σ_b^e (mm level), are much smaller than the error introduced by the GNSS positioning inaccuracy, σ_{meas} (cm - dm level).

[4]The running edge is defined as the point on the track where the wheels of the train and the track are in contact

The final step in RILA track processing is to merge the TCL data of all (4) individual runs into a single TCL to increase the accuracy of the estimated absolute trajectory and reduce the potential impact of outliers / faulty measurements (Wang et al. 2019). In this merging process, a weighted averaging algorithm is used that weighs each of the individual trajectory solutions with the inverse of the distance to the mean TCL. The further the TCL is from the mean, the less weight it is assigned in the merged solution (Secco 2022). Furthermore, when a Fugro operator overseeing the merging process deems a certain part of a run to deviate 'too' much from the mean solution, he/she can decide to remove that data from the solution entirely (called patching). This is currently a manual and very superficial process. Furthermore, it is also important to note that the averaged trajectory, although likely more accurate than the TCL of an individual run, may still deviate from the true position of the track.

3.2.4. Products Processing

When the processing of the merged TCL is complete, the other data collected by RILA sensors can be processed (see Figure 3.2). This is done to create a variety of products that can be relevant for railway engineering companies. These output products include for example georeferenced point clouds and digital representations (combining video and pointcloud data) of the railcorridor. The coordinates of the georeferenced products will all be determined relative to the TCL obtained by RILA track. Furthermore, the merged TCL itself is also an output product (absolute track geometry) together with the relative track geometry measurements obtained by the railstripers, processed in RILA track. It is important to note that all output data is presented to the end-user on a mileage (along-track distance in km) based axis.

3.3. Trajectory Accuracy

To evaluate a trajectory solution on its accuracy, general practice is to compare it to a *ground truth*- or so-called *reference trajectory*. The distance between the estimated trajectory solution and the reference trajectory can directly be used as the 'error' in the estimated trajectory solution. It is very important to unambiguously define what is understood by trajectory accuracy. In this report, *precision* and *trueness* are used to describe the trajectory accuracy, in line with the definition confirmed by the ISO (International Organization for Standardization). The precision of the trajectory solution describes the repeatability (spread) of the measurements. Trueness, however, is defined as a metric for the distance between the navigation solution and the actual, true (reference) trajectory (ISO 5725-1 1994). A graphical representation of the accuracy metrics can be found in Figure 3.6a. The *accuracy* is defined as a combination of both the *trueness* and *precision* of a set of observations. The relation between the accuracy and confidence level, trueness and precision is displayed in Figure 3.6b. Therefore, the combination of the trueness and precision metrics gives an indication of both the accuracy of the trajectory solution and the level of uncertainty that needs to be accounted for.

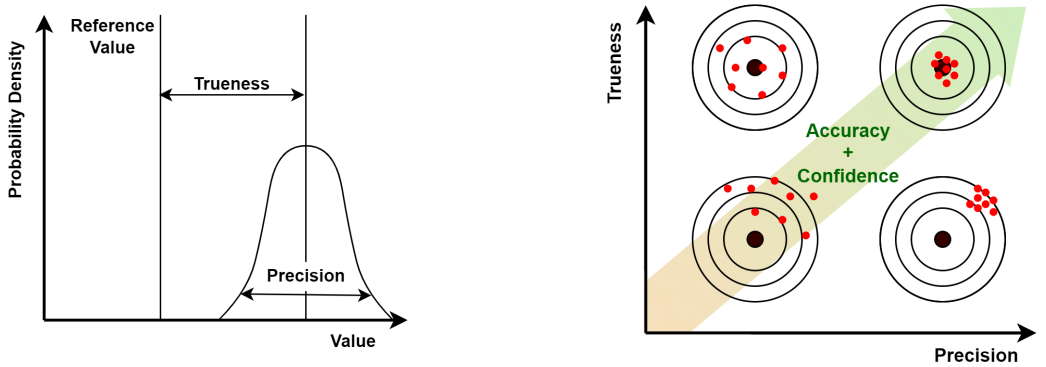

(a) Trajectory accuracy metrics *trueness* and *precision* (Perakis et al. 2015)

(b) *Trueness* versus *precision* as metrics for the accuracy and certainty (Weitzel 2015)

Figure 3.6: Accuracy defined by the precision and trueness

The main requirement for a suitable ground-truth trajectory, is that its level of accuracy is at least an order higher than the evaluated trajectory solution. Therefore, the reference trajectory would need to

have an accuracy of 1 cm (or lower) in order to compare the trajectory solution of the RTSS. Obtaining a (reference) trajectory with such high accuracy levels is usually expensive, as land surveying crews have to come to take the measurements. Furthermore, as railway tracks are long and stretched out over many kilometres, acquiring reference trajectories takes a long time and costs would progressively rise.

Therefore, the availability of adequate reference trajectories along railway segments is very limited. Furthermore, Fugro, as owner of the RILA system, also has not made significant investments in the acquisition of reference trajectories to evaluate trajectory accuracy. The geo-referenced output data of the RILA system is usually corrected (shifted) using physical control points placed along the track (see section 2.4) with known, 'ground-truth' coordinates provided by end-users of the track data. Ground-truth, in this case, is not necessarily objectively defined, but rather what the client or end-user of the track data perceives/determines is ground-truth.

In absence of a reference trajectory, the best alternative for the quality analysis of a trajectory solution is to use precision as an evaluation metric. The options and implications of evaluating the trajectory accuracy on the precision only will be further discussed in this section.

3.3.1. Single Pass Accuracy

To provide insight into the quality of the integrated GNSS/IMU trajectory solution, Inertial Explorer (IE) - the navigation software used for the trajectory processing of the RILA system - provides some quality control output data. A variety of qualitative metrics defining the trajectory solution can be plotted on the time axis. One of these metrics is the estimated position accuracy, of which an example output of a 10-minute interval of the survey is given in Figure 3.7.

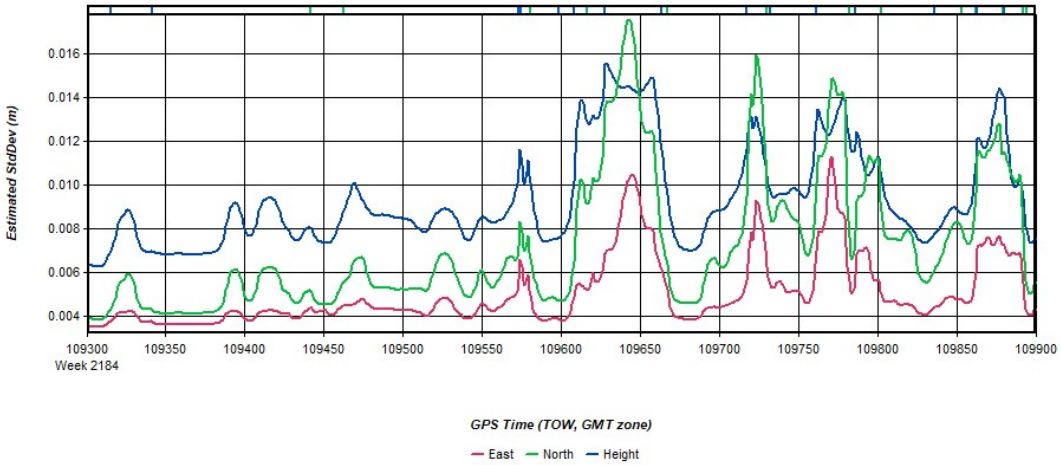

Figure 3.7: Example output of IE software: Estimated position accuracy plot (10-minute interval)

As one can observe from Figure 3.7, the estimated position accuracy consists of the estimated standard deviation of the trajectory solution in North, East and Height directions. There are two things important to understand about the estimated position accuracy: (1) What metrics are used as input for the estimated standard deviation and (2) what the implications are on the true (real-life) trajectory accuracy.

1. Input parameters for the estimated standard deviation

According to the manual of the IE-software[5], the estimated standard deviation is a "summary" of a number of measured trajectory quality metrics. The most important metrics are the satellite geometry and the float/fixed status of the 'resolved' integer carrier phase ambiguity. Furthermore, other quality metrics - such as the separation between the forward- and backwards-processed trajectory solutions - could impact the estimated standard deviation of the position error. However, qualitative information on these metrics is not provided by the documentation of IE.

[5] `https://novatel.com/support/waypoint-software/inertial-explorer`

2. Implications of the estimated standard deviation

According to the IE manual:

"Please note that the estimated error plot contains no knowledge of any systematic error (such as biased base station coordinates or incorrectly fixed integer ambiguities), and as such the values reported are only (by definition) estimates."

As quoted, there is no information on any systematic bias. Therefore, the estimated standard deviation only provides an estimation of the *precision* of the trajectory solution and not the *trueness*. This means that the magnitude of the values of the estimated STDev is not indicative of the true magnitude of the standard deviation of the trajectory solution. A scaling factor can be applied to the estimated STDev values to more closely represent the true magnitude of the errors, which can only be obtained by comparing the navigation solution to a reference trajectory.

Therefore, the estimated standard deviation is a direct estimation of the *precision* of the trajectory solution and does not say anything about the *trueness*.

3.3.2. Multi Pass Accuracy

A significant benefit to the way that the RILA survey is performed, is that the same track segment is measured at least four times in the baseline survey. This means that, at any arbitrary point along the trajectory, there should be four, individual measurements of the same track position. This repetitiveness of the dataset can be used to provide further insights into the accuracy of the trajectory estimate.

Using the multitude of measurements of the same track segment, an analysis of the spread of the different trajectory solutions can be made. This analysis will yield a measure of the observed trajectory *precision*. In absence of a reference trajectory or *trueness*, this observed trajectory *precision* is the best alternative for evaluating a trajectory on its accuracy.

The observed trajectory *precision* is derived from multiple observations taken under different conditions. As the passes of the RTSS over an arbitrary track segment happen at different times during the day, the observed GNSS satellite constellation will also have a different geometry. Furthermore, including measurements from runs taken in different driving directions may (partially) eliminate specific GNSS outages resulting from environmental obstructions, such as railway underpasses. Given that the number of runs used for the computation of the trajectory *precision* is sufficiently large with sufficient variation, one could argue that the systematic error (bias) is reduced, and therefore the *trueness* is relatively high.

In that case, the observed *precision* of a trajectory can be used as an accuracy metric. Therefore, the accuracy of the estimated trajectory will increase with increasing observed trajectory *precision*, as seen in Figure 3.6b.

3.3.3. Trajectory Similarity Metrics

To make a meaningful comparison between the different runs of the RTSS over the same track segment, a selection must be made on metrics to define trajectory *precision*. A paper by Tao et al. (2021) presents an analysis of a variety of trajectory similarity measures. Most of the discussed measures, such as the Lock-step Euclidean Distance (LSED), Dynamic Time Warping (DTW) and Discrete Fréchet Distance (DFD) are discrete. This has the distinct disadvantage that it could potentially lead to problems when comparing trajectories with non-uniform sampling, which is the case in the RILA trajectories.

Although LSED (Vlachos et al. 2002), DTW (Berndt et al. 1994) and DFD (Eiter et al. 1994) are widely used and extensively applied in trajectory comparison, there is another disadvantage to these comparison metrics. All of these metrics provide a single-valued 'score' for trajectory similarity. However, for the analysis in this report, it would be more relevant to obtain an insight into the (changing) local similarity along the trajectory path. One such continuous metric is the Fréchet Distance (FD) Tao et al. (2021). FD evaluates trajectories on the distance between the two curves on all points by making use of interpolated trajectories. The disadvantage to an FD analysis is that only provides a

comparison between two trajectories (Alt et al. 1995), making it less suitable for comparing three or more. Therefore, for this research, two other continuous trajectory comparison metrics are used.

Standard Deviation of the Cross-Track Trajectory Spread

The first metric is the cross-track trajectory spread, defined by the standard deviation. Different to the estimated standard deviation as an output of the IE software, the standard deviation of the measured trajectories gives a direct metric for the cross-track spread of the trajectory solutions. A decrease in this spread will therefore lead to an increase in the confidence level of the accuracy of the trajectory solutions. This continuous metric will also allow for the identification of local changes in the trajectory spread along the full track segment.

By definition, the interpolated trajectory epochs are in the same cross-track plane, a combination of the standard deviations of the X_{ECEF}, Y_{ECEF} and Z_{ECEF} coordinates computes the standard deviation of the cross-track spread. The standard deviation of the cross-track trajectory spread (σ_{ct}) is therefore computed using Equation 3.2.

$$\sigma_{ct} = \sqrt{\sigma^2_{X_{ECEF}} + \sigma^2_{Y_{ECEF}} + \sigma^2_{Z_{ECEF}}} \tag{3.2}$$

Smallest Enclosing Circle Analysis

The second proposed continuous metric for evaluating the *precision* of the trajectory solutions, is to perform a smallest enclosing circle analysis. The smallest circle problem aims to find the properties of the smallest circle enclosing a given set of points in the Euclidean plane, as seen in Figure 3.8 (Sylvester 1857). For the trajectory accuracy metric, the Euclidean plane is defined as a vertical, cross-track plane defined in the local navigation frame at an arbitrary point along the track.

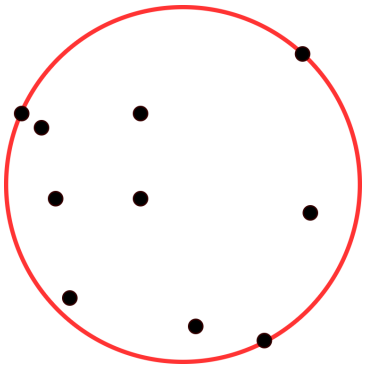

Figure 3.8: Smallest enclosing circle of a given set of points in the Euclidean plane[6]

To compute the radius of the smallest circle, the `smallestenclosingcircle.py`[7] python module is used. The algorithm uses a set of 2D coordinates as input to describe the location of the points in the Euclidean plane. For simplicity's sake, these 2D coordinates will be referred to as the horizontal- (P_{EN}) and vertical (P_U) coordinates. However, the location of the RILA system is provided in 3D ECEF coordinates. To account for the varying orientation of the 2D Euclidean plane along the trajectory, the ECEF coordinates used to define the RILA trajectory need to be transformed to the local East-North-Up (ENU) frame. To do so, Equation 3.3 is used (Sanz Subirana et al. 2011).

$$\begin{bmatrix} E \\ N \\ U \end{bmatrix} = \begin{pmatrix} -\sin\lambda & \cos\lambda & 0 \\ -\cos\lambda\sin\varphi & -\sin\lambda\sin\varphi & \cos\varphi \\ \cos\lambda\cos\varphi & \sin\lambda\cos\varphi & \sin\varphi \end{pmatrix} \left(\begin{bmatrix} x_i \\ y_i \\ z_i \end{bmatrix} - \begin{bmatrix} x_O \\ y_O \\ z_O \end{bmatrix} \right) \tag{3.3}$$

In Equation 3.3, φ and λ are the respective latitude and longitude of the origin of the ENU frame, defined in ECEF by (x_O, y_O, z_O). To define the origin of the ENU frame, the coordinate (see subsection on trajectory interpolation) of the baseline run in the Euclidean plane is used. The coordinates of the other

[6] Source: `http://www.algorithmic-solutions.info/leda_guide/geo_algs/extremal_circles.html`
[7] `https://pypi.org/project/smallestenclosingcircle/`

points, defined by (x_i, y_i, z_i) in the ECEF frame in Equation 3.3, are then transformed to the same ENU frame as the baseline coordinate. In the local ENU-frame, the horizontal coordinate P_{EN} is defined in the East- and North plane, and the vertical coordinate P_U is defined along the local Up-axis. Therefore, the inputs required for the smallest circle algorithm (P_{EN}, P_U) are defined using Equation 3.4.

$$\begin{aligned} P_{EN} &= \sqrt{E^2 + N^2} \\ P_U &= U \end{aligned} \tag{3.4}$$

Finding the radius of the circle enclosing all trajectory solutions in this local, cross-track plane, gives a measure of the distance between all trajectories. Different to the cross-track standard deviation, the smallest circle radius does not give a statistical measure, but rather an absolute one. The smaller the smallest-circle radius, the higher the trajectory *precision* and the more accurate the trajectory solution.

3.3.4. Trajectory Interpolation

The trajectory output (both quality control and coordinates) is provided on a time-based output. As the velocity of the RTSS along a certain trajectory and the starting time is arbitrary, the different trajectory solutions will have an unequal sampling rate when comparing trajectories at a distance along the trajectory. Therefore, to be able to perform the cross-track standard deviation and smallest circle analyses on a continuous basis, interpolation is needed. The interpolation of the trajectory solution could introduce errors to the calculation of the trajectory *precision*. To quantify this potential error, a case study is performed to quantify the largest interpolation error that could occur.

As the trajectory is evaluated on the cross-track spread, when interpolating *linearly*, the largest interpolation error would occur in a tight curve. An (exaggerated) example of such a curve between points P_i and P_{i+1} is presented in Figure 3.9. In this figure, point A is the point at which the coordinates of the arc segment $P_i - P_{i+1}$ need to be determined by interpolation, point A' is the linearly interpolated point of which the coordinates are actually retrieved and h is the interpolation error.

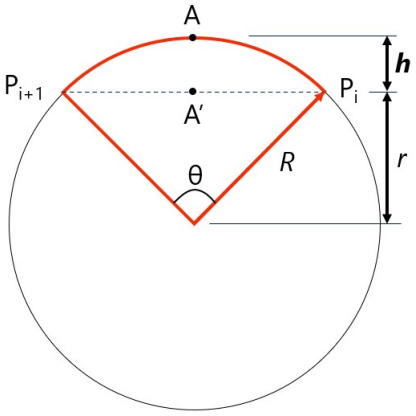

Figure 3.9: Maximum error introduced by linear interpolation along an arbitrary arc segment

The interpolation error $A - A'$ is largest when point A is exactly halfway on arc-segment $P_i - P_{i+1}$, where $A - A' = h$. Furthermore, the interpolation error is dependent on the radius of the curve R and the length of the arc-segment $P_i - P_{i+1}$. Using the relations from Equation 3.5, the maximum (linear) interpolation error h can be determined (Harris et al. 1998).

$$\begin{aligned} \theta &= \frac{P_i - P_{i+1}}{R} \\ r &= R\cos\left(\frac{1}{2}\theta\right) \\ h &= R - r \end{aligned} \tag{3.5}$$

According to the (Dutch) main railway infrastructure regulations, the minimum radius of a railway track curve must be 190 [m] for trains travelling less than 40 [km/h] and at least 400 [m] for trans

travelling at speeds higher than 40 [km/h] (VWS 2005). With this information, the interpolation error at the tightest curve radius ($R = 190$ [m]) at maximum speed ($v = 11.11$ [m/s]) can be computed. Provided that the Inertial Explorer software provides position outputs at every 0.5-second interval, the arc-segment $P_i - P_{i+1}$ is 5.56 [m]. The computed absolute maximum cross-track interpolation error h is therefore, using the relations from Equation 3.5, 2.03 [cm].

It is likely that the interpolation error could be reduced when using other forms of interpolation such as polynomial- or cubic-spline interpolation (Brus et al. 1996). However, linear interpolation was specifically selected as this stage of the research for ease of implementation in the complex datasets provided by Fugro.

3.3.5. Conclusion on Trajectory Accuracy Metrics

To provide a comparison for the accuracy of the processed, integrated trajectory solution, two main quality metrics have been selected. First of all the cross-track trajectory spread, defined by the observed standard deviation and second, the radius of the smallest (enclosing) circle of the navigation solutions. However, with these quality metrics, there are a few considerations to keep in mind.

- **Precision vs Trueness:** In absence of a ground-truth trajectory, both the selected trajectory quality metrics are a measure of the precision of the trajectory solution, rather than the trueness. However, when the dataset consists of a sufficient number of samples of the same track segment, sampled at different time intervals during a day, it can be assumed that systematic errors in the dataset are limited, leading to relatively high trueness. With this assumption, the trajectory precision is a measure of the accuracy of the integrated GNSS/IMU trajectory solution. Therefore, increasing the *precision* of the trajectory solution will increase the trajectory accuracy. However, it must be kept in mind that no relation to the true position of the tracks (reference trajectory) is available to validate the measure of accuracy.
- **Interpolation Error:** As the trajectory *precision* is a continuous measure of the cross-track trajectory spread, comparing multiple trajectories with unequal sampling rate, interpolation is needed. Linear interpolation of a trajectory will yield a maximum cross-track interpolation error at the minimum railway curve radius ($R = 190$ [m]) at maximum allowed velocity ($v = 40$ [km/h]). This maximum (linear) interpolation error is c. 2 [cm]. Therefore, when evaluating the trajectories on the precision, especially in curves, this interpolation error must be kept in mind.

3.4. Trajectory Research Methodology

In order to formulate an answer to the main research question posed in section 2.6, a research methodology or framework has been devised. This research framework aims to find a correlation between the Quality Control (QC) metrics for the processed trajectory provided by the Inertial Explorer software, and the observed trajectory accuracy metrics (cross-track trajectory spread and smallest enclosing circle). When a correlation can be identified, it can be used to develop a targeted error mitigation strategy in order to improve the accuracy of the integrated trajectory solution. First of all, an overview of the Inertial Explorer Quality Control (QC) metrics is provided.

Inertial Explorer Quality Control Metrics

The trajectory QC metrics of the individual runs form, together with the cross-track trajectory spread, the basis for the hypothesis and execution of the accuracy improvement strategies. Therefore, it is important to select meaningful QC variables from the vast array of trajectory metrics available in the trajectory processing software. Apart from the QC metrics selected in this report, the correlation of many others with the cross-track trajectory spread could be investigated in the search for accuracy gains. As a starting point, three metrics are selected:

1. Estimated Standard Deviation (Est. STD)

As explained in section 3.3, the estimated standard deviation is a summary of a number of measured trajectory quality metrics. It, therefore, provides an indication of the expected trajectory accuracy but does not in itself provide an absolute measure of the accuracy. However, in a comparative analysis where the estimated trajectory is benchmarked against the values for other runs, it does provide insight into the relative accuracy. In other words, if the estimated standard deviation of a run is high compared to the other runs at the same track segment, it can be expected that the accuracy of the trajectory solution of that run is lower.

2. Position Dilution Of Precision (PDOP)

The Position Dilution Of Precision (PDOP) is a measure of the satellite geometry and is a mapping of an observations' measurement error (Langley et al. 1999). If the geometry is bad - i.e. the observed GNSS satellites are all located close to each other - the PDOP value is high and the measurement error is multiplied with a large value, as seen in Figure 3.10. The measurement error or User Equivalent Range Error (UERE) is the error in the psuedo-range measurement between the GNSS satellite and receiver (Chen et al. 2002). This measurement error is multiplied by a Dilution Of Precision factor in order to determine the true positioning error (Langley et al. 2017). The PDOP represents the 3-Dimensional dilution of precision, relevant as the RTSS trajectory needs to be accurate in 3 dimensions.

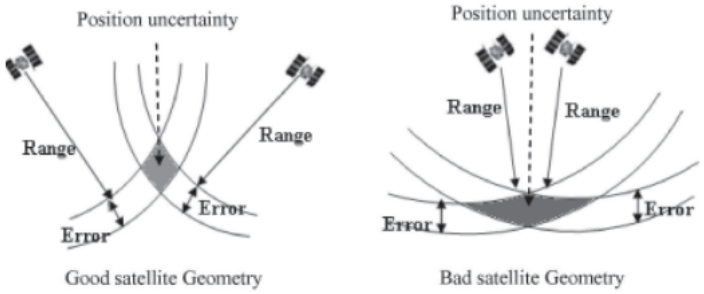

Figure 3.10: Concept of dilution of precision in a situation with good satellite geometry (low PDOP) and bad satellite geometry (high PDOP) for a simplified satellite constellation consisting of two satellites (Dutt et al. 2009)

In order to assess what can be considered acceptable PDOP values for high-accuracy trajectory processing applications, literature is consulted. Where some studies implement a very strict, limited 3-tier (Acosta et al. 2012) ($PDOP > 3$ = poor), many incorporate the same qualitative classifications with slight variations (Dutt et al. 2009), (Kaya et al. 2005). Research by Isik et al. (2020) aims to classify the DOP parameters under conditions most similar to the research performed in this report. Hence, their qualitative classification is selected (see Table 3.2).

Table 3.2: Qualitative PDOP classification (Isik et al. 2020)

Tier	PDOP Value	Qualitative Rating
1	<1	Ideal
2	1-2	Excellent
3	2-5	Good
4	5-10	Moderate
5	10-20	Fair
6	>20	Poor

3. Number of Satellites used in the trajectory solution (NS)

As the name suggests, the number of satellites used in the trajectory solution (NS) represents the number of GNSS observations that are used in the GNSS position update of the integrated GNSS/IMU trajectory estimate. This is an important note, as NS does not represent the number of actual GNSS observations. GNSS observations rejected by the receiver or the trajectory processing software are therefore not included in this number. As the research aims to improve the trajectory solution at points where the GNSS signal is *reduced*, NS is an important metric for GNSS environment classification and detection.

Research Framework

With the QC metrics defined, the next step is to find a correlation with the quality metrics discussed in section 3.3 quantifying the observed trajectory accuracy. To do so, first of all, a track segment needs to be identified where a distinct 'peak' is observed in the accuracy metrics, indicating a decreased accuracy of the integrated trajectory solution. Although this 'peak' is not unambiguously defined, it should be a short interval where the trajectory accuracy metrics are significantly higher than the observed nominal values of the metrics. After such a track segment has been identified, the research framework consists of three distinct steps:

1. **Find a correlation between the trajectory QC metrics and trajectory segments with low accuracy**
   When a track segment with an increased cross-track trajectory spread is identified, the next step is to find a correlation between the cross-track trajectory spread increase and the observed QC metrics of the trajectory solution. This allows for the identification of an error source that is the potential cause of the decreased trajectory accuracy. With an identified correlation between a certain QC metric and the decreased trajectory accuracy, a hypothesis can be formed to mitigate the error source's effects on trajectory accuracy. It is valuable to form a hypothesis based on deviating (unfavourable) QC metrics observed for a single run, as this allows for isolation of the problem. In other words, in the first instance, it would be valuable to find a correlation between the observed QC metrics for a single run, indicating decreased accuracy of the trajectory solution, and the observed increased cross-track trajectory spread.

2. **Apply trajectory error mitigation strategies**
   Once a potential GNSS error source in one of the runs has been identified, error mitigation strategies can be applied. These error mitigation strategies can be the inactivation of certain GNSS measurements (at epochs, of constellations or of individual satellites) or updating selected values for the trajectory processing thresholds. By reprocessing the trajectory of only one of the runs with the updated settings, the effects on the observed cross-track trajectory spread can be analysed.

3. **(Re-)analyse the trajectory accuracy after application of error mitigation strategies**
   Once the trajectory of a run has been reprocessed using the updated settings, the trajectory accuracy metrics will be recomputed. This allows for one-on-one comparison of the observed trajectory with the original, and the reprocessed run. If the accuracy metrics show a decrease in standard deviation and radius of the smallest enclosing circle, the reprocessed trajectory is more accurate than the original, under the assumptions that are implicit in the accuracy metrics.

A more elaborate description of the algorithm developed for the research framework, together with flowcharts, data sources, settings and verification can be found in Appendix C.

This page was intentionally left blank.

4

Results: Case Study Trajectory Analysis

In this chapter, an accuracy analysis will be performed on a case study track segment within the survey scope `MLG1-2_0-39`. First of all, in section 4.1, a track segment for the case study is identified and a situational overview is presented. Next, in section 4.2, the observations of the quality metrics at the track segment are summarized and a hypothesis is formed. In section 4.3, the analysis performed on the case study is further explained followed by an elaboration on the validation cases in section 4.4. The results of the case study are presented in section 4.5 followed by the conclusions in section 4.6.

4.1. Track Segment Identification for Research

With the research methodology and the data analysis algorithm established, it is important to find a suitable track segment for the research. Track segments are surveyed according to a surveying scope defined by the end-user of the data. Such a survey scope is usually designated with a code like `AAA1_2-3`. In this code 'AAA' represents a three-letter code representing the location at which the scope starts, '1' indicates the survey number, and '2' and '3' represent the start and end mileage (in local units). Together with Fugro, a list of requirements has been established in order to find a suitable survey scope for the analysis:

- The survey scope needs to include varying levels of GNSS signal availability along the trajectory. This allows for the comparison of trajectory accuracy between environments and for isolation of an environment with 'reduced GNSS signal access', as required by the research question.
- The observations at the survey scope need to have been acquired by the *RILA04* measurement unit as this unit is one of the newer and more accurate models. It also contains a very accurate IMAR IMU system[1] with accessible processing software
- The survey scope needs to be mostly single-track as this generally increases the number of runs over the same railway track and therefore the sample size of the dataset.
- The survey scope needs to have a sufficient number of measurement runs to make a meaningful analysis of the cross-track trajectory spread (see section 3.3). In general, the larger the sample size (number of runs over a track segment), the better.

4.1.1. Research Scope Selection

With the requirements in mind, survey scope `MLG1-2_0-39` has been selected as the research dataset. As can be seen in Figure 4.1, `MLG1-2_0-39` is situated in the northeast of Scotland, the 'highlands'. Furthermore, data has been acquired by means of six measurement runs over the entire scope by the *RILA04* measurement unit.

[1] `https://www.imar-navigation.de/en/`

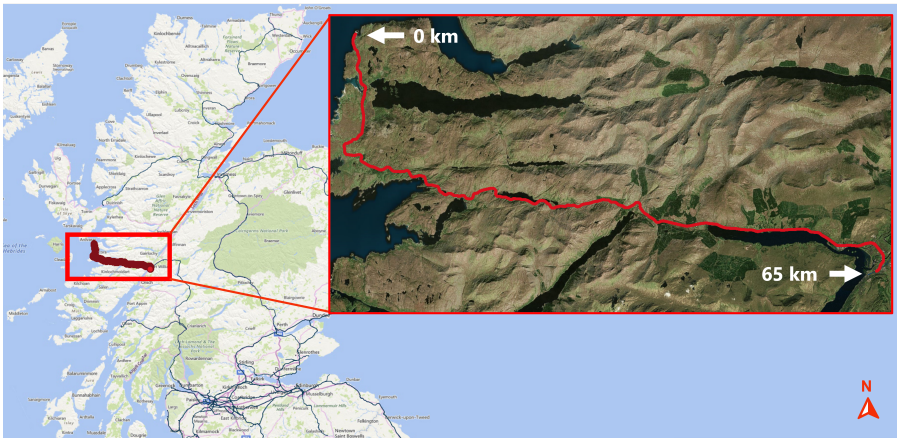

Figure 4.1: Overview of survey scope `MLG1-2_0-39`

The scope is nearly fully single-track (apart from railway stations etc.) and is, by nature of the highlands' coastline, very twisty including many railway underpasses and has high canyons along the track. Furthermore, dense vegetation can be found along the track that can cause a potential GNSS signal obstruction. Therefore, all the GNSS environments as established in section 2.3 are present and, according to Fugro, data engineers encountered many inaccurate GNSS/IMU trajectory segments along the selected survey scope (needing manual adjustment). Finally, the survey scope is situated in a 'middle latitude' region, which should allow for accurate GNSS positioning under ideal conditions using only the GPS and GLONASS constellations (same constellations as used by *RILA04*) (Zheng et al. 2022). This makes scope `MLG1-2_0-39` a good starting point for the analysis of the trajectory accuracy. An overview of the available measurement runs, together with their direction, is presented in Table 4.1.

Table 4.1: Runs in survey scope `MLG1-2_0-39`

Runs in Forward Direction	Runs in Backward Direction
`15_run1`	`2021-11-15_run2`
`15_run3`	`2021-11-15_run4`
`16_run1`	`2021-11-16_run2`

Note on MLG1-2_0-39 Railhead Detection & Case Study Analysis

Upon conducting the research (see chapter 4), it was discovered that the Railhead Detection for this track segment was unreliable resulting in inaccurate track centre line computations. This can be caused by many circumstances such as wet tracks, broken railstripers or inaccurate system calibration. The unreliable TCL trajectories made it impossible to compare the trajectories of the track centre lines of the different runs. Hence, the decision was made to compare the integrated GNSS/IMU trajectories provided in the output of Inertial Explorer.

As the train with the RTSS runs on fixed tracks, apart from small variances resulting from the train suspension, the cross-track position variation of the RTSS across the different passes is very limited. when the RILA system is mounted on the same train, in the same orientation. Therefore, the case study analysis is performed on runs in the same direction (`15_run1`, `15_run3` and `16_run1`.)

An assumption is made, based on literature on train suspension (Fu et al. 2020), that the variance in the position of the RILA body w.r.t. the TCL, caused by the train suspension, is in the order of 1 [cm] in cross-track direction. Therefore, in the analysis of the trajectory accuracy, this (potential) error needs to be accounted for.

Case Study Requirements

The selected surveying scope is c.65[2] [km] long and therefore too long in order to make a qualitative analysis of the trajectory accuracy along the entire track. Therefore, a case study analysis will be performed on a subset (or track segment) of the selected scope. For the selection of a case study track segment, again, a couple of requirements have been constructed:

- The scale, or length of the case study track segment shall be small enough to analyse local changes in the trajectory accuracy and QC metrics. The scale must also be large enough to put these local changes into perspective of the trajectory trends. A case study track segment with a 500 [m] to 3 [km] length is considered suitable.
- As the research aims to improve the trajectory solution where the GNSS signal access is reduced, there must be satellite observations used in the trajectory solution (*Environment 2*, chapter 2).
- The case study track segment is not allowed to include a segment where the velocity of the system is 0. A 'standstill' of the system provides, by nature, very irregular and relatively inaccurate position updates for the interval that the system is stationary. These standstill effects are only partly removed when in the conversion from the time-based to mileage-based representation.

4.1.2. Case Study Track Segment Selection

When looking at the quality metrics along the railway track from survey `MLG1-2_0-39`, a significant increase in the cross-track trajectory spread can be observed between kilometre 55 and 56. This trajectory accuracy decrease, defined by a short interval where the trajectory accuracy metrics are significantly higher than the observed nominal values (section 3.4), is highlighted in red in Figure 4.2a. This leads to a critical question: *What is the cause of the increase in the cross-track trajectory spread between kilometre 55 and 56 of the research track segment?*

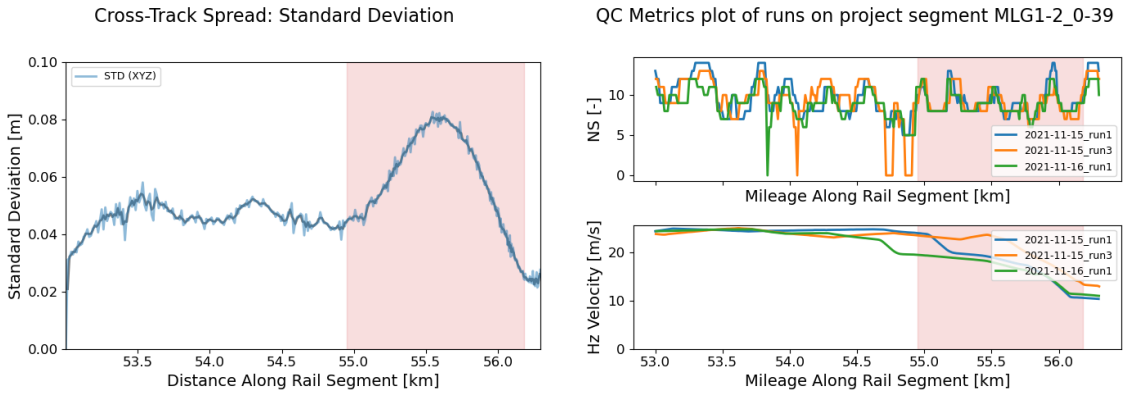

(a) Standard deviation of the cross-track trajectory spread for case study track-segment

(b) Number of satellites used in trajectory solution and velocity for the SBET case study track segment

Figure 4.2: Case study initial observations

A potential cause for the decrease in trajectory accuracy would be the loss of satellite signals. From Figure 4.2b, where the number of satellites used in the trajectory solution (NS) (exported from Inertial Explorer) is plotted, this is proven not to be the case. The number of satellites used in the trajectory solution is approximately 8 to 10 between kilometres 55 and 56. Generally, with good satellite geometry, this can be considered a healthy number of satellites for a good GNSS position estimate (Maciuk 2015). Furthermore, from the velocity profile in Figure 4.2b, the system is also it can be observed that the system has a sufficiently high velocity (> 10 [m/s]) to avoid being impacted by 'standstill' effects.

From the above, it can be concluded that the increase in the cross-track trajectory spread is caused by something other than loss of satellite signal or standstill effects. Furthermore, the track segment conforms to the requirements for the case study track segment discussed in subsection 4.1.1. Therefore, the track segment between kilometres 55 and 56 is suitable for the case study analysis. The track segment

[2] 39 miles

Figure 4.3: Satellite image of the case study track-segment, indicated by the purple dots (km 53 to km 56.3). The measurement system moves, in forward direction, from left to right

between kilometres 53 and 56.3 is situated close and parallel to a riverbank. A satellite image with the track segment indicated by purple dots can be found in Figure 4.3. Along the track segment, open areas, good for GNSS reception, are alternated with dense vegetation such as trees and semi-forested areas limiting the 'sky view'[3](Hussain et al. 2020). This is in accordance with *Environment 2* identified in chapter 2.

4.2. Observations & Hypothesis

From section 4.1, it was concluded that, in first instance, there was no obvious cause for the observed increase in the cross-track trajectory spread. Therefore the question remains: *What is the cause of the increase in the cross-track trajectory spread, given that NS is sufficient for adequate GNSS positioning and there are no 'standstill' effects?* To find a solution to this question, the QC metrics for the individual runs are plotted in Figure 4.4 as discussed in section 3.4.

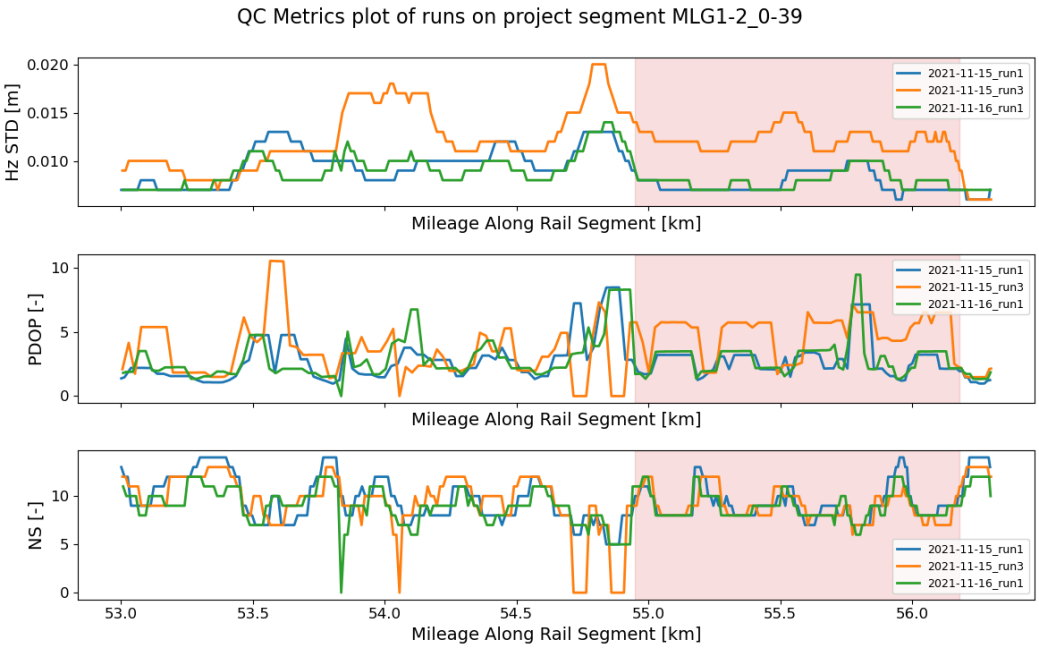

Figure 4.4: Quality Control metrics (IE output) for the SBET case study track segment, with the area at which the cross-track trajectory spread spike is observed highlighted in red

In Figure 4.4, the track segment at which the increased cross-track trajectory spread is observed is highlighted in red. A couple of important observations can be made when observing the QC metrics of the case study track segment at the highlighted trajectory interval. First of all, the number of satellites used in the trajectory solution (NS) is approximately the same for all runs included in the analysis. This therefore, by itself, cannot be the cause for the increase in the cross-track trajectory spread observed.

[3]Amount of sky that can be observed - spherical area at which GNSS signals can be observed

To better analyse the effect of obstructions along the track, one can look at a subset of the trajectory QC-metrics when the system travels from a more open, to a more enclosed track segment. A detailed view of the case study track segment, indicated by the white box, is presented in Figure 4.5.

Figure 4.5: Quality metrics with corresponding location on the map, RTSS moving from 'open area' into 'vegetated area'. Train direction is from left to right.

In line with expectations, when looking at Figure 4.5, it can be observed that NS decreases when moving onto a track segment surrounded by more vegetation. When the RTSS moves from a relatively open area (green), further into the vegetated area (red), for all runs, some satellites are lost and the PDOP increases. However, it can be observed that the PDOP values of `15_run3` increase about twice as much as the PDOP values for `15_run1` and `16_run1`. Where, the PDOP values of runs `15_run1` and `16_run1` show an increase of approximately $\Delta PDOP \approx 1.3$, from 1.8 to 3.1, `15_run3` shows an increase of approximately $\Delta PDOP \approx 3.4$, from 1.8 to 5.4. From Figure 4.4, it is observed that the increased PDOP values of `15_run3` compared to the other runs are consistent along the track segment highlighted in red.

In Figure 4.4, it can also be seen that the Estimated Standard Deviation values of `15_run3` are significantly higher (c 30%) than that of the other runs. According to the Inertial Explorer Manual[4]: *"spikes in DOP caused by loss of satellite signals are typically correlated with spikes in estimated position accuracy"*. The increase of the PDOP metric as a result of the loss of 2 satellite observations (NS) is therefore the likely cause of the increase in the estimated standard deviation for run `15_run3`.

As explained in section 3.4, GNSS positioning solution with a higher PDOP has, by definition, a lower accuracy. Because of the PDOP increase in all runs going from the green to the red epoch in Figure 4.5, it can be expected that the cross-track trajectory spread increases. However, the PDOP increase in runs `15_run1` and `16_run1` is only marginal compared to `15_run3`. This leads to think that the GNSS position updates with increased PDOP values observed for `15_run3`, could have a profound effect on the increase of the cross-track trajectory spread (Figure 4.2a). A good method to check the effect of the GNSS position updates on the trajectory solution, is to inactivate the raw measurements and reprocess the trajectory. If the trajectory spread where to decrease after the inactivation of the GNSS position updates with high PDOP of `15_run3`, one could state that the GNSS position updates lead to decreased accuracy of the integrated trajectory solution. This leads to the following hypothesis:

Hypothesis
By removing the GNSS observations for `15_run3` at the case study track segment, therefore forcing the processing software to rely on IMU measurements for the position updates, the cross-track trajectory spread can be decreased.

[4]page 113 on: Estimated Standard Deviation

4.3. Analysis

In order to test the hypothesis, the GNSS observations are inactivated for the trajectory segment where the high PDOP values for `15_run3` are observed. It is decided not to include the (bordering) GNSS epochs where the NS= 0 at kilometres 54.72 and 54.86. The complete loss of satellite signals might have a different cause and is therefore better to remove from this analysis. Furthermore, the GNSS epochs are inactivated up to the point where the PDOP values for `15_run3` are excellent ($PDOP < 2$). In Table 4.2, the alterations to the raw GNSS observations used for re-processing 1 (RP1) of the trajectory solution in IE are presented.

Table 4.2: RP1: GNSS epoch inactivation for the reprocessing of the trajectory of the case study

Run	Metric	Unit	Start	End	Delta
`15_run3`	GNSS Time	s	126950	127018	69
	Kilometre along axis	km	54.95	56.28	1.33

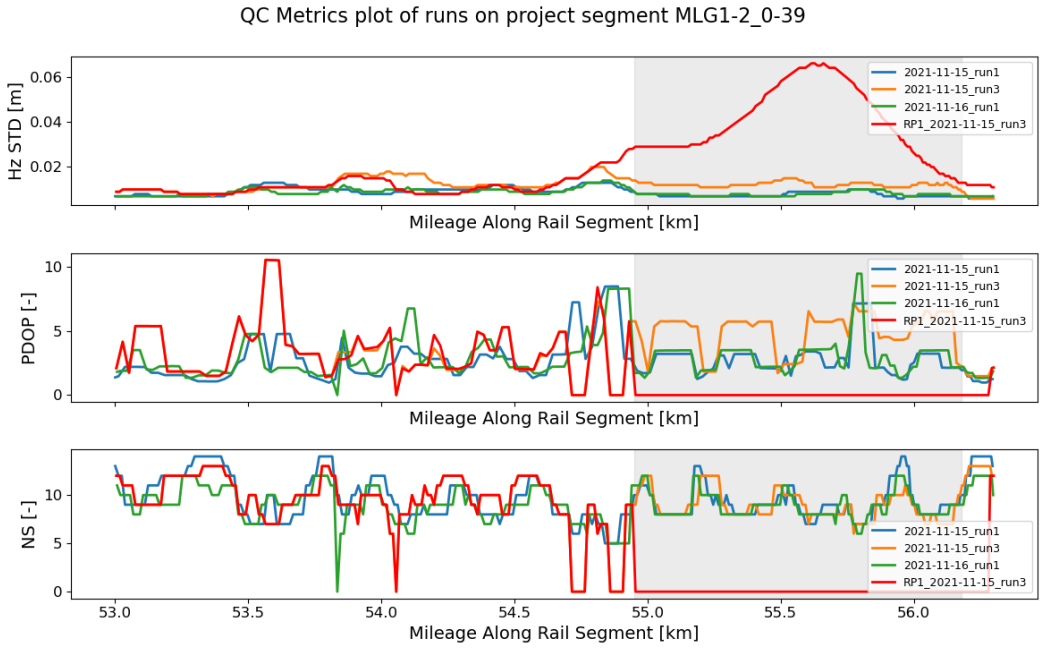

Figure 4.6: Quality Control metrics (IE output) for the SBET case study track segment, including the QC-metrics of the reprocessed trajectory solution (red) and the interval at which the raw GNSS epochs are adjusted highlighted in grey

The effect of the reprocessed trajectory solution on the quality metrics can be found in Figure 4.6, where the reprocessed trajectory, `RP1_15_run3`, is presented in red. The interval where the raw GNSS data is modified is highlighted in grey. From Figure 4.6, a few observations can be made. First of all, obviously, the NS (and PDOP) statistic goes to 0 for `RP1_15_run3`. This forces the IE software to rely on IMU-derived position updates for the reprocessed trajectory in the grey interval. As the position error of these IMU position updates is cumulative over time, so is its effect on the accuracy of the trajectory solution. This effect can be observed as the increase in the estimated position error in Figure 4.6. As the trajectory solution is forwards- and backwards-processed, it is expected that the peak of the increase in the estimated position error can be found approximately halfway through the modified trajectory interval.

4.4. Validation

To check if potential results obtained in the case study analysis can be reproduced, a validation strategy is constructed. In order for the results to be considered validated, similar levels of accuracy gains, indicated by decreased cross-track trajectory spread, must be able to be obtained when GNSS position updates with high PDOP values are inactivated. Furthermore, similar results must be achieved when high PDOP GNSS position updates are observed and inactivated for different runs than `15_run3`. Finally, an increased accuracy should be realised when high PDOP GNSS position updates are inactivated for multiple runs at the same time. The validation requirements only apply to track segments compliant with the case study track segment requirements (sufficient NS, no standstill). Three Validation Cases (VC), along different track segments of the survey `MLG1-2_0-39`, have been developed.

VC1: High PDOP, 1 run inactivated

In validation case 1, along a 1.2-kilometre tack segment between km 59.6 and 60.8, multiple intervals are observed where the PDOP values are significantly higher than the other runs. Similar to the case study analysis, the run for which this is observed is `15_run3`. However, for the validation case, the intervals are shorter and more widely spread along the track segment. Therefore, GNSS positioning updates have been inactivated for three distinct intervals, presented in Table 4.3.

Table 4.3: VC1: GNSS epoch inactivation for the reprocessing of the trajectory of the validation case

Interval	Run	Metric	Unit	Start	End	Delta
1	`15_run3`	GNSS Time	s	127382	127399	17
		Kilometre along axis	km	59.80	60.11	0.31
2	`15_run3`	GNSS Time	s	127414	127418	4
		Kilometre along axis	km	60.35	60.40	0.05
3	`15_run3`	GNSS Time	s	127435	127453	18
		Kilometre along axis	km	60.60	60.74	0.14

VC2: High PDOP, 2 runs inactivated

In the second validation case, a situation is identified where two runs have significantly higher PDOP values compared to the other run in the analysis. Reprocessing the trajectories of two runs at the same location leaves only one run in the original position. This could lead to an increased, or reduced effect in the change of the cross-track trajectory spread. A short, c. 70 [m] interval is identified for this analysis at kilometre 40.8. The GNSS inactivation settings are presented in Table 4.4.

Table 4.4: VC2: GNSS epoch inactivation for the reprocessing of the trajectory of the validation case

Run	Metric	Unit	Start	End	Delta
`15_run1`	GNSS Time	s	111316	111320	4
	Kilometre along axis	km	40.78	40.83	0.31
`16_run1`	GNSS Time	s	197668	197675	7
	Kilometre along axis	km	40.77	40.86	0.05

VC3: High PDOP around zero NS

In the analysis performed on the case study, it has been explicitly decided not to include the GNSS epochs at and surrounding a track segment where the NS statistic. This is because there is no use inactivating the GNSS position updates where NS is already zero. However, at the epochs surrounding the interval with NS= 0, high PDOP values are observed with NS> 0. In the case study, these epochs have also been omitted as the effect of these very short high PDOP intervals on the cross-track trajectory spread was expected to be limited. In order to confirm if that expectation was correct, the third validation case identifies a track segment where this situation occurs. Along the track segment at 20.5 to 23.5 [km], there are three instances where NS= 0. After the GNSS signals are re-acquired, for a few epochs, the PDOP values for `15_run3` are significantly higher. This can be seen in Figure 4.7.

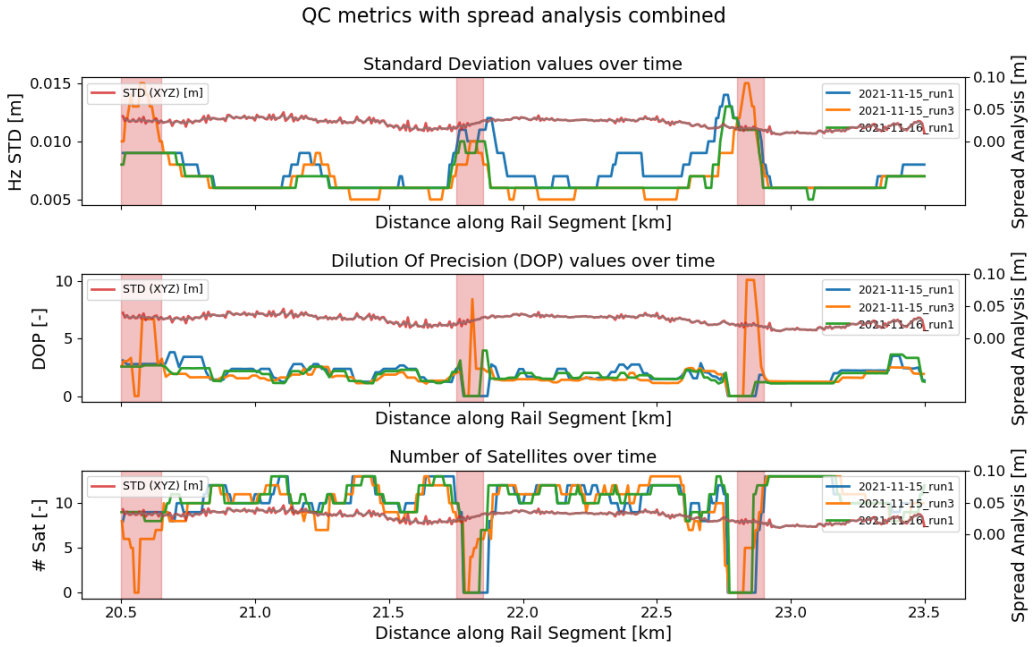

Figure 4.7: VC3: QC metrics and cross-track trajectory spread along the track segment

However, as can be seen from the standard deviation of the cross-track trajectory spread, also plotted in Figure 4.7, no significant spike can be observed in the trajectory accuracy metric. Therefore, it can be concluded that the spikes in PDOP values before and after short intervals with NS= 0 do not have a deteriorating effect cross-track trajectory spread and therefore on the trajectory accuracy. This in turn, confirms the expectation made in the case study analysis and proves that GNSS epochs with high PDOP 'spikes' surrounding short NS= 0 intervals can be ignored. It is likely that the Inertial Explorer is able to mitigate the effects of the short PDOP spikes on the integrated trajectory solution.

4.5. Results

4.5.1. Case Study Results

Recomputing the trajectory accuracy metrics for the case study trajectory using the reprocessed trajectory `RP1_15_run3`, allows for an analysis of the impact on the cross-track trajectory spread. The results for the standard deviation and smallest circle analysis are presented in Figure 4.8. First of all, a

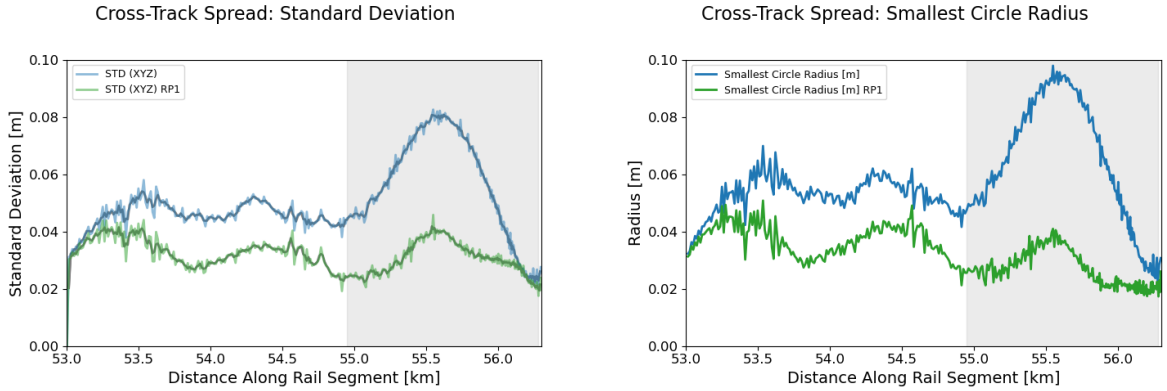

(a) RP1: cross-track standard deviation analysis

(b) RP1: smallest circle analysis

Figure 4.8: RP1: results on the trajectory accuracy metrics of the reprocessed trajectory solution

decrease of approximately 50% can be observed in the standard deviation of the cross-track trajectory spread and the radius of the smallest enclosing circle at the reprocessed trajectory interval. When comparing the (ECEF) coordinates of the original and reprocessed trajectories of `run3` at the peak of the cross-track trajectory spread (GNSSTime = 126973 [s]), the total, absolute position change can be computed. This results are presented in Table 4.5.

Table 4.5: Comparison of (re)processed trajectory coordinates for `15_run3` at GNSS epoch 126976 [s]

Value	Unit	15_run3	RP1_15_run3	Delta (abs)
X (ECEF)	m	3481064.570	3481064.664	0.094
Y (ECEF)	m	-317512.082	-317512.100	0.018
Z (ECEF)	m	5317167.609	5317167.682	0.073
Position Change	**m**			**0.120**

The magnitude of the absolute position shift, 12.04 [cm], is an order of magnitude larger than the maximum linear interpolation error (2 [cm], section 3.3) that could have been introduced in the trajectory accuracy analysis. Furthermore, the position change is an order of magnitude larger than the potential error introduced by the variance in the random position of the measurement system w.r.t. the track centre line, as a result of train suspension movement (1 [cm], section 3.4). This excludes the possibility that the increase in trajectory accuracy is caused by the introduced linear interpolation error or random variations in the position of the RTSS w.r.t. the railway track.

A second important observation from Figure 4.8, is that the trajectory accuracy computed using the reprocessed trajectory is also affected outside of the modified GNSS interval. As the SBET trajectory solutions are used in the comparison, it is likely that the LC IMU measurement integration also impacts the position of the trajectory outside of the modified GNSS interval. To analyse if this is true, the cross-track trajectory spread using the original and reprocessed trajectory for the GNSS-only trajectory solution are plotted in Figure 4.9.

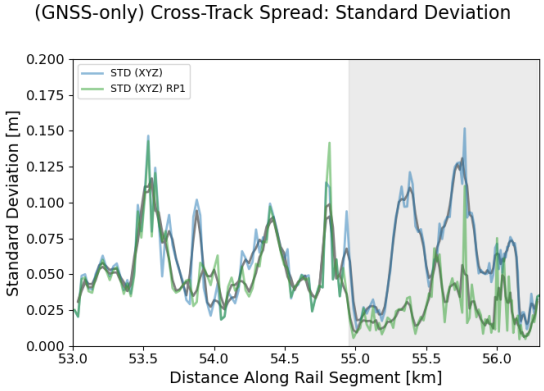

Figure 4.9: RP1: cross-track standard deviation of the GNSS-only trajectory solution

From Figure 4.9, the difference in the GNSS-only cross-track trajectory spread including `15_run3` or `RP1_15_run3` along the inactivated GNSS positioning update interval is clear. Furthermore, with differences in standard deviation in the 10 [cm] range, the accuracy increase can be attributed to the different positions of the reprocessed trajectory. From this, it can also be concluded that the error of the GNSS only trajectory solution, therefore the high PDOP GNSS position updates, is in the order of 10 [cm]. Outside of the inactivated GNSS interval, there are also differences in the standard deviation of the cross-track trajectory spread to be observed. These differences are mostly in the 2 [cm] range, similar to the order of magnitude of the linear interpolation error, 2 [cm] (see section 3.3). The discrepancies between the original and reprocessed accuracy metrics in Figure 4.9, are therefore likely caused by linear interpolation errors. Therefore, it can be assumed that the difference in trajectory accuracy metrics of the original and reprocessed integrated GNSS/IMU trajectory solutions observed

outside of the modified GNSS interval (Figure 4.8), is caused by the integration of GNSS and IMU measurements. This proves that epochs with high PDOP values have a more widespread negative effect on trajectory accuracy than just the interval at which they are observed.

4.5.2. VC 1: High PDOP, 1 run inactivated - Results

The results of reprocessing the trajectory using the manipulated raw GNSS observations input file on the trajectory accuracy metrics are presented in Figure 4.10. For context on the validation case, such as SBET QC metrics and a situational overview, please refer to Appendix D. Due to the inactivation of the GNSS epochs with high PDOP values, a significant decrease in both the standard deviation cross-track trajectory spread as the smallest circle radius can be observed in the metrics using the reprocessed trajectory solution (Figure 4.10). The increase in the trajectory accuracy metrics in the original analysis is nearly completely eliminated in the accuracy metrics for the reprocessed trajectory.

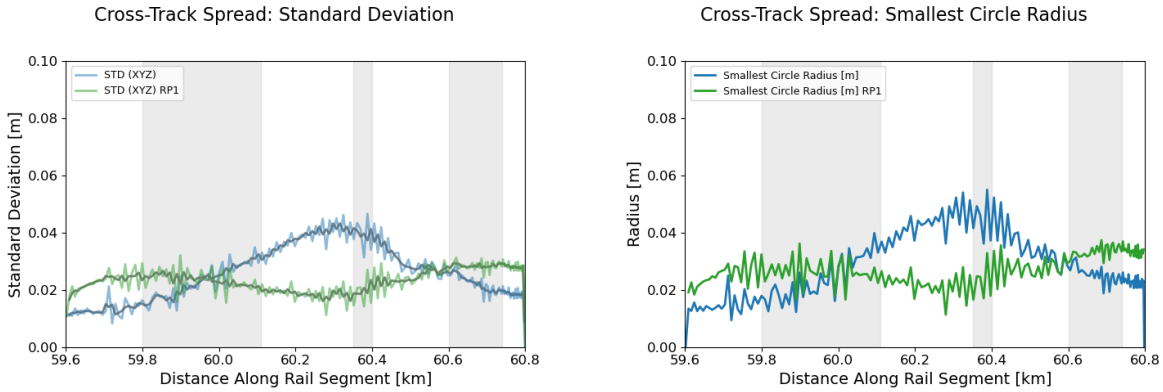

(a) VC1: cross-track standard deviation analysis

(b) VC1: smallest circle analysis

Figure 4.10: VC1: results on the trajectory accuracy metrics of the reprocessed trajectory solution for the validation case

4.5.3. VC 2: High PDOP, 2 runs inactivated - Results

The results of reprocessing the trajectory using the manipulated raw GNSS observations input file on the trajectory accuracy metrics are presented in Figure 4.11. Although an improvement in trajectory accuracy can be observed from Figure 4.11, it is significantly smaller than the accuracy gains observed in the case study and VC1. Two potential causes for this observation have been identified. First of

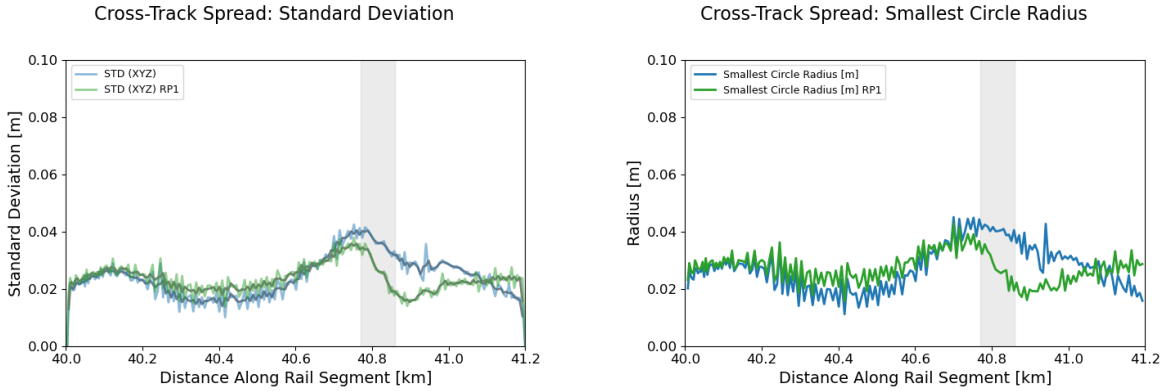

(a) VC2: cross-track standard deviation analysis

(b) VC2: smallest circle analysis

Figure 4.11: VC2: results on the trajectory accuracy metrics of the reprocessed trajectory solution for the validation case

all, as the trajectories of two runs are reprocessed, two trajectories have different locations. Therefore, as indicated in section 4.4, the effect on the cross-track trajectory spread might not be as profound as

when the trajectory of one run is reprocessed. A more likely explanation is the short duration of the GNSS interval at which the GNSS observations are inactivated. This is significantly shorter than for the case study and VC1. Therefore, the negative effect of the GNSS position updates with high PDOP values are likely limited compared to situations where longer high-PDOP intervals are observed.

4.6. Conclusions

Inactivating GNSS epochs of a run with significantly higher PDOP values compared to other runs at the same location does decrease the absolute cross-track trajectory spread of the SBET trajectory solutions. Forcing the trajectory processing software to rely on IMU measurements provides, provided that the inactivated interval is not too long, a more accurate trajectory compared to a trajectory with GNSS position updates with high PDOP values. High PDOP values are defined as PDOP>5, or moderate according to Table 3.2. This confirms the hypothesis posed in section 4.2. Furthermore:

- Accuracy (trajectory precision) gains of up to 50% can be obtained along track segments where sustained periods of high PDOP (>5) values are observed.
- The accuracy gain is significantly higher than the accuracy error that can be expected from the interpolation error and random position variation of the measurement system w.r.t. the track.
- The negative effect of GNSS position updates with high PDOP (>5) values on the trajectory accuracy is noticeable in the integrated SBET trajectory estimate outside of the GNSS interval at which the high PDOP (>5) values are observed.
- Short spikes ($1-2$ [s]) in PDOP values after a complete signal loss do not cause a significant increase in the cross-track trajectory spread and are likely handled well by Inertial Explorer.

From the conclusions of the case study analysis, it is likely that the amount of accuracy gain is dependent on the length of the interval at which the original trajectory is affected by high PDOP GNSS epochs. This would make sense as it can be expected that the impact of a short interval of inaccurate GNSS position updates on the trajectory solution is less than that of a long interval. It must be noted that the conclusions constitute no direct proof of improvement of the accuracy of the trajectory solution, but rather of improvement of the trajectory precision. However, under the assumption that the measurements of the individual runs are unbiased, it does provide proof that the accuracy of the trajectory solution has increased. In the absence of a ground-truth trajectory, trajectory precision is the best alternative for a measure of trajectory accuracy. However, as indicated by the note in section 4.1, the analysis was intended to performed on the TCL trajectory and a larger dataset (6 runs). Increasing the sample size (number of runs), increases the confidence that can be put in the conclusions found in this report as a larger sample size limits the effect of systematic errors in the individual runs.

However, following the case study performed in section 4.3, there are a few questions that remain. Understanding and answering these questions would provide a better insight into the problem, its root causes and its implications. Up until now, it is not clear exactly why the PDOP values of `15_run3` are approximately twice as high as the other runs. Hence, the first question:

Q1 Why are the PDOP values of `15_run3` so much higher than runs `15_run1` and `16_run1`, when they all use a similar number of satellites for the GNSS position update?

In the case study analysis, trajectory accuracy improvement has been established when deactivating the GNSS position updates for only one of the runs. It is important to further investigate if similar accuracy gains can be achieved for all runs and a larger dataset. Furthermore, it might be worth exploring the possibilities of processing with PDOP thresholds, above which the GNSS position updates are inactivated. Hence, questions 2 and 3:

Q2 Does the current 3-run dataset have a sufficiently large sample size and can comparable accuracy gains to the case study be obtained, when the sample size of runs is increased?

Q3 What is the effect on the accuracy of the trajectory solution of processing the entire trajectory solution using strict constraints for the PDOP thresholds?

In the following chapters, chapter 5 and chapter 6, the questions will be extensively discussed along with methods to find relevant answers. Furthermore, results of the research performed will be presented.

This page was intentionally left blank.

5

Results: Position Dilution of Precision Scrutinization

One of the questions that remained after the case study performed in chapter 4, is what could have caused the significant increase in PDOP values for one of the runs compared to the other. More specifically, what explains the increased PDOP values of `15_run3` (PDOP $\approx$ 5.4) compared to runs `15_run1` and `16_run1` (PDOP $\approx$ 3.2), given the fact that the observations are made at the same distance along the track, using a similar number of satellite observations. In order to answer that question, the PDOP values of the different runs at the same railway track location will be analysed. This railway track location will be designated as the *critical epoch*. The critical epoch, defined by the red vertical line in Figure 4.5, is the first epoch in the case study track segment where the PDOP values for all runs increase, and for `15_run3` are found to be significantly higher than the other runs in the analysis. In Table 5.1, an overview of the quality statistics is given for the critical epochs of all runs.

Table 5.1: Trajectory statistics at the critical epoch of the runs in `MLG1-2_0-39` (ΔPDOP = PDOP$_i$ - PDOP$_{i-1}$)

Critical Epoch Value	Unit	`15_run1`	`15_run3`	`16_run1`
GPSTime	s	112014	126953	198371
Mileage	km	55.03	55.02	55.03
ΔPDOP at epoch	-	1.44	3.52	1.58
NS	8	9	8	

Where normally, the PDOP is directly computed from the observed satellite geometry, it could be the case that the derivation of the PDOP in Inertial Explorer is not as direct. As Inertial Explorer performs many edits, weighting algorithms and smoothing to the dataset, potentially, the PDOP is computed using a more complex algorithm. For example, from Table 5.1, it would be expected that the satellite with the highest NS, has the lowest PDOP. However, this is not the case. In this chapter, four theories that could provide a potential explanation for the PDOP increase of `15_run3` will be explored. First of all, the time of data acquisition of the RILA system is analysed in section 5.1. Secondly, the skyplots of the raw GNSS observations at the critical epochs will be analysed in section 5.2, followed by a manual (re)computation of the PDOP values in section 5.3. In section 5.4, a thorough analysis of the precise GNSS ephemeris files is performed. The chapter is concluded with a summary of the conclusions found throughout the chapter in section 5.5.

5.1. Data Acquisition Time

Dilution Of Precision (DOP) metrics are a function of the observable satellite constellation and the position of the receiver alone (Driver 2007). When the position of the receiver is fixed, changes in the satellite geometry will therefore also imply changes in the observed DOP. Furthermore, as GNSS satellites are in orbit at c. 20,000 [km] altitude with an orbital period of c. 12 [h], the constellation

approximately repeats itself every 12 hours (Petrovski 2014). This means that, w.r.t. a fixed receiver, different values for the DOP can be obtained at different times during the day. In order to quantify the effect of the data acquisition time on the PDOP values observed by the RTSS system, the data acquisition times and PDOP values are analysed at the critical epoch. The results are presented in Table 5.2.

Table 5.2: Time stamps of the data acquisition of the different RILA runs for survey scope `MLG1-2_0-39`

Metric	Unit	`15_run1`	`15_run3`	`16_run1`
Date	-	15 Nov 2021	15 Nov 2021	16 Nov 2021
GPS Week	-	2184	2184	2184
GPSTime Run Start	s	108263	123112	194631
GPSTime @ crit. epoch	s	112014	126953	198371
UTC Time Run Start	hh:mm:ss	06:04:05	10:11:34	06:03:33
UTC Time @ crit. epoch	hh:mm:ss	07:05:53	11:15:35	07:06:36
PDOP	-	3.21	5.35	3.45
NS	-	8	9	8
Δt to `15_run3`	hh:mm	00:00	04:10	24:01

From Table 5.2, it can be observed that time difference between `15_run1` and `16_run1` is 24 hours and 1 minute. This means that the constellation at the critical epochs of these runs is nearly the same. As expected, the observed PDOP values for `15_run1` and `16_run1` are approximately the same. The relative (12-hour cycle) time difference between `15_run3` and `15_run1`, is 4 hours, leading to a significantly different GNSS constellation. Hence, the following hypothesis can be formed:

Hypothesis
The increased PDOP values of the GNSS observations for `15_run3` in the track segment between km 55 and 56,3 could be caused by the significant difference in constellation geometry, due to the difference in data acquisition point in time of the runs (+4 hours).

Analysis

Not only is the PDOP related to the position of the satellite constellation but also the amount of GNSS observations impacts the satellite geometry and PDOP value. In general, the higher the number of satellite observations, the lower the DOP statistic (Hofmann-Wellenhof et al. 2008). When looking at the NS statistic in Table 5.2, a higher number of satellites is used for `15_run3` (NS = 9) compared to the other runs (NS = 8). Therefore, a lower PDOP value would have been expected.

In general, having 8 or 9 satellite observations leads to high-quality PDOP values. Research shows that 7 to 9 satellite observations, from any GNSS constellation, lead to average PDOP values in the $1.5 < PDOP < 2.5$ range[1] (Pan et al. 2020) (Fang et al. 2021). Therefore PDOP values of > 5 are not expected when 9 satellite observations are used in its computation.

Conclusion

The small relative time difference (1 [min]) between the different runs passing the critical epoch in the case study track segment does explain why similar PDOP values are observed for `15_run1` and `16_run1`. As the time at which `15_run3` passes the critical epoch is significantly different, it can be expected that the satellite geometry, and therefore PDOP value, is different.

However, due to the sufficient, and increased number of satellite observations at the critical epoch of `15_run3` (compared to the other runs), it is not obvious why the PDOP value is much worse (PDOP> 5). In order to find out, a more thorough analysis of the satellite constellation is needed. More detailed information on the satellite geometry observed by the receiver could be obtained by looking at the receiver *skyplots*.

[1] Apart from extreme latitudes

5.2. Skyplot Analysis

In order to gain a better understanding of the satellite geometry, one could look at the receiver *skyplots*. A skyplot is a graphical representation of the azimuth and elevation of all satellites observed by the receiver at a certain time instance (Shen et al. 2019). By comparing the satellite geometries at the critical epochs of the different runs, an indication can be obtained of the PDOP values. As explained in section 3.4, if satellites are more spread-out - i.e. at lower elevation angles distributed across the horizon - the geometry will be better and the PDOP value lower. With this in mind, the following hypothesis can be constructed:

Hypothesis
The increased PDOP values of the GNSS observations for `15_run3` in the track segment between km 55 and 56,3 could be caused by poorly situated satellites (unlucky geometry).

Analysis

To find out if the hypothesis is true, the skyplots of the receiver at the critical epochs of `15_run1` and `15_run3` are compared at the critical epoch, and the epoch prior. These skyplots can be found in Figure 5.1. The green- and red colours of the skyplots, Figure 5.1a and Figure 5.1a respectively, correspond to the green- and red line in the QC metrics plotted in Figure 4.5.

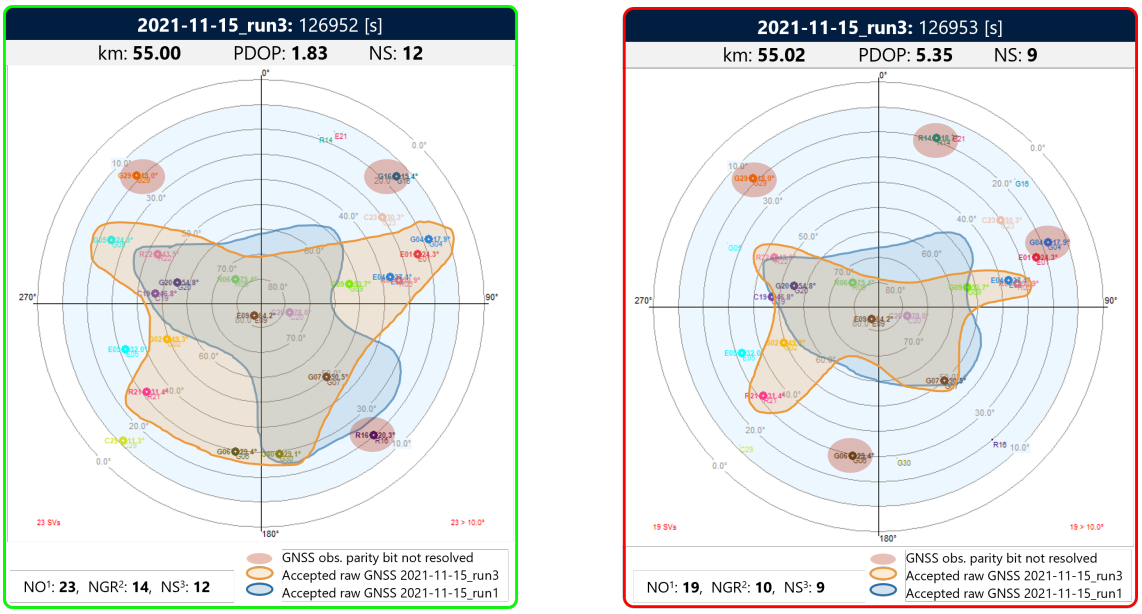

(a) Skyplot analysis at epoch prior to the critical epoch

(b) Skyplot analysis at the critical epoch

Figure 5.1: Skyplot analysis of `15_run3` & `15_run1`

In Figure 5.1, the areas enclosing the satellite geometry for `15_run3` and `15_run1` are presented in orange and blue respectively. The number of satellite observation statistics given in Figure 5.1 are for `15_run3` only. First of all, from Figure 5.1, it can be observed that the number of satellite observations decreases for both `15_run1` (blue) and `15_run1` (orange). As can be expected from Figure 4.5, most satellites are lost at lower elevation angles in the south (180°) to east (90°) area. In this azimuth range ($90° - 180°$), the (dense) vegetation is located which is causing the obstruction for the GNSS signals. With the loss of satellite signals, the area enclosing the satellite geometry becomes smaller for both runs at the critical epoch. This is the direct cause of the PDOP increase experienced for both runs at the critical epoch.

[1]NO: Number of GNSS Observations
[2]NGR: Number of GPS + Glonass observations (used in trajectory processing), with resolved parity bit solution
[3]NS: Number of Satellites used in the trajectory processing

The second observation that can be made from Figure 5.1, is that the total number of satellite observations (NO) is much higher than the number of satellites used in the trajectory solution (NS). First and foremost, this is because the skyplots show the GNSS observations for the G4[2] constellation. However, the trajectory is processed using only the GPS and GLONASS observations (G2), as explained in Table 3.1. Therefore, the Galileo and Beidou observations are discarded. However, when counting the GPS and GLONASS observations, the sum still exceeds NS. This is because a satellite observation can be rejected at multiple stages during trajectory acquisition and processing.

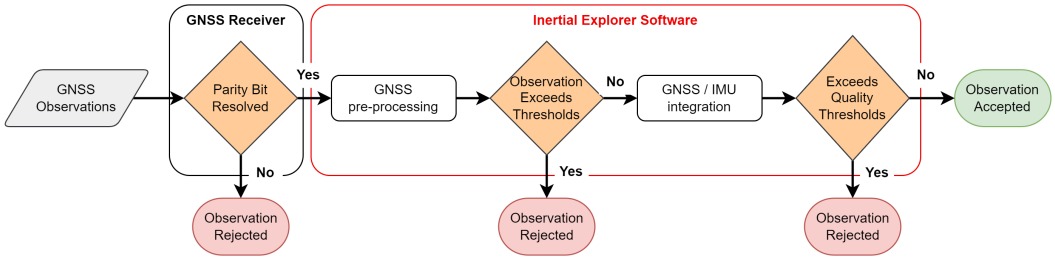

Figure 5.2: Different stages of GNSS observation rejection in the trajectory processing flow

In Figure 5.2, the three stages at which a GNSS observation can be rejected is presented in a flow chart. First of all, an observation can be rejected at the receiver if the parity bit check, performed for signal robustness and reliability, cannot be resolved (Anghileri et al. 2013). Secondly, if the quality metrics of a GNSS observation exceed the GNSS pre-processing thresholds, the observation is rejected by Inertial Explorer. Finally, if the quality metrics of the positioning solution of a certain GNSS epoch exceed the GNSS / IMU (LC) integration thresholds, the GNSS observations can be rejected. The rejections at the receiver level are indicated with a red circle in Figure 5.1, however, the GNSS observations that are rejected during the actual processing of the trajectory (in the red box in Figure 5.2) are not present in the skyplot.

The third important observation that can be made from Figure 5.1 is that the geometry of the accepted satellite observations is more favourable - more satellite observations at lower elevation angles - for `15_run3` at the critical epoch. Therefore, it is not expected that the PDOP value at the critical epoch for `15_run3` indicates an inferior geometry. For further analysis, a count of the raw GNSS measurements is presented Table 5.3.

Table 5.3: Overview of satellite observations at the critical epochs for the skyplot analysis

Metric	**Unit**	`15_run1`	`15_run3`
GPSTime	s	108263	123112
Mileage	km	55.033	55.025
PDOP	-	3.21	5.35
Total Raw Sat Obs.	-	19	19
Total G[3]+ R[4]Obs	-	11	15
Total G + R Obs. with PBR[5]	-	8	10
Total G + R Obs. used in traj. solution	-	8	9
Software Satellite Rejections	-	0	1

[2]G4: GPS + GLONASS + Galileo + Beidou
[3]G: GPS observation
[4]R: GLONASS observation
[5]PBR: Parity Bit check Resolved

From Table 5.3, it becomes clear that at the critical epoch of `15_run3`, a satellite observation is rejected by the processing software. As this observation rejection is not excluded in the skyplot, it could be that the geometry of `15_run3` is worse than `15_run1` when removing the rejected satellite from the constellation. Unfortunately, Inertial Explorer does not provide logs or records on what GNSS observations are rejected and why, making it difficult to perform the analysis.

Conclusion

When looking at the skyplots of the different runs at the critical epoch, a loss of GNSS signals compared to the previous epoch can be observed. As the 'lost' signals are at lower elevation angles, it has a negative impact on the satellite geometry an therefore, explains the increase in PDOP values that can be observed for all runs. However, from the skyplot analysis, it seems that the satellite geometry for `15_run3` at the critical epoch is better than the other runs in the analysis, contrary to what is expected from the higher PDOP values observed for this run.

It is found that one of the satellite observations is rejected by the processing software for `15_run3` at the critical epoch. This potentially has a negative effect on the satellite geometry for `15_run3`. However, no information is present on what satellite is rejected (and why). Therefore, rejecting each satellite at a time, to see if the PDOP values for the `15_run3` at the critical epoch can be reproduced, could provide a solution.

5.3. PDOP Reconstruction

The PDOP is a direct function of the position of the ephemeris of the observed GNSS satellites and the location of the receiver. Records of the Ephemerides of all GNSS satellites are constructed, published and kept by the International GNSS Service (IGS)[6]. These ephemeris files are publicly available. Furthermore, the position of the receiver along the trajectory is known. This information allows for the recomputation of the PDOP observed by the RTSS receiver at the critical epoch. If the PDOP value computed by the IE software can be recreated manually, a sensitivity analysis on the rejected satellite can be performed to identify the rejected satellite observation (see section 5.2). If the rejected satellite can be identified, it would provide an explanation as to why the PDOP values for `15_run3` are high compared to the other runs. With this information, the following hypothesis can be formed for a manual PDOP analysis.

Hypothesis
The increased PDOP values of the GNSS observations for `15_run3` in the track segment between km 55 and 56,3 could be caused by the rejection of a satellite observation by Inertial Explorer.

Analysis

To compute the PDOP, equations and definitions as presented by Langley et al. (2017) and Chen (2015) are used. First of all, the design matrix $\mathbf{A}$ for the satellite observations is constructed in Equation 5.1.

$$\mathbf{A} = \begin{bmatrix} \frac{x_0 - x^1}{\rho} & \frac{y_0 - y^1}{\rho} & \frac{z_0 - z^1}{\rho} & 1 \\ \frac{x_0 - x^2}{\rho} & \frac{y_0 - y^2}{\rho} & \frac{z_0 - z^2}{\rho} & 1 \\ \frac{x_0 - x^3}{\rho} & \frac{y_0 - y^3}{\rho} & \frac{z_0 - z^3}{\rho} & 1 \\ \vdots & \vdots & \vdots & \vdots \\ \frac{x_0 - x^m}{\rho} & \frac{y_0 - y^m}{\rho} & \frac{z_0 - z^m}{\rho} & 1 \end{bmatrix} \tag{5.1}$$

In Equation 5.1, the $(x_0,\ y_0,\ z_0)$ represent the coordinates of the receiver, $(x^i,\ y^i,\ z^i)$ represent the coordinates of GNSS satellite i and pseudo-distance ρ is given by equation Equation 5.2.

$$\rho = \sqrt{(x_0 - x^1)^2 + (y_0 - y^1)^2 + (z_0 - z^1)^2} \tag{5.2}$$

[6] `https://igs.org/`

The next step is to compute the covariance matrix **Q** from the design matrix (**A**) and weighting matrix **W** using Equation 5.3.

$$\mathbf{Q} = \left(\mathbf{A}^T\mathbf{W}\mathbf{A}\right)^{-1} \tag{5.3}$$

The weighting matrix (**W**) contains a weighting scheme to account for the differences in variances of each measurement. Variation in variances can occur because, for example, multiple satellite constellations are used in the position determination (Chen 2015). However, due to environmental effects and other error sources, it can be that the variance of a single observation deviates from the others. The weighing matrix, computed by the receiver and/or trajectory processing software, assigns less weight to the measurement with greater variance. As the weighting matrix used in the PDOP computation is unknown (and untraceable), the weighting matrix is assumed to be the identity matrix (**I**). This assumption is widely used in DOP computations (Langley et al. 2017). Therefore, the covariance matrix can be computed using Equation 5.4.

$$\mathbf{Q} = \left(\mathbf{A}^T\mathbf{A}\right)^{-1} = \begin{bmatrix} \sigma_{xz}^2 & \sigma_{xy} & \sigma_{xzz} & \sigma_{xt} \\ \sigma_{xy} & \sigma_{yy}^2 & \sigma_{yz} & \sigma_{yt} \\ \sigma_{xz} & \sigma_{yz} & \sigma_{z}^2 & \sigma_{zt} \\ \sigma_{xt} & \sigma_{yt} & \sigma_{zt} & \sigma_{t}^2 \end{bmatrix} \tag{5.4}$$

In Equation 5.4, σ_{ab} represents the variance of a measurement mapped to its respective (a, b) coordinate. Finally, the PDOP can be computed using the relation in Equation 5.5.

$$\text{PDOP} = \sqrt{\sigma_{xx}^2 + \sigma_{yy}^2 + \sigma_{zz}^2} \tag{5.5}$$

The results of manually recomputing the PDOP at the critical epoch of `15_run3` are presented in Table 5.4. Furthermore, a sensitivity analysis is included where, in turn, a single satellite observation is excluded from the design matrix. Also, a sensitivity analysis is performed on the inactivation of an entire satellite constellation.

Table 5.4: Results of the manual PDOP computation analysis at the critical epoch of `15_run3`

Sat in Analysis: G02, G07, G09, G20, R05, R06, R07, R15, R21, R22					
Critical Epoch Metrics			Sensitivity Analysis		
Metric	**Value**	**Unit**	**Excluded Sat.**	**Computed PDOP**	**NS**
GPSTime	126953	s	G02	2.56	9
Mileage	55.025	km	G07	2.75	9
Δt to nearest ephemeris	58	s	G09	2.52	9
NR of Sats (NS)	10	-	G20	2.58	9
PDOP Observed	5.35	-	R05	2.76	9
PDOP Computed	2.48	-	R06	3.04	9
ΔPDOP	2.87	-	R07	2.56	9
GLONASS PDOP	57.69	-	R15	2.74	9
GPS PDOP	3.18	-	R21	2.55	9
			R22	2.96	9

From Table 5.4, a couple of observations can be made. First of all, manually computing the PDOP with all 10 GNSS observations, yields a value of PDOP= 2.48. A lower value compared to the PDOP generated by the IE processing software (PDOP= 5.35) can be expected, as no satellites are rejected and therefore, an extra satellite observation is present (see Table 5.3). However, when performing the sensitivity analysis - where all 10 satellites are alternately 'rejected' - no computed PDOP value is of the same order of magnitude as the observed PDOP= 5.35. Rejecting satellite `R06`, yields the largest PDOP value, PDOP= 3.04, at 56% of the observed value. When computing the PDOP for another epoch, for example, the critical epoch of `15_run1`, the results (PDOP= 5.17) also do not match the PDOP values of Inertial Explorer (PDOP= 3.21). For a full table of the results at the critical epoch of `15_run1`, please refer to Appendix D. It is important to note, that all ephemerides files published by the IGS, are sampled at 15-minute intervals. This means that a discrepancy can exist between the constellation observed by the receiver at a certain epoch and the constellation that can be retrieved

using the ephemeris files. At the critical epoch of `15_run3`, the time discrepancy to the closes ephemeris update is 58 [s]. It can be assumed that the change in the GNSS satellite constellation (with altitude c. 20,000 [km]), observed by the receiver, is negligible for PDOP computation.

As per Equation 5.3, the different GNSS observations can be assigned different weights, to prioritise their relevance in the GNSS positioning solution. These weights can be assigned at the receiver, to provide an initial positioning solution and PDOP value, but can also be assigned by Inertial Explorer. It is likely that the Inertial Explorer software implements a (proprietary) weight matrix to, for example, eliminate discrepancies in the variance between the measurements of different GNSS constellations and improve the GNSS positioning solution. The discrepancies between the manually computed PDOP and the PDOP value provided by the software are therefore likely caused by the simplification of the weight matrix to the identity matrix ($\mathbf{W} = \mathbf{I}$). The weight matrix used by the software cannot be traced, and estimating its contents is very ambiguous.

Conclusion

From the manual PDOP sensitivity analysis, of which the results are presented in Table 5.4, it cannot be determined which satellite is rejected at the critical epoch of `15_run3`. Furthermore, from the manual PDOP analysis, much lower PDOP values have been obtained than those provided by the Inertial Explorer software, in all cases. In validation cases, it was also not possible to recreate the IE-generated PDOP values by means of manual computations. The discrepancies between the software-generated, and manual PDOP values is likely due to the simplification of the weight matrix ($\mathbf{W} = \mathbf{I}$) in the manual computation. Therefore, the reconstruction of the PDOP computation at the critical epoch cannot provide a decisive answer to the hypothesis posed at the beginning of this sector. Further analysis of the raw GNSS observations within Inertial Explorer could provide more insights.

5.4. GLONASS Precise Ephemerides

When looking into the raw GNSS observations using the Inertial Explorer *GPBViewer*[7], a discrepancy can be found. In Figure 5.3, the raw GLONASS observations at the critical epoch are presented.

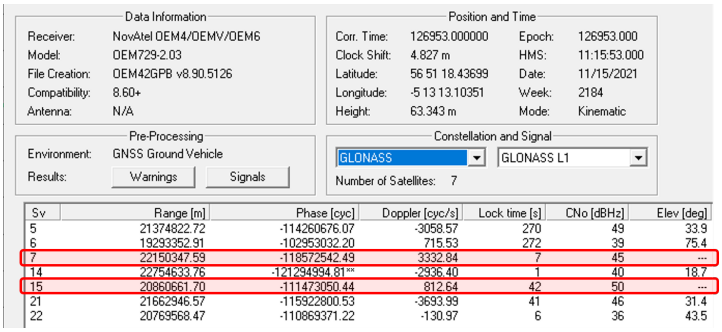

Figure 5.3: Analysis of the Raw GLONASS measurements at the critical epoch of `15_run3`

Furthermore, in Figure 5.3, the satellite observations of *R07* and *R15* have no data for the satellite elevation statistic. Counting the GPS (G) + GLONASS (R) raw observations, a total of 15 GNSS measurements is present. When deducting the non-contributing *G30* observation, and the observations rejected at the receiver[8] (indicated with **), a total of 10 observations is present at the critical epoch. This corresponds to the observations from section 5.2. This means that the observations of which the elevation statistic is missing, *R07* and *R15*, are used in the GNSS positioning solution. The elevation data of a satellite originates from the satellite broadcast- or precise ephemeris files, present in Inertial Explorer. The absence of the elevation statistics raises the question if the ephemerides of these satellites are corrupted, or contain inaccurate data. From this, the following hypothesis can be formed:

[7] IE Manual, page 170 (`https://docs.novatel.com/Waypoint/Content/PDFs/Waypoint_Software_User_Manual_OM-20000166.pdf`)

[8] measurements of which the parity bit cannot be resolved

Hypothesis
The increased PDOP values of the GNSS observations for `15_run3` in the track segment between km 55 and 56,3 could be caused by corrupted ephemerides of GLONASS satellites present in Inertial Explorer.

Analysis

In order to establish if the missing PDOP values are due to corrupted ephemerides files, precise ephemeris files can be added to Inertial Explorer. Currently, the RILA trajectory is processed using only the GPS ultra-rapid ephemeris files, and GLONASS broadcast ephemerides. GLONASS preliminary- and precise ephemeris files take longer to publish (Bezmenov 2020), (Weber et al. 2002). Hence, in practical applications, it is not always possible to wait. In general GNSS positioning techniques, significant positioning accuracy gains can be obtained by using the final precise ephemeris files published by the IGS (Lu et al. 2011). However, in differential positioning applications in commercial software, as is the case for the RILA system, only millimetre accuracy gains are to be expected (David et al. 2003). This is because in differential GNSS positioning, the orbital errors are mostly cancelled out (David et al. 2003)

As only elevation statistics are missing for the GLONASS constellation, only the precise ephemerides of the GLONASS satellites will be uploaded to the navigation software. The aim of this analysis is to find if any improvements of the PDOP values of satellites *R07* and *R15* can be found. It is however likely that the reprocessed trajectory has limited to no effect on the accuracy metrics of the trajectory solution, as the ephemeris errors mostly cancel out in differential positioning.

After analysis of the reprocessed trajectory, it was found that still, no elevation data for satellites *R07* and *R15* are present in the output of Inertial Explorer. Furthermore, identical PDOP values are observed for `15_run3` at the critical epoch. A more elaborate overview of the results is presented in Table 5.6. Finally, the cross-track trajectory spread and smallest circle analysis of the reprocessed trajectory using the precise GLONASS ephemerides are identical to the original. The results are therefore not plotted in this report.

A solution to find and quantify if the GNSS measurements with missing elevation statistics do have an effect on the accuracy of the trajectory solution is to inactivate the observations for *R07* and *R15* specifically. This inactivation is performed for the same trajectory interval as for the case study (see Table 5.5).

Table 5.5: GNSS epoch inactivation for satellites *R07* & *R15* for the reprocessing of the trajectory of the case study

Run (Satellites excluded)	Metric	Unit	Start	End	Delta
`15_run3` - (*R07*, *R15*)	GNSS Time	s	126950	127018	69
	Kilometre along axis	km	54.95	56.28	1.33

The results on the standard deviation of the cross-track trajectory spread and on the QC metrics of the reprocessed trajectory solution are presented in Figure 5.4. Again, the interval at which the GNSS observations are modified is highlighted in grey.

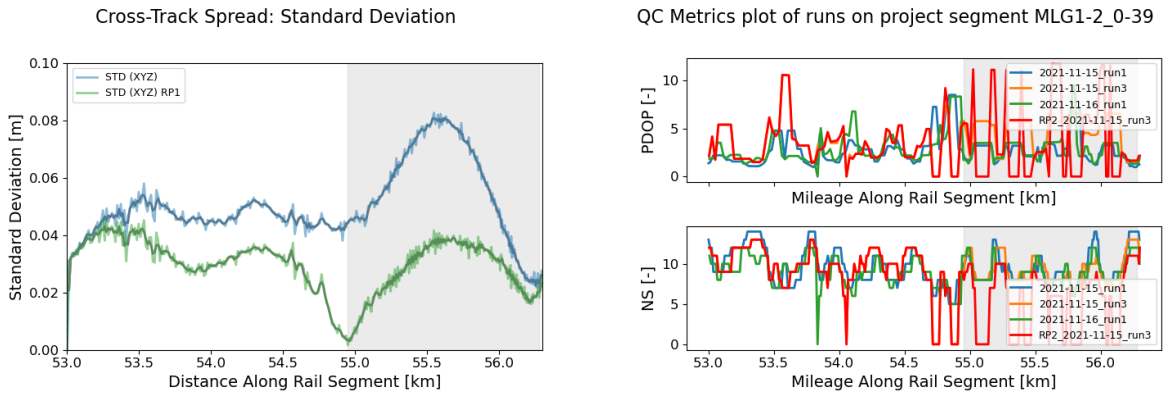

(a) Results on the cross-track trajectory spread

(b) Results on the QC metrics of the reprocessed trajectory

Figure 5.4: Results of the reprocessed trajectory solution with observations for *R07* & *R15* inactivated

As one can observe from Figure 5.4a, the standard deviation of the cross-track trajectory spread is significantly lower than the original trajectory. Furthermore, at c. 54.9 [km], the cross-track spread seems to go to 0. This could be caused by the 3 trajectories intersecting each other at this point. The decrease in cross-track spread can be explained when looking at the qc metrics of the track segment in Figure 5.4b. The NS statistic for the reprocessed trajectory (NS_{RP}) is 0 at a large part of the modified interval. This is caused by the trajectory software deeming it has not enough GNSS observations with sufficient quality for an accepted position fix. In the segments where NS= 0, the processing software will rely on the IMU measurements for position updates. At the locations where NS> 0, $NS_{RP} = NS_0 - 2$ (the 2 excluded observations).

Inertial Explorer constantly accepts new integer ambiguity fixes with only a limited number of satellite observations. This results in high PDOP values where the GNSS observations are used in the trajectory solution ($NS_{RP} > 0$). However, because the IMU measurements, proven to be more accurate than the high PDOP GNSS position updates, are weighted heavily in the modified track segment, it improves the trajectory accuracy of `RP_15_run3` compared to the original. The results of the PDOP and NS statistics at the critical epoch are presented in Table 5.6.

Table 5.6: Qualitative PDOP classification (Isik et al. 2020)

Metric	Original	Precise Ephemeris	Without *R07* & *R15*
GPSTime	126953	126953	126953
PDOP	5.35	5.35	11.12
NS	9	9	7

Conclusion

Reprocessing a trajectory using added GLONASS precise ephemeris files does not provide the missing elevation statistics observed in the raw GNSS data for `15_run3`. Therefore, the missing satellite elevation statistics are not the cause of the increased PDOP values of `15_run3` (compared to the other runs) experienced at the critical epoch. This, therefore, denies the hypothesis. Furthermore, reprocessing the trajectory using the precise ephemeris files does not contribute (significantly) to the accuracy of the trajectory solution.

Although an improvement of the trajectory accuracy is obtained by excluding the GNSS observations for satellites *R07* and *R15*, it is likely caused by the increased weight assigned to the IMU-derived position updates. As NS= 0 for most of the modified track segment, the software relies heavily on the IMU measurements, yielding similar results as obtained in the case study analysis (chapter 4).

5.5. Conclusions on PDOP Scrutinization

In this chapter, several methods have been discussed to determine why the PDOP of `15_run3` (PDOP≈ 5.4) are so much higher at the critical epoch than the PDOP values of the other runs (PDOP≈ 3.2), given the fact that a similar number of satellite observations was used for the trajectory processing of all runs. However, using all methods, no definitive answer on the root cause of the observed, increased PDOP values has been found. Following the analyses performed, the following conclusions can be made:

- The small (1 [min] relative time difference, based on the 12-hour orbital period of the GNSS constellation, does provide an explanation why the observed PDOP values for `15_run1` and `16_run1` are the same. This is because the observed satellite constellation is nearly identical. Therefore, it can be expected that at `15_run3` with a relative time difference of 4 [hrs], the PDOP value deviates due to the differences in the observed constellation.
- When looking at the skyplots of the runs at the critical epoch, the geometry of `15_run3` seems more favourable than that of `15_run1`. However, it was found that a GNSS observation has been rejected by the receiver. This could potentially have a detrimental effect on the observed constellation and PDOP value.
- Manually reconstructing the PDOP values that are provided by the IE software does not lead to a definitive answer on what satellite is rejected by the software. The manually computed PDOP values deviate too much from the values exported by Inertial Explorer. This is likely due to the application of a weighting matrix in Inertial Explorer, which cannot be traced, estimated or reconstructed.
- Although GLONASS observations are found in the raw GNSS measurements with incomplete statistics, it is unlikely that they are the source of the increased PDOP values. Uploading and reprocessing the trajectory using precise ephemeris files does not yield the missing data and does not significantly impact the trajectory accuracy metrics. Although the exclusion of the satellite observations with missing elevation statistics does (in this case) provide an increase in the trajectory accuracy, the gain is likely due to the increased importance of IMU measurements in the integrated GNSS/IMU trajectory solution.

In general, it can be concluded that no definitive cause of the increased PDOP values of `15_run3` can be identified. Therefore, also no targeted error mitigation strategy can be applied to improve on the accuracy of the GNSS position updates. As there are more satellites available to Inertial Explorer than it uses, it is likely rejecting a satellite due to one (or more) of the processing constraints. Tweaking the constraints, making them more lenient or more strict, could provide some additional information on the GNSS data processing in IE. However, this is a very labour intensive sensitivity analysis that, without starting point, is likely to bring little added value.

Although the PDOP value could not be reconstructed, in chapter 4, it was proven that inactivating the GNSS position updates with high PDOP values (> 5) does increase the accuracy of the trajectory solution. This is still a valid conclusion. GNSS position updates with High PDOP values do more harm than good to the integrated trajectory solution. It would have an added benefit to perform a sensitivity analysis on the exact value of a PDOP processing threshold, were all GNSS observations with PDOP values exceeding that threshold are inactivated.

6

Results: Increasing the Number of Runs

The trajectory accuracy metrics used for the quantification of the trajectory accuracy in the case study, are statistical metrics that are used to represent accuracy, based on the assumption that the trajectories of the individual measurement runs are unbiased (see section 3.3). To increase the *trueness* of the dataset, more samples are to be added to the analysis. In other words, it would increase the support for the results obtained in the case study, if similar results can obtained on a larger dataset. Therefore, an answer is to be found on the second question posed in the conclusion of the case study (section 4.6): Can similar accuracy gains be obtained, under similar conditions, when the sample size of the measurements over the same track segment is increased?

First, in this chapter, a track segment is identified for the trajectory accuracy analysis with multiple runs in section 6.1. Next, in section 6.2, an elaboration of the TCL analysis is provided together with any existing considerations followed by the results in section 6.3. Finally, the chapter is concluded with the conclusions on the analysis in section 6.4.

6.1. Survey Scope Identification

When comparing trajectories at the IMU body frame, only runs in the same direction can be used in order to avoid misalignment in the mounting position of the RTSS system on the train. However, when a certain track segment is surveyed using the RILA system, the system usually travels an i-amount of runs in one direction, and an i-amount of runs in the opposite direction. Therefore, to be able to compare the trajectories of all the runs over the same track segment, a comparison of the TCL trajectory, which corrects for any body frame misalignment, is required (see section 3.2).

Figure 6.1: Overview of survey scope `ANI2_0-30`

At the survey scope of the case study analysis, `MLG1-2_0-39`, the railhead detection, and therefore TCL computation was notoriously inaccurate and unreliable. Therefore, in close collaboration with the RILA track processing team, a survey scope has been identified where the TCL computation is reliable, and the survey meets the requirements posed in section 4.1. This survey scope is `ANI2_0-30` and is located in the northwest of Scotland (see Figure 6.1).

The survey of `ANI2_0-30` is, similar to the survey of the case study, obtained by the *RILA04* measurement unit in order to prevent any potential inconsistencies in the different measurement units. Furthermore, the survey consists of five individual measurement runs presented in Table 6.1.

Table 6.1: Runs in survey scope `ANI2_0-30`

Run	Direction
`2022-05-11_run1`	forward
`2022-05-11_run2`	backward
`2022-05-12_run2`	forward
`2022-05-12_run3`	backward
`2022-05-12_run4`	forward

6.2. Track Centre Line Analysis

For the analysis of the track centre line trajectory spread of the measurement runs along the same track segment, a similar research strategy is applied as for the case study analysis (see chapter 4). First of all, a track segment is identified where the RTSS velocity and the number of satellites used in the trajectory solution are greater than zero, and, the PDOP values of one of the runs are higher than the other runs. Such a track segment along `ANI2_0-30` has been selected between 39 [km] and 41.5 [km]. The observations of the QC metrics and standard deviation of the cross-track trajectory spread at this track segment can be found in Figure 6.2a and Figure 6.2b respectively.

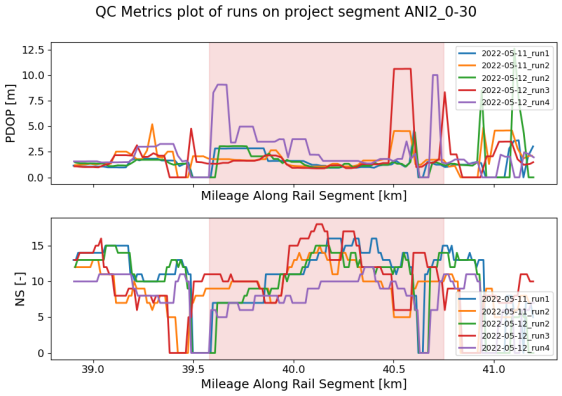

(a) QC metrics of the TCL of the runs

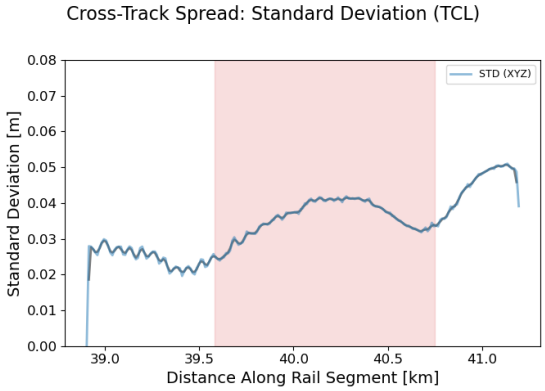

(b) Cross-track TCL trajectory spread of the runs

Figure 6.2: Initial observations of the trajectory metrics of the TCL of the runs along a track segment of scope `ANI2_0-30`

In Figure 6.2, the track interval at which the increase in the standard deviation of the cross-track trajectory spread is observed is indicated in red. Although multiple runs show 'spikes' in PDOP values at certain segments along the track, only `12_run4` shows increased PDOP values for a significant distance along the track. As concluded from the case study analysis (section 4.6), 'spikes' in PDOP values seem to have a limited negative effect on the trajectory accuracy as the trajectory processing software is able to cope with these incidental increases.

Trajectory Reprocessing

In the established research procedure, normally, the trajectory of `12_run4` would be reprocessed. Next, the effect of the reprocessed trajectory of the run on the trajectory accuracy would be analysed. Reprocessing the IMU trajectory of `12_run4` is straightforward following the process explained in section 3.2. However, reprocessing the TCL trajectory using the reprocessed IMU trajectory as input, requires a lot more effort and is unfortunately, due to practical considerations, not possible at this time. There is a few factors that obstruct this process:

- First of all, RILA track processing is a semi-automated process. This means that a Fugro operator needs to monitor the TCL computation and perform manual quality control and reprocessing once the initial TCL computation is complete. Acquiring an accurate TCL can take up to 3 days for a 50 [km] track segment, according to Figure 2.6. Currently, Fugro does not have the resources to perform TCL reprocessing for research purposes.
- During the TCL processing, the operator has applied manual corrections to the initial TCL coordinates. In order to obtain an accurate comparison, the reprocessed TCL should be subject to exactly the same adjustments as the original. This is difficult to obtain as only limited documentation on the adjustments is available.

As for all epochs, coordinates are available on the IMU- and TCL trajectory, a workaround solution has been considered. This workaround solution consists of computing the offset between the IMU coordinate and the TCL coordinate at all epochs for the original trajectories. This offset would then be applied to the reprocessed IMU trajectory, in order to obtain the coordinates of the reprocessed TCL trajectory. However, this workaround solution is currently not possible.

The coordinates of the IMU body frame are given in an ECEF global coordinate system (selected in IE). However, when processing the track data and computing the TCL, Fugro converts the global ECEF coordinates to a local coordinate system selected by the end-user of the data. The transformation of the coordinates is performed using proprietary conversion systems, in order to allow Fugro to exactly tailor the output TCL coordinates to the client's demands. Therefore, when trying to convert the global ECEF coordinates to the local grid using Inertial Explorer or open-source software, the coordinate transformation will differ from the one performed by Fugro. The discrepancy (depending on the latitude and orientation of the trajectory) can be as large as 0.5 [m] according to Fugro operators. In the TCL trajectory, 1 [cm] level accuracies are required, making it impossible to refer the TCL trajectory coordinates to the IMU coordinates without using Fugro's proprietary coordinate conversion system.

Alternative Analysis

An alternative method to establish the effect of the runs with comparatively high PDOP values on the trajectory accuracy is applied. By excluding individual runs from the trajectory accuracy analysis, conclusions can be drawn about its effect on the trajectory accuracy. If the standard deviation of the cross-track trajectory spread decreases after excluding a certain run, it can be concluded that the trajectory of this run had a negative effect on the observed trajectory *precision*. Therefore, under the assumption that the dataset is unbiased, the trajectory of the run was less accurate. If the trajectory accuracy metrics are to be unchanged after the exclusion of a certain run, the accuracy of this run has been similar to the other runs.

6.3. Results

The results of the alternative analysis of the track segment between kilometres 39 and 41.5 on the trajectory accuracy metrics are presented in Figure 6.3. The PDOP metric and standard deviation of the cross-track trajectory spread are given in the same figure. Furthermore, the excluded run `12_run4` is indicated with a dotted line.

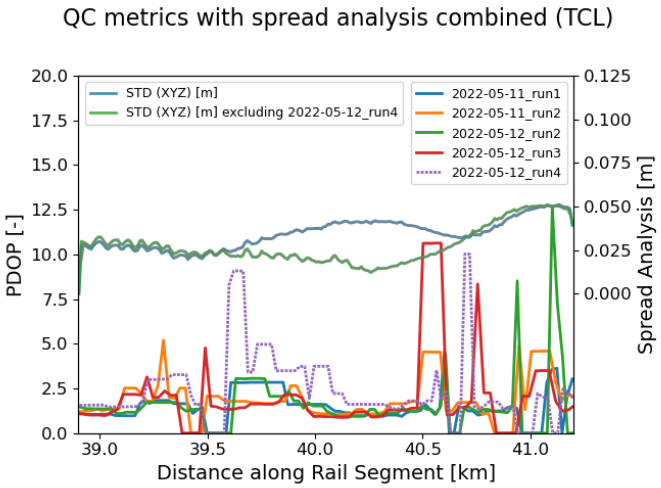

Figure 6.3: Results of the exclusion of high PDOP `12_run4` on the cross-track TCL trajectory spread

From Figure 6.3, it can be observed that indeed, the standard deviation of the cross-track trajectory spread decreases after the exclusion of `12_run4`. As explained in section 6.2, this indicates that the TCL trajectory of `12_run4` deviates from the TCL trajectories of the rest of the runs. With the conclusions from the case study (section 4.6) in mind, it is very likely that the trajectory of `12_run4` is less accurate due to the GNSS position updates with high PDOP values. However, it is not possible to reprocess the trajectory to get a definitive answer.

Furthermore, it can be observed that a standard deviation decrease of c. 60% is achieved at kilometre 40.3. This can be considered significant. From kilometre 40.7 onward, the cross-track trajectory spreads of the analysis in- and excluding `12_run4` are approximately similar but increasing. This is likely due to the irregular PDOP values of all the runs experienced at this interval. Nearly all runs show PDOP increases or complete signal loss. It is therefore likely that that has a negative effect on the trajectory accuracy.

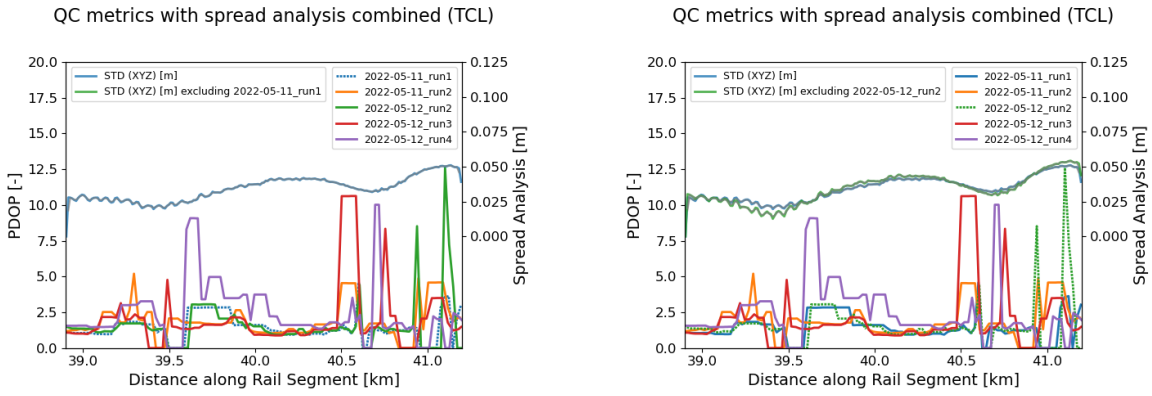

(a) Results of the exclusion of `11_run1`

(b) Results of the exclusion of `12_run2`

Figure 6.4: Results of the exclusion of nominal PDOP runs on the cross-track TCL trajectory spread

Computing the standard deviation of a data set before and after the removal of a sample, the standard deviation can by definition never increase. Therefore, to check the significance of the removal of the TCL with high PDOP values (`12_run4`), the same test has been performed in Figure 6.4 for the removal of runs `11_run1` and `12_run2` with nominal PDOP values.

From Figure 6.4, it can be clearly observed that the change in the cross-track trajectory spread is minimal, especially compared to the results from Figure 6.3. This proves that the excluded runs from Figure 6.4, `11_run1` and `12_run2`, lie in-between all the other runs where `12_run4` is clearly an outlier. This is conform the conclusions from the case study performed in chapter 4. Also conform the results of the case study, from Figure 6.3 it can be observed that there is a difference in cross-track trajectory accuracy outside of the intervals where GNSS position updates with high PDOP values are observed. This is in line with the conclusions from the case study analysis, as it was established that the effect of the inaccurate GNSS position updates propagates through the integrated GNSS/IMU (SBET) trajectory.

Validation

In order to validate if similar results can be obtained using the alternative analysis on the TCL trajectories, two validation track segments (VC1 & VC2) with similar characteristics to the segment presented in section 6.2 have been identified along the survey scope. The results of the validation analyses are presented in Figure 6.5.

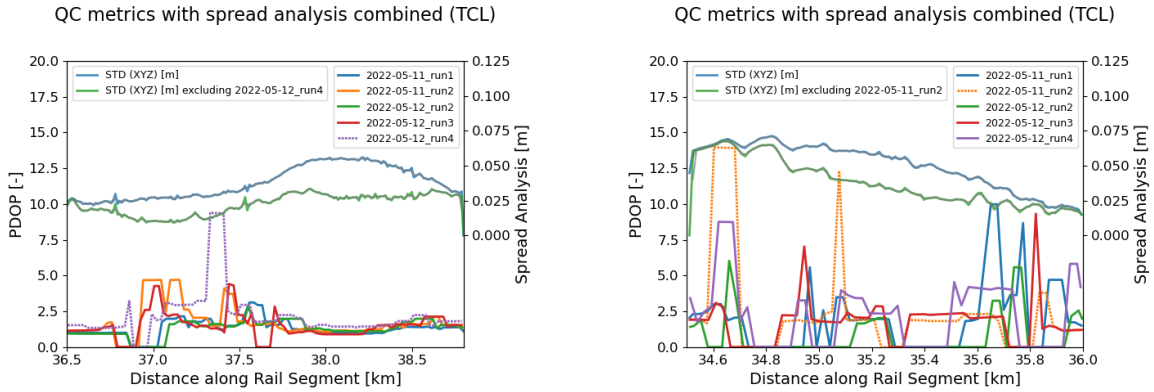

(a) VC1: Results of the exclusion of `12_run4`

(b) VC2: Results of the exclusion of `11_run2`

Figure 6.5: Validation results on the PDOP and cross-track TCL trajectory spread metrics along track segments `ANI2_0-30`

In Figure 6.5a, the results of the exclusion of run `12_run4` between km 36.5 and 40 is presented. Exclusion of the run leads to a significant reduction in the standard deviation of the cross-track trajectory spread. Although the interval at which the PDOP values are very high ($PDOP > 5$) is relatively short, the PDOP values of `12_run4` are, with a few exceptions, the highest during the entire analysed trajectory interval.

A decrease in the cross-track TCL trajectory spread can also be obtained when excluding the TCL trajectory of `11_run2` between km 34.6 and 36. Although significant increases in PDOP values can be observed, they are relatively short. It could be that the PDOP increase at km 34.6 causes inaccurate GNSS position updates to be used for the trajectory determination. This could lead the TCL of `11_run2` to be positioned further away from the other runs, of which the effect propagates through the entire 1.4 [km] track segment. However, as spikes in the PDOP values have only had limited effects on the positioning accuracy in previous analyses, it cannot be stated with certainty. It would be interesting to reprocess the IMU- and TCL-trajectory of `11_run2` with IMU measurements only to isolate the effect of the epochs with increased PDOP values.

6.4. Conclusions on Increasing the Number of Runs

Performing a cross-track trajectory spread analysis to determine the accuracy of the trajectory solution on the trajectory of the Track Centre Line (TCL) does propose some challenges. First of all, a track segment with known high-quality railhead detection and TCL computation must be selected. This has been found to be along the survey scope of `ANI2_0-30`. While it is possible to reprocess the IMU trajectory of a run, due to current practical limitations, it is not possible to reprocess the trajectory of the TCL of a given run. This is because recomputing the TCL using the exact same QC modifications as the original is difficult and very labour-intensive and time-consuming. A workaround solution, where the offset between the original IMU- and TCL trajectories is reapplied to the reprocessed IMU trajectory is not possible due to the unknown parameters for the accurate coordinate system transformation.

However, by comparing the trajectory spread metrics before and after the exclusion of a single run, some conclusions can be made regarding the accuracy of the excluded run. It was observed that excluding the trajectory of a run in which sustained relatively high PDOP values are observed, does decrease the cross-track trajectory spread. This implies that the TCL trajectory of the excluded run was of inferior quality compared to the other runs. This conclusion is further supported by the exclusion of runs with nominal PDOP values. When these runs were excluded from the analysis, the change in the cross-track trajectory spread was limited. This indicates that the high PDOP runs were in-fact, outliers.

To definitively prove that this loss in accuracy is due to the high PDOP values and quantify the inaccuracy, an analysis including the reprocessed TCL of that excluded run is needed. This is an important recommendation made in this report, as it allows for both further validation of the results obtained in chapter 4, and for assessment of the practical use of the high PDOP GNSS observation removal in daily trajectory processing performed for RILA.

7

Conclusions & Recommendations

This chapter will summarise the main conclusions of this thesis research report. Furthermore, recommendations will be presented for further research on the topic, and for practical implementations of the research findings. First of all, in section 7.1, conclusions and answers to the research questions posed in section 2.6 are presented. Furthermore, in section 7.2, recommendations for the processing and research of the trajectory of a rail-based track surveying system, based on the findings in this report, will be presented.

7.1. Conclusions

To formulate an answer to the main research question posed in chapter 2, first of all, a summary of the conclusions from the report supporting answers to the subquestions is presented.

Subquestion 1:

What would be a good quality metric to represent the accuracy of the integrated GNSS/IMU estimated trajectory solution?

In order to find an answer to the first research subquestion, research was performed on the available accuracy metrics in section 3.3. The conclusions on the trajectory accuracy metrics are the following:

- **The observed cross-track trajectory spread provides a qualitative metric to quantify the accuracy of multiple passes over the same track segment.**
  In absence of a ground-truth reference trajectory, which can be used as a benchmark to determine the accuracy of the integrated GNSS/IMU trajectory solution, different quality metrics needed to be constructed. The trajectory accuracy is defined by the *trueness* and *precision* (spread). Assuming the trajectory estimates of the passes over a certain track segment are unbiased and the sample size is sufficiently large, the *accuracy* of the trajectory can be determined by its *precision*. Although the *precision* is only a measure of the *accuracy* under this specific assumption, there are no better alternatives feasible with the current available RILA data. Therefore, when comparing cross-track trajectory spread metrics, a higher *precision* indicates more accurate individual trajectory solutions.
- **The standard deviation and the radius of the smallest enclosing circle are selected as metrics to provide a statistical- and absolute measure of the cross-track trajectory spread.**
  To quantify the cross-track trajectory spread, or *precision*, two metrics have been selected. First of all, the standard deviation of the observed cross-track spread. With the multiple runs over the same track segment present, the standard deviation can be used to provide a statistical measure of the trajectory *precision*. Secondly, the radius of the smallest enclosing circle is selected as an absolute metric to indicate how far the trajectory solutions of different runs are apart in a local cross-track plane. It is important to note that the true performance of the accuracy metrics (compared to ground truth) is not investigated in this report.

Subquestion 2:

In a GNSS signal-constrained environment, what is the magnitude of degradation in the accuracy of GNSS positioning updates, and what strategies can be employed to improve the accuracy of the GNSS positioning update?

To answer the second subquestion, an extensive case study analysis was performed. The results and conclusions of the case study and supporting research, performed in chapter 4, chapter 5 and chapter 6, are presented below.

- **Inaccurate GNSS position updates can be identified at track segments where both the cross-track trajectory spread and the amount of GNSS observations in the SBET solution are high.**
  In this report, the time-based trajectory and Quality Control (QC) output generally provided by commercial trajectory processing software has been transformed to show the data on a mileage-based scale. This allows for comparison of the GNSS quality metrics of the (generally 4-6) individual runs and the computed quality metrics at an arbitrary track location. When a sufficient number of satellites (>7) is used for the GNSS positioning update in the integrated trajectory solution, and the cross-track trajectory spread shows a significant increase, it can be concluded that the GNSS position updates are of decreased accuracy. Because the increase in the cross-track trajectory spread does not correlate to the known error-propagation curve of the IMU-derived positioning updates, the error in the trajectory solution is predominantly caused by inaccurate GNSS position updates.
- **The decreased accuracy of GNSS positioning updates is strongly correlated with observed high PDOP values but mitigating the GNSS position update inaccuracy is not feasible.**
  Runs with large PDOP values (PDOP> 5) were shown to have a significant correlation with increased cross-track the trajectory spread, indicating a decreased accuracy of the GNSS position updates. In chapter 4 it was found that the error in the GNSS-only processed trajectory solution of a run, at a track segment with increased PDOP and cross-track trajectory spread, was in the order of 10 [cm]. High PDOP values indicate a bad satellite geometry, which cannot be 'fixed' in post-processing. However, in chapter 5, it was concluded that the observed 'raw' PDOP indicates a better satellite geometry than the PDOP values reported by Inertial Explorer. This discrepancy can be caused by GNSS observation rejections by the software and by the software-assigned weighting matrix of the individual GNSS observations. However, the exact cause of the discrepancy could not be traced, making error mitigation unfeasible.

Subquestion 3:

What is the effect of inaccurate GNSS position updates on the accuracy of the integrated trajectory solution of an RTSS, and what measures can be taken to mitigate these effects?

From the case study analysis and supporting research, the third and final research subquestion can be answered. The conclusions are:

- **The accuracy of the integrated GNSS/IMU trajectory solution is decreased where at segments where high PDOP (inaccurate) GNSS position updates are present.**
  In the Loosely Coupled (LC) integration of the GNSS- and IMU-derived position updates in Inertial Explorer, the software assigns less weight to GNSS position updates of lower quality. With this, the software aims to account for the decreased accuracy of the high PDOP GNSS position updates. However, there is still a strong correlation between the existence of high PDOP (PDOP> 5) in one of the measurement runs and the increased cross-track spread of the integrated GNSS/IMU trajectories. It can therefore be concluded that the GNSS position updates with increased PDOP values (PDOP> 3) are assigned too much weight in the LC Kalman filter at the GNSS/IMU integration. The effect on the integrated trajectory solution is the same whether the observed satellite geometry or the weighted satellite geometry is considered 'bad'. This leads to an accuracy decrease in the integrated trajectory estimate.

- **By inactivating the GNSS position updates for a trajectory at a track segment where high PDOP values are observed, a significant contribution (50%) to the trajectory accuracy can be made.**
  For high-precision measurement systems featuring a very high-quality Inertial Measurement Unit (IMU), position updates derived from the IMU can be more accurate than position updates obtained by the GNSS receiver under sub-optimal conditions. Inactivating the GNSS measurements entirely, at the interval at which they are known to provide position updates with decreased accuracy, forces the software to rely on the IMU-derived position updates. After the inactivation of high PDOP (> 5) GNSS positioning updates, the position of the SBET trajectory shifted by c.12 [cm]. Furthermore, the trajectory *precision* increased by 50%, indicated by the standard deviation decreasing from 8 [cm] to 4 [cm], and the radius of the smallest enclosing circle decreasing from 10 [cm] to 5 [cm]. This is a very significant result for precise (railway) surveying applications where the trajectory accuracy required for rapid rail surveying is in the order of 3 [cm] (Specht et al. 2016). However, due to the cumulatively IMU-introduced positioning error, the interval for which the GNSS observations are inactivated cannot be too long.
- **An increase in the accuracy of the reprocessed trajectory can be observed outside of the inactivated high PDOP interval.**
  The Smoothed Best Estimate Trajectory (SBET) solution undergoes multiple 'smoothing' steps after integration of the forwards and backwards processed trajectory solution. Therefore, the trajectory solution is affected by inaccurate GNSS positioning updates even outside of the interval at which they are observed. Therefore, when inactivating these inaccurate GNSS position updates, or mitigating their effects, an increase in the trajectory accuracy can be observed even outside of the modified interval.

All in all, when combining the answers to the subquestions, an answer can be formulated to the main research question formulated in chapter 3. To reiterate, the main research question investigated in this report is the following:

What would be a way to improve the accuracy of the GNSS/IMU integrated trajectory solution of a rail-based track surveying system, in environments with reduced GNSS signal access?

In short: The accuracy of the integrated GNSS/IMU trajectory solution can be increased by limiting the negative effects experienced by inaccurate GNSS position updates. Especially in areas with limited GNSS signal access, it can occur that either the satellite geometry observed at the receiver or the weighted satellite geometry computed by Inertial Explorer can be considered 'bad' (PDOP$>$ 5). This causes inaccuracies in the GNSS position updates in the integrated trajectory solution, which in turn causes a decrease in the accuracy of the GNSS/IMU integrated trajectory solution. By inactivating the GNSS position updates at these high PDOP epochs, increases the integrated trajectory accuracy by as much as 50%.

However, the discrepancy found between the satellite geometry observed by the receiver and the satellite geometry presented by Inertial Explorer, could not be traced. A better understanding of this discrepancy might lead to a successful strategy for improvement of the accuracy of the GNSS position update. Potentially, this could eliminate the need for 'inactivation', which is generally considered to be preferable as less costly data is deleted. The research framework presented in this report can also be used to establish other correlations between GNSS- or trajectory QC metrics and the cross-track trajectory spread. Also, sensitivity analyses of the different processing settings and thresholds (see section 3.2) can be performed to find other (GNSS) error sources and methods to mitigate their effects.

7.2. Recommendations

Based on the findings in this report, recommendations are provided for further research on the problem at hand. The recommendations focus on both practical implementations in trajectory processing operations, and on further research on the topic. The recommendations are prioritised based on an indication of the estimated implementation time.

- **Recommendation 1:** *Short-term*

  Using the research framework presented in this report, the effect of different trajectory processing settings and thresholds on trajectory accuracy can be quantified. The current settings and thresholds, discussed in section 3.2, are not yet thoroughly investigated. Performing a sensitivity analysis on these processing thresholds, such as the *C/N0* tolerance, *L1 Locktime Cutoff* and *Max. RMS* to find optimal values could lead to increased accuracy of the trajectory estimates.

- **Recommendation 2:** *Short-term*

  Currently, in the daily processing flow of the RILA trajectories, no feedback loop is present between the Quality Control (QC) of the Inertial Explorer output and the provided processing settings and threshold as input (see Figure 3.3). Although QC is performed, it is merely to observe if the trajectory processing has not failed. However, now the QC output can be linked to trajectory accuracy metrics, it is recommended to implement a feedback loop between (quality thresholds in) the cross-track trajectory spread and the QC metrics of the individual runs. For an individual survey, the RILA data engineer could reprocess the trajectory to increase the trajectory accuracy. A suggested trajectory processing flow is presented in Appendix B.

- **Recommendation 3:** *Short-term*

  Currently, as discussed in chapter 3, a linear interpolation method is used to interpolate the different trajectories, in order to compute the cross-track trajectory spread and accuracy metrics. However, it can well be that other interpolation methods would provide more accurate representations of the interpolated trajectories, thereby limiting the potential interpolation error (currently 2.03 [cm]). For this application, a good recommendation would be to implement a cubic-spline interpolation method (Kucuk 2017).

- **Recommendation 4:** *Medium-term*

  From chapter 4 and chapter 6, it was concluded that the reprocessing of trajectories with GNSS updates removed for high PDOP observations, significantly increases the trajectory accuracy. Therefore it is recommended to process the trajectory with a tight PDOP constraint. As no such feature is currently present in Inertial Explorer, a tool will need to be developed to inactivate the GNSS measurements at the epochs which, in the originally processed trajectory, have a PDOP value exceeding the threshold. Additional research will be needed to determine the optimal value of this PDOP threshold. Due to the availability of a high-quality IMU and the positive results presented in chapter 4, where the GNSS position updates with PDOP$>$ 2 were inactivated, the threshold can be expected to be in the order of 2 $<$PDOP Threshold$<$ 3.

- **Recommendation 5:** *Medium-term*

  In chapter 6, a trajectory spread analysis is performed on the TCL obtained by the different runs. It was proven that a decrease in cross-track trajectory spread could be obtained by removing the trajectory of a run with high PDOP values. However, due to resource constraints, it was not possible to perform the TCL spread analysis using reprocessed TCL trajectories based on improved IMU trajectories. Therefore, it is recommended to redo the analysis with a reprocessed TCL trajectory in order to quantify the potential (TCL) trajectory improvement.

- **Recommendation 6:** *Medium-term*

  Currently, the RTSS trajectory is processed using only the GPS + GLONASS constellations (G2), Differential GNSS positioning (DGNSS) and a Loosely-Coupled (LC) IMU integration scheme. However, research has proven that trajectory processing using four GNSS constellations (G4[1]) (An et al. 2020) (Delikaraoglou et al. 2016), GNSS Precise Point Positioning (PPP) (Ramachandran et al. 2019) (Héroux et al. 2004) and Tightly-Coupled (TC) integration schemes (Shi et al. 2021b) (Liu et al. 2018) can provide significant (accuracy) advantages in challenging GNSS environments for high-precision, land-surveying applications. Therefore, it is recommended to quantify the effect of these processing settings on the accuracy of the trajectory estimates. It is recommended to prioritise the implementation of G4 constellations in the trajectory processing.

[1] G4: GPS + GLONASS + Beidou + Galileo

- **Recommendation 7:** *Medium-term*
  As concluded from chapter 5, it has been proven difficult to recreate PDOP values at a certain epoch of the trajectory estimate, because the GNSS observation weighting applied by the software is untraceable. It is recommended to further research and better understand this weighting algorithm. This potentially allows for tuning of the weighting matrix, for example in the Kalman filter settings of the GNSS/IMU integration, could prevent the need for inactivation of GNSS observations in order to obtain a similar accuracy increase. In general, it is preferred to not 'delete' costly obtained GNSS epochs altogether as the observations can contribute to an accurate trajectory solution. For example, it might be that significant performance gains can be obtained by eliminating only an individual GNSS observation, or implementing a different observation weight matrix.

- **Recommendation 8:** *Long-term*
  Improvements in trajectory accuracy have been quantified using statistical metrics under the assumption that the individual trajectory measurements are unbiased. As discussed in section 3.3, this is a critical assumption where the individual measurements are assumed to be *true*. However, the actual *trueness* is very important for high-accuracy surveying and the acquisition of the true absolute track geometry measurements. Therefore, it is recommended to obtain a ground-truth reference trajectory to quantify the accuracy and performance of the trajectory accuracy metrics. As indicated by Fugro, this has been previously attempted and is a very costly process. Furthermore, the measurements of the reference trajectory did not have much higher accuracies than what can be obtained by the RILA system. However, there is added benefit as the reference trajectory allows for a true comparison of the accuracy of the trajectory solutions of the different runs.

- **Recommendation 9:** *Long-term*
  In the absence of a ground-truth trajectory, the cross-track trajectory spread of the multiple runs over the same track segment is used in this report. However, research by Tombrink et al. (2023), suggests geospatial sorting of the runs along the track in order to benchmark the accuracy of different trajectory solutions. Contrary to the current chronological (time-based) sorting of the position epochs, geospatial sorting arranges the epochs along the trajectory. Where chronological sorting yields four 'individual' runs over a track segment separated by time, geospatial sorting integrates all epochs into a single trajectory solution. Geospatial sorting, therefore, leads to a trajectory estimate based on a much higher sampling rate, which in turn could lead to higher trajectory accuracy. It is therefore recommended to explore its applications for multi-run trajectory processing.

This page was intentionally left blank.

References

Acosta, HÃctor Nelson and Juan Manuel Toloza (Aug. 2012). "A tool for prototyping a precision GPS system". In: *International Journal of Computers & Technology* 3 (1), pp. 15–23. DOI: 10.24297/ijct.v3i1a.2722.

Alt, Helmut and Michael Godau (1995). "Computing the Fréchet distance between two polygonal curves". In: *International Journal of Computational Geometry & Applications* 05.01n02, pp. 75–91. DOI: 10.1142/S0218195995000064. URL: https://doi.org/10.1142/S0218195995000064.

An, Xiangdong, Xiaolin Meng, and Weiping Jiang (Dec. 2020). "Multi-constellation GNSS precise point positioning with multi-frequency raw observations and dual-frequency observations of ionospheric-free linear combination". In: *Satellite Navigation* 1. ISSN: 26621363. DOI: 10.1186/s43020-020-0009-x.

Anghileri, M., M Paonni, D Fontanella, and B Eissfeller (2013). "GNSS data message performance: A new methodology for its understanding and ideas for its improvement". In: *Proceedings of the 2013 International Technical Meeting of The Institute of Navigation*, pp. 638–650.

Angrisano, Antonio, Mark Petovello, Mario Vultaggio, and Lorenzo Turturici (2010). *GNSS/INS Integration Methods*. Universita' Degli Studi Di Napoli, Schulich School of Engineering, Dipartimento di Scienze Applicante.

Berndt, Donald J. and James Clifford (1994). "Using Dynamic Time Warping to Find Patterns in Time Series". In: *Proceedings of the 3rd International Conference on Knowledge Discovery and Data Mining*, pp. 359–370.

Bezmenov, Igor (Jan. 2020). "Estimation of precise orbits and clock corrections of GLONASS and GPS navigation satellites in ultra-rapid regime based on observation data". In: *Izmeritel'naya Tekhnika*, pp. 11–17. DOI: 10.32446/0368-1025it.2020-1-11-17.

Birk, Andreas and Max Pfingsthorn (2016). *Simultaneous Localization And Mapping (SLAM)*. Encyclopedia of Electrical and Electronics Engineering.

Briers, Mark, Arnaud Doucet, and Simon Maskell (June 2009). *Smoothing Algorithms for State-Space Models*. The Institute of Statistical Mathematics.

Bronsvoort, E. and N. Van Den Hurk (2013). "The RILA system - now in the UK". In: *Rail Infrastructure*, pp. 57–59.

Brus, D.J., J. J. de Gruijter, B.A. Marsman, R. Visschers, A.K. Bregt, A. Breeuwsma, and J. Bouma (1996). "The performance of spatial interpolation methods and choropleth maps to estimate properties at points: a soil survey case study." English. In: *Environmetrics* 7, pp. 1–16. ISSN: 1180-4009. DOI: 10.1002/(sici)1099-095x(199601)7:1<1::aid-env157>3.0.co;2-y.

CEN (Mar. 2019). *EN 13848-1:2019 Railway applications - Track - Track geometry quality - Part 1: Characterization of track geometry*. CEN.

Charron, Nicholas, Stephen Phillips, and Steven Waslander (May 2018). "De-noising of Lidar Point Clouds Corrupted by Snowfall". In: pp. 254–261. DOI: 10.1109/CRV.2018.00043.

Chaube, Vishwesh, V. K. Agnihotri, Rakesh Goyal, and N. C. Bindlish (Sept. 2019). *Tamping Machine and Dynamic Track Stabilizer*. 2nd ed. Government of India, Ministry of Railways, pp. 201–300.

Chen, Chien Sheng (Jan. 2015). "Weighted geometric dilution of precision calculations with matrix multiplication". In: *Sensors (Switzerland)* 15 (1), pp. 803–817. ISSN: 14248220. DOI: 10.3390/s150100803.

Chen, Qijin, Xiaoji Niu, Lili Zuo, Tisheng Zhang, Fuqin Xiao, Yi Liu, and Jingnan Liu (Feb. 2018). "A railway track geometry measuring trolley system based on aided INS". In: *Sensors (Switzerland)* 18. ISSN: 14248220. DOI: 10.3390/s18020538.

Chen, Yuan K., Jya-Syin Chien, Kamran Ghassemi, Tom Simundich, Jack Taylor, and Nicholas Nyema (2002). "User range error evolution and projected performance". In: *Proceedings of the 15th International Technical Meeting of the Satellite Division of The Institute of Navigation (ION GPS 2002)*, pp. 1575–1584.

Clinnick, Richard (Dec. 2013). "A pressing engagement". In: *Rail Magazine - Current Trains*. URL: https://www.railmagazine.com/trains/a-pressing-engagement.

Cosandier, D, H Martell, and G Roesler (2018). *Direct Utilization of LiDAR Data in GNSS/IMU Processing for Indoor and Mobile Mapping Applications*. NovAtel Inc.

Czaplewski, Krzysztof, Zbigniew Wisniewski, Cezary Specht, Andrzej Wilk, Wladyslaw Koc, Krzysztof Karwowski, Jacek Skibicki, Paweł Dabrowski, Bartosz Czaplewski, Mariusz Specht, Piotr Chrostowski, Jacek Szmaglinski, Slawomir Judek, Slawomir Grulkowski, and Roksana Licow (2020). "Application of Least Squares with Conditional Equations Method for Railway Track Inventory Using GNSS Observations". In: *Sensors*. DOI: 10.3390/s20174948. URL: www.mdpi.com/journal/sensors.

David, L. M., David Warren, and John F. Raquet (Jan. 2003). "Broadcast vs. precise GPS ephemerides: A historical perspective". In: *GPS Solutions* 7, pp. 151–156. DOI: 10.1007/s10291-003-0065-3.

Delikaraoglou, Demitris and Dimitrios Vasileios Psychas (2016). "Accuracy improvement techniques in Precise Point Positioning method using multiple GNSS constellations". In: *Technische Universit¨at M¨unchen, Ingenieurfakult¨at Bau Geo Umwelt*. DOI: 10.13140/RG.2.1.1386.5365. URL: https://www.researchgate.net/publication/301553055.

Driver, Ted (2007). "Long-term prediction of GPS accuracy: Understanding the fundamentals". In: *Proceedings of the 20th International Technical Meeting of the Satellite Division of The Institute of Navigation (ION GNSS 2007)*, pp. 152–163.

Durrant-Whyte, Hugh and Thomas C. Henderson (2008). "Multisensor Data Fusion". In: *Springer Handbook of Robotics*. Ed. by Bruno Siciliano and Oussama Oussama Khatib. Berlin, Heidelberg: Springer Berlin Heidelberg, pp. 585–610. ISBN: 978-3-540-30301-5. DOI: 10.1007/978-3-540-30301-5_26. URL: https://doi.org/10.1007/978-3-540-30301-5_26.

Dutt, V.B.S. Srilatha Indira, G.Sasi Bhushana Rao, S.Swapna Rani, Swarna Ravindra Babu, Rajkumar Goswami, and Ch.Usha Kumari (Jan. 2009). *Investigation of GDOP for Precise user Position Computation with all Satellites in view and Optimum four Satellite Configurations*. Andhra University College of Engineering. URL: https://www.researchgate.net/publication/267257339.

Eiter, Thomas and Heikki Mannila (Apr. 1994). *Computing Discrete Fréchet Distance*. Technische Universtat Wien.

Elkhoury, Najwa, Lalith Hitihamillage, Sara Moridpour, and Dilan Robert (Mar. 2018). "Degradation Prediction of Rail Tracks: A Review of the Existing Literature". In: *The Open Transportation Journal* 12 (1), pp. 88–104. ISSN: 1874-4478. DOI: 10.2174/1874447801812010088.

Falco, Gianluca, Marco Pini, and Gianluca Marucco (Feb. 2017). "Loose and tight GNSS/INS integrations: Comparison of performance assessed in real Urban scenarios". In: *Sensors (Switzerland)* 17 (2). ISSN: 14248220. DOI: 10.3390/s17020255.

Fang, Rongxin, Huanghui Lv, Yuanming Shu, Jiawei Zheng, Kunlun Zhang, and Jingnan Liu (Oct. 2021). "Improved performance of GNSS precise point positioning for high-rate seismogeodesy with recent BDS-3 and Galileo". In: *Advances in Space Research* 68 (8), pp. 3255–3267. ISSN: 18791948. DOI: 10.1016/j.asr.2021.06.012.

Fontul, Simona, André Paixão, Mercedes Solla, and Lara Pajewski (Apr. 2018). "Railway track condition assessment at network level by frequency domain analysis of GPR data". In: *Remote Sensing* 10 (4). ISSN: 20724292. DOI: 10.3390/rs10040559.

Fu, Bin, Rocco Libero Giossi, Rickard Persson, Sebastian Stichel, Stefano Bruni, and Roger Goodall (Mar. 2020). "Active suspension in railway vehicles: a literature survey". In: *Railway Engineering Science* 28 (1), pp. 3–35. ISSN: 26624745. DOI: 10.1007/s40534-020-00207-w.

Fu, Chao-Yang and Jaan-Rong Tsay (2017). *The Performance Analysis of Visual Odometry Based on Disparity Changing*. Dept. of Geomatics, National Cheng Kung University. URL: https://www.researchgate.net/publication/324942382.

Guo, Yunlong, Jiale Xie, Zheng Fan, Valeri Markine, David P. Connolly, and Guoqing Jing (Aug. 2022). "Railway ballast material selection and evaluation: A review". In: *Construction and Building Materials* 344. ISSN: 09500618. DOI: 10.1016/j.conbuildmat.2022.128218.

Habibzadeh, Yashar (Mar. 2023). *Trajectory Improvement of Railway Mobile Mapping System using Monocular Visual Inertial SLAMM*. Delft University of Technology - Faculty of Aerospace Engineering.

Harris, John and Horst Stoecker (Jan. 1998). *The Handbook of Mathematics and Computational Science*. ISBN: 978-1-4612-5319-8. DOI: 10.1007/978-1-4612-5317-4.

Héroux, Pierre, Yang Gao, Jan Kouba, François Lahaye, Yves Mireault, Paul Collins, K. MacLeod, Pierre Tétreault, and K. Chen (Sept. 2004). "Products and Applications for Precise Point Positioning - Moving Towards Real-Time". In: *Proceedings of the 17th International Technical Meeting of the Satellite Division of The Institute of Navigation*, pp. 1832–1843.

Hofmann-Wellenhof, Bernhard, Herbert Lichtenegger, and Elmar Wasle (2008). *More on GNSS*. Vienna: Springer Vienna, pp. 397–430. ISBN: 978-3-211-73017-1. DOI: 10.1007/978-3-211-73017-1_12. URL: https://doi.org/10.1007/978-3-211-73017-1_12.

Hu, Can and Xiang Liu (Apr. 2016). "Modeling Track Geometry Degradation Using Support Vector Machine Technique". In: vol. 2016 Joint Rail Conference. ASME/IEEE Joint Rail Conference. V001T01A011. DOI: 10.1115/JRC2016-5739. URL: https://doi.org/10.1115/JRC2016-5739.

Hussain, Arif, Arslan Ahmed, Hina Magsi, and Rajesh Tiwari (2020). "Adaptive GNSS receiver design for highly dynamic multipath environments". In: *IEEE Access* 8, pp. 172481–172497. ISSN: 21693536. DOI: 10.1109/ACCESS.2020.3024890.

IEA, International Energy Agency (2019). *The Future of Rail*. Licence: CC BY 4.0. URL: https://www.iea.org/reports/the-future-of-rail.

Isik, Oguz Kagan, Juhyeon Hong, Ivan Petrunin, and Antonios Tsourdos (Sept. 2020). "Integrity analysis for GPS-based navigation of UAVs in urban environment". In: *Robotics* 9 (3). ISSN: 22186581. DOI: 10.3390/ROBOTICS9030066.

ISO 5725-1 (Dec. 1994). *Accuracy (trueness and precision) of measurement methods and results — Part 1: General principles and definitions*. CEN. URL: https://www.iso.org/standard/11833.html.

Judek, Slawomir, Andrzej Wilk, Wladysław Koc, Lszek Lewiński, Artur Szumisz, Piotr Chrostowski, Sławomir Grulkowski, Jacek Szmagliński, Michal Michna, Krzysztof Karwowski, Jacek Skibicki, and Roksana Licow (Oct. 2022). "Preparatory Railway Track Geometry Estimation Based on GNSS and IMU Systems". In: *Remote Sensing* 14, p. 5472. ISSN: 2072-4292. DOI: 10.3390/rs14215472. URL: https://www.mdpi.com/2072-4292/14/21/5472.

Kaya, Fevzi and Muzeyyen Saritas (Jan. 2005). "A Computer Simulation of Dilution of Precision in the Global Positioning System Using Matlab". In.

Kersting, A. P. and P. Friess (2016). "Post-mission quality assurance procedure for survey-grade mobile mapping systems". In: vol. 2016-January. International Society for Photogrammetry and Remote Sensing, pp. 647–652. DOI: 10.5194/isprsarchives-XLI-B1-647-2016.

Khajehei, Hamid, Alireza Ahmadi, Iman Soleimanmeigouni, and Arne Nissen (Dec. 2019). "Allocation of effective maintenance limit for railway track geometry". In: *Structure and Infrastructure Engineering* 15 (12), pp. 1597–1612. ISSN: 17448980. DOI: 10.1080/15732479.2019.1629464.

Kraft, S., J. Causse, and F. Coudert (2016). "An approach for the classification of track geometry defects". In: *The Dynamics of Vehicles on Roads and Tracks - Proceedings of the 24th Symposium of the International Association for Vehicle System Dynamics, IAVSD 2015*, pp. 1135–1144. DOI: 10.1201/b21185-121.

Kucuk, Serdar (2017). "Optimal trajectory generation algorithm for serial and parallel manipulators". In: *Robotics and Computer-Integrated Manufacturing* 48, pp. 219–232. ISSN: 0736-5845. DOI: https://doi.org/10.1016/j.rcim.2017.04.006. URL: https://www.sciencedirect.com/science/article/pii/S0736584516302927.

Kukko, Antero (Dec. 2013). *Mobile laser scanning - system development, performance and applications*.

Langley, Richard B et al. (1999). "Dilution of precision". In: *GPS world* 10.5, pp. 52–59.

Langley, Richard B, Peter J. G. Teunissen, and Oliver Montenbruck (2017). "Introduction to GNSS". In: *Springer Handbook of Global Navigation Satellite Systems*. Ed. by Peter J.G. Teunissen and Oliver Montenbruck. Springer International Publishing, pp. 3–23. ISBN: 978-3-319-42928-1. DOI: 10.1007/978-3-319-42928-1_1. URL: https://doi.org/10.1007/978-3-319-42928-1_1.

Liao, Yingying, Lei Han, Haoyu Wang, and Hougui Zhang (Oct. 2022). "Prediction Models for Railway Track Geometry Degradation Using Machine Learning Methods: A Review". In: *Sensors* 22 (19). ISSN: 14248220. DOI: 10.3390/s22197275.

Liu, Yue, Fei Liu, Yang Gao, and Lin Zhao (Dec. 2018). "Implementation and analysis of tightly coupled global navigation satellite system precise point positioning/inertial navigation system (GNSS PPP/INS) with insufficient satellites for land vehicle navigation". In: *Sensors (Switzerland)* 18. ISSN: 14248220. DOI: 10.3390/s18124305.

Løvås, Marianne (Oct. 2017). "Increasing the Accuracy of Positioning in Mobile Mapping Systems A method supported by Simultaneous Localization And Mapping". Norwegian University of Science and Technology. ISBN: 9789177252627.

Lu, Fumin and Jin Li (2011). "Precise point positioning study to use different IGS precise ephemeris". In: *2011 IEEE International Conference on Computer Science and Automation Engineering*. Vol. 3, pp. 592–595. DOI: 10.1109/CSAE.2011.5952748.

Maciuk, Kamil (Mar. 2015). "DOP coefficients in GNSS observations". In: *Budownictwo i Architektura* 14 (1), pp. 065–072. ISSN: 2544-3275. DOI: 10.35784/bud-arch.1668.

Mattheuwsen, L., M. Bassier, and M. Vergauwen (2019). "Theoretical accuracy prediction and validation of low-end and high-end mobile mapping system in urban, residential and rural areas". In: vol. 42. International Society for Photogrammetry and Remote Sensing, pp. 121–128. DOI: 10.5194/isprs-archives-XLII-2-W18-121-2019.

El-Mohammedy Sabaa, Nasr and Ahmed Abd-Elhai Ahmed (2019). "Studying the Effects of Broadcast and Precise Ephemeris form GNSS and GPS only on Position Accuracy". In: *Australian Journal of Basic and Applied Sciences* 13 (8), pp. 147–153. ISSN: 2309-8414. DOI: 10.22587/ajbas.2019.13.8.19. URL: www.ajbasweb.com.

Odijk, Dennis and Lambert Wanninger (2017). "Differential Positioning". In: *Springer Handbook of Global Navigation Satellite Systems*. Ed. by Peter J.G. Teunissen and Oliver Montenbruck. Springer International Publishing, pp. 753–780. ISBN: 978-3-319-42928-1. DOI: 10.1007/978-3-319-42928-1_26. URL: https://doi.org/10.1007/978-3-319-42928-1_26.

Ong Kim Sun, G. and P. Gibbings (2005). "How well does the virtual reference station (VRS) system of GPS base stations perform in comparison to conventional RTK?" In: *Journal of Spatial Science* 50 (1), pp. 59–73. ISSN: 14498596. DOI: 10.1080/14498596.2005.9635038.

Pan, Lin, Xuanping Li, Wenkun Yu, Wujiao Dai, Cuilin Kuang, Jun Chen, Fade Chen, and Pengfei Xia (Nov. 2020). "Performance evaluation of real-time precise point positioning with both BDS-3 and BDS-2 observations". In: *Sensors (Switzerland)* 20 (21), pp. 1–20. ISSN: 14248220. DOI: 10.3390/s20216027.

Perakis, Harris, Vassilis Gikas, P Clausen, P-Y Gilliéron, H Perakis, V Gikas, and I Spyropoulou (Dec. 2015). *Positioning Accuracy of Vehicle Trajectories for Road Applications*. 22nd ITS World Congress. URL: https://www.researchgate.net/publication/283741764.

Petrovski, Ivan G. (2014). *Part 1 - GNSS: orbits, signals and methods*. Cambridge University Press. DOI: 10.1017/CBO9781139565455.

Puente, I., H. González-Jorge, J. Martínez-Sánchez, and P. Arias (2013). "Review of mobile mapping and surveying technologies". In: *Measurement: Journal of the International Measurement Confederation* 46, pp. 2127–2145. ISSN: 02632241. DOI: 10.1016/J.MEASUREMENT.2013.03.006.

Ramachandran, Duraisamy, Ami Hassan Md Din, Siti Aisah Ibrahim, and Abdullah Hisam Omar (2019). *Real-time precise point positioning (RT-PPP) for positioning and mapping*. Vol. 9. Springer, pp. 891–913. DOI: 10.1007/978-981-10-8016-6_64.

Retscher, Guenther (June 2002). "Accuracy Performance of Virtual Reference Station (VRS) Networks". In: *Journal of Global Positioning Systems* 1, pp. 40–47. DOI: 10.5081/jgps.1.1.40.

Sanz Subirana, J, Juan Zornoza J.M., and M. Hernandez-Pajares (2011). *Transformations between ECEF and ENU coordinates*. URL: https://gssc.esa.int/navipedia/index.php/Transformations_between_ECEF_and_ENU_coordinates.

Secco, Pablo (Apr. 2022). *Point cloud based improvement of the trajectory of a Railway Mobile Mapping System*. URL: http://resolver.tudelft.nl/uuid:7eb73102-59c4-440e-9ee1-c3dafb5f88f0.

Selig, E. T. and J. M. Waters (1994). *Track geotechnology and substructure management*. Thomas Telford.

Shen, Nan, Liang Chen, Jingbin Liu, Lei Wang, Tingye Tao, Dewen Wu, and Ruizhi Chen (May 2019). "A review of Global Navigation Satellite System (GNSS)-based dynamic monitoring technologies for structural health monitoring". In: *Remote Sensing* 11 (9). ISSN: 20724292. DOI: 10.3390/rs11091001.

Shi, Bo, Yuntian Bai, Shun Zhang, Ruofei Zhong, Fanlin Yang, Shizhu Song, and Guoyu Li (Feb. 2021a). "Reference-plane-based approach for accuracy assessment of mobile mapping point clouds". In: *Measurement: Journal of the International Measurement Confederation* 171. ISSN: 02632241. DOI: 10.1016/j.measurement.2020.108759.

Shi, Bo, Mengke Wang, Yunpeng Wang, Yuntian Bai, Kang Lin, and Fanlin Yang (Jan. 2021b). "Effect analysis of GNSS/INS processing strategy for sufficient utilization of urban environment observations". In: *Sensors (Switzerland)* 21, pp. 1–25. ISSN: 14248220. DOI: 10.3390/s21020620.

Specht, Cezary and Wladyslaw Koc (2016). "Mobile Satellite Measurements in Designing and Exploitation of Rail Roads". In: *Transportation Research Procedia* 14, pp. 625–634. ISSN: 23521465. DOI: 10.1016/j.trpro.2016.05.310.

Specht, Mariusz, Cezary Specht, Paweł D¸ Abrowski, Krzysztof Czaplewski, Leszek Smolarek, and Oktawia Lewicka (Aug. 2020). "Road Tests of the Positioning Accuracy of INS/GNSS Systems Based on MEMS Technology for Navigating Railway Vehicles". In: *Energies* 13 (13(17)), p. 4463. DOI: 10.3390/en13174463. URL: www.mdpi.com/journal/energies.

Specht, Mariusz, Cezary Specht, Andrzej Stateczny, Paweł Burdziakowski, Paweł Dabrowski, and Oktawia Lewicka (June 2022). "Study on the Positioning Accuracy of the GNSS/INS System Supported by the RTK Receiver for Railway Measurements". In: *Energies* 15 (11). ISSN: 19961073. DOI: 10.3390/en15114094.

Sylvester, J. J. (1857). "A question in the geometry of situation". In: *Quarterly Journal of Mathematics* (1), p. 79.

Tamparas, Dimitrios (Nov. 2016). "Railway Track Geometry, A framework to optimally evaluate track condition and assess maintenance needs based on vehicle response". Delft University of Technology.

Tao, Yaguang, Alan Both, Rodrigo I. Silveira, Kevin Buchin, Stef Sijben, Ross S. Purves, Patrick Laube, Dongliang Peng, Kevin Toohey, and Matt Duckham (2021). "A comparative analysis of trajectory

similarity measures". In: *GIScience and Remote Sensing* 58 (5), pp. 643–669. ISSN: 15481603. DOI: 10.1080/15481603.2021.1908927.

Tiberius, Christian and Edward Verbree (Jan. 2004). *GNSS positioning accuracy and availability within Location Based Services: The advantages of combined GPS-Galileo positioning*. Delft University of Technology (TU Delft).

Tombrink, Gereon, Ansgar Dreier, Lasse Klingbeil, and Heiner Kuhlmann (2023). "Trajectory evaluation using repeated rail-bound measurements". In: *Journal of Applied Geodesy*. DOI: doi:10.1515/jag-2022-0027. URL: https://doi.org/10.1515/jag-2022-0027.

Valtonen Ornhag, Marcus, Patrik Persson, Marten Wadenback, Kalle Astrom, and Anders Heyden (2022). "Trust Your IMU: Consequences of Ignoring the IMU Drift". In: *Proceedings - 2022 IEEE/CVF Conference on Computer Vision and Pattern Recognition Workshops, CVPRW 2022*. IEEE Computer Society Conference on Computer Vision and Pattern Recognition Workshops. United States: IEEE Computer Society, pp. 4467–4476. DOI: 10.1109/CVPRW56347.2022.00493.

Vlachos, M., G. Kollios, and D. Gunopulos (2002). "Discovering similar multidimensional trajectories". In: pp. 673–684. DOI: 10.1109/ICDE.2002.994784.

VWS, Ministerie van Verkeer en Waterstaat (2005). "Regeling hoofdspoorweginfrastructuur, Artikel 8". In: URL: https://wetten.overheid.nl/jci1.3:c:BWBR0017712%5C&paragraaf=3%5C&artikel=8%5C&z=2005-11-01%5C&g=2005-11-01.

Wakker, Karel (Jan. 2015). *Fundamentals of Astrodynamics*. Delft University of Technology. ISBN: 978-94-6186-419-2.

Wang, Haoyu and Jos Berkers (July 2019). "Absolute and Relative Track Geometry: Closing the Gap". In: *railwayengineering.com*. URL: https://www.researchgate.net/publication/338223570.

Wang, Haoyu, Jos Berkers, Nick van den Hurk, and Nasir Farsad Layegh (Feb. 2021). "Study of loaded versus unloaded measurements in railway track inspection". In: *Measurement: Journal of the International Measurement Confederation* 169. ISSN: 02632241. DOI: 10.1016/j.measurement.2020.108556.

Weber, R and E Fragner (2002). *The Quality of Precise GLONASS Ephemerides*. Insitute of Geodesy and Geophysics; University of Technology, pp. 271–279. URL: www.elsevier.com/locate/asr.

Weitzel, Jane (Mar. 2015). "Accuracy, Trueness, Error, Bias, Precision, and Uncertainty: What Do These Terms Mean?" In: *AOAC International - Inside Laboratory Management*. URL: http://tdrm.aoac.org/rm_docs/RM%5C%20Documents/ILM_Accuracy_Trueness_2015_Weitzel.pdf.

Wienia, Rikkert (2015). "Combined aerial and train mounted lidar system provide a fast and innovative approach to surrveying railway infrastructure and track geometry". In: *International conference railway engineering*.

Zhang, Xinchun, Ximin Cui, and Bo Huang (June 2021). "The design and implementation of an inertial gnss odometer integrated navigation system based on a federated kalman filter for high-speed railway track inspection". In: *Applied Sciences (Switzerland)* 11. ISSN: 20763417. DOI: 10.3390/app11115244.

Zheng, Yanli, Fu Zheng, Cheng Yang, Guigen Nie, and Shuhui Li (Sept. 2022). "Analyses of GLONASS and GPS+GLONASS Precise Positioning Performance in Different Latitude Regions". In: *Remote Sensing* 14 (18). ISSN: 20724292. DOI: 10.3390/rs14184640.

Zhou, Yukun, Qijin Chen, and Xiaoji Niu (2019). "Kinematic Measurement of the Railway Track Centerline Position by GNSS/INS/Odometer Integration". In: *IEEE Access* 7, pp. 157241–157253. ISSN: 21693536. DOI: 10.1109/ACCESS.2019.2946981.

Zhu, Guoliang (2014). *Trajectory-aided GNSS Land Navigation: Application to Train Positioning*. Universite de Technologie Troyes. URL: https://hal.archives-ouvertes.fr/tel-01352620.

A

Track Geometry Parameters

In Table 2.1, an overview with the definitions of the different track geometry parameters can be found. In Figure A.1, a graphical representation of the different relative track geometry parameters is presented.

Table A.1: Definitions of absolute- and relative track geometries

Geometry	Type	Definition
Gauge	Relative	Distance between the inner sides of both rail heads perpendicular to the track centre
Twist	Relative	Elevation difference between the topside of both rail heads over a certain segment
Alignment	Relative	Deviations in lateral position between both rail heads from the mean distance (gauge)
Longitudinal Level	Relative	Deviations in the vertical position between the topside of both rail heads from the ideal running plane
Cant (Cross Level)	Relative	Elevation difference between the topside of both rail heads perpendicular to the track centre line
Position	Absolute	True position of the track (centre line) in a three-dimensional space
Radius	Absolute	Radius of the track centre line
Gradient (Slope)	Absolute	Gradient of the track centre line

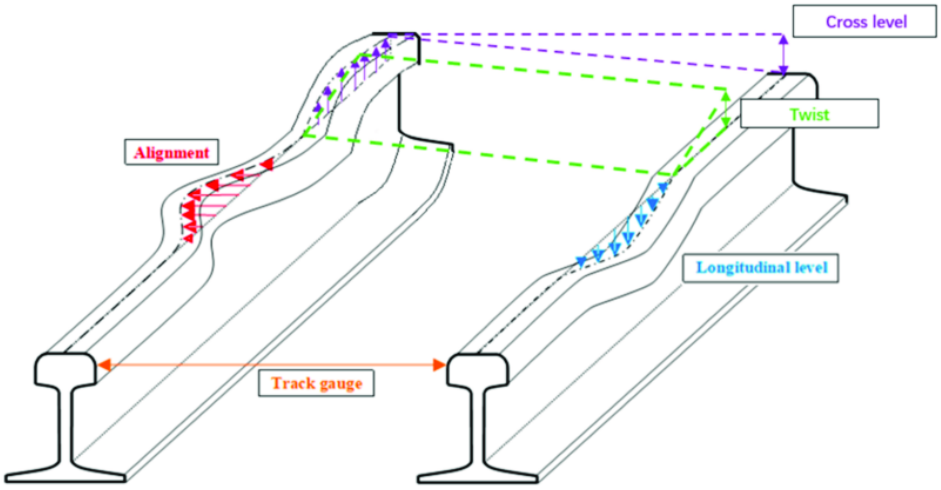

Figure A.1: Schematic overview of the relative track geometry measurements (Liao et al. 2022)

This page was intentionally left blank.

B

RILA Data Acquisition & Processing

B.1. RILA Data Acquisition

Below, an overview of the RILA sensors can be found together with their sampling interval and statistics in Table B.1

- **GNSS Antenna** The Global Navigation Satellite System antenna provides the absolute position to which all measurements of the RILA system are related.
- **IMU** The Inertial Measurement Unit measures accelerations and rotations along all axis of its internal reference frame. The data is used to complement the GNSS measurements by calculating the change of position between GNSS measurements using the observed accelerations.
- **LiDAR Scanner** The 360° LiDAR scanner, measuring perpendicular to the track centre line, provides a point cloud representation of the railcorridor and track that the train travels through.
- **Railstripers** There are two optical (laser) railscanners on the bottom of the RILA system pointed at the rails. These scanners provide accurate relative measurements of the track, trackbed, ballast and sleepers.
- **Video Camera** The three video cameras mounted on the RILA system provide a geo-referenced video representation of the rail corridor. This data, together with the point cloud, is used to make a virtual representation of the rail corridor.

Table B.1: Overview of parameters of RILA sensors

Sensor	Sampling Frequency [Hz]	Amount	Along-track Sampling Interval [m]	
			@ 100 kph	@ 160 kph
GNSS Antenna	5	1	5.56	8.89
IMU	300	1	0.09	0.15
LiDAR scanner	250 x 4000	1	0.11	0.18
Railscanner	500 x 2352	2	0.06	0.09
Video Camera	15	3	1.85	2.96

B.2. RILA Trajectory Processing Settings

B.2.1. Current Trajectory Processing Settings

Table B.2: Current RILA GNSS-only trajectory processing settings

Parameter	Unit	Current Setting
Processing direction	n/a	*foward + backward*
Processing method	n/a	*Differential GNSS*
GNSS Constellations	n/a	*GPS + GLONASS*
Elevation Mask	deg	10
L1 Locktime Cutoff	s	0.00
C/N0 rejection tolerance	dB-Hz	*disabled*
ARTK Engine	n/a	*default*
ARTK Quality Acceptance Criterion	n/a	Q2-99%
Minimum Reliability	n/a	3.00
Maximum RMS	mm	3.00

In Table B.2 ARTK is Novatel's proprietary software used to resolve integer carrier phase ambiguities. In its *default* processing mode, the ARTK engine is constantly re-checking its resolved ambiguities when the observed satellite geometry changes. This can lead to a new position fix (set of integer ambiguities) being accepted when a more favourable geometry is observed. The quality acceptance criterion determines the confidence level required in residual testing for an ARTK fix to be accepted. A higher quality criterion reduces the chance of an incorrect fix being accepted but increases the possibility of no fix being achieved in environments with limited GNSS coverage. The minimum reliability is the ratio between the second-best RMS and the best RMS of the individual GNSS observations. High-reliability values indicate a high confidence level that can be placed in the solution.

Table B.3: Current RILA GNSS/IMU integration processing settings

Parameter	Unit	Current Setting
Processing direction	n/a	*foward + backward*
Require fixed ambiguities	n/a	*disabled*
SD tolerance	m	2.0
GNSS Quality Number	n/a	6 (2 - 10 [m])

In Table B.3, the SD-tolerance is a threshold for the standard deviation of the baseline as calculated by the LC Kalman Filter. The GNSS quality number threshold allows for the specification of a certain level of estimated accuracy for a GNSS position update to be accepted.

B.2.2. Processing settings definitions

In this section of the appendix, more context is provided, based on the Inertial Explorer user manual, on the RILA trajectory processing settings defined in section 3.2, Table B.2 and Table B.3.

- **Processing Method**
  [Differential GNSS] "Differential processing can be selected if base station(s) have been added to the project. This method of processing provides access to ARTK, where carrier phase ambiguities may be fixed for high accuracy applications."

  [Precise Point Positioning] "PPP is an autonomous positioning method where data from only the remote receiver is used. If base station data has been added to the project, it will not be used when processing PPP. By design, both differential and PPP trajectories can be processed within the same project without over-writing each other"

- **Elevation Mask**
  "Satellites below this elevation (relative to the horizon) are ignored. Common elevation masks for differential kinematic processing are 10-12 degrees. Static processing generally benefits from a higher elevation mask (15 degrees).

  Low elevation signals are more affected by multipath and tropospheric error, and are more likely to be affected by cycle slips due to signal blockages and/or signal attenuation by the antenna. Thus, pre-filtering low elevation signals is generally beneficial to post-processed accuracy. Increasing this value too high may cause satellite geometry to become poor which can affect the performance of integer carrier phase determination."

- **L1 Locktime Cutoff**
  "This is the number of seconds that continuous carrier phase tracking is required before measurements will be used. Lowering this value will help to maximize GNSS position availability following a total loss of carrier phase lock. However, using low values increases the likelihood of an incorrect ambiguity fix. This is because the quality of carrier phase measurements may be suspect within the first few seconds the receiver achieves carrier phase lock"

- **C/N0 Rejection Tolerance**
  "Most often, pre-filtering GNSS signals by elevation mask and L1 locktime cutoff is effective. For specialized applications, introducing an alternative or additional pre-filtering method based on the signal to noise ratio may also be effective.

  This option is not engaged by default as not every receiver provides a C/N0 value, and different receivers may output this value at different stages of signal processing. Care should be used if applying this option."

- **Default-mode ARTK Engine**
  "When ARTK is used in default mode, it is constantly re-checking its solved ambiguities when the satellite geometry changes (i.e. when new satellites come into the solution or when individual satellites are lost). Thus it is possible, even under open sky conditions where no loss of lock occurs, that ARTK will accept a new set of integer ambiguities when there is a change in satellite geometry. This may result in a position jump where the new ambiguities are accepted.

  Using ARTK in default mode is thus mostly preferred for ground vehicle applications, as this method provides a high level of solution accuracy over the entire length of a trajectory."

- **ARTK Quality Acceptance Criterion**
  "This is the confidence level required in residual testing for an ARTK fix to be accepted. Using lower quality acceptance criteria increases both the likelihood of achieving a fix and the possibility the fix may be incorrect. Conversely, increasing the quality acceptance criteria helps reduce the likelihood of incorrect ambiguity fixes, but also the chance that no fix is achieved when conditions are marginal for ambiguity determination."

- **Maximum Reliability**
  "The reliability of an ARTK fix is the ratio of the second best RMS and the best RMS. It indicates how much better, statistically, the best solution is from the second best solution. High reliability values indicate the best RMS is significantly better (lower) than the second best RMS, and thus a high degree of confidence can be placed in the solution. This option provides direct control over the minimum reliability ARTK will accept as a pass."

- **Maximum RMS**
  "An RMS is computed for every possible ARTK fix within a given search area. This RMS, output by Inertial Explorer in units of mm, represents the mathematical fit of the solution or how well the carrier phase measurements in the solution agree with each other. Low values (mm level or sub-mm) represent well fitting solutions, or measurements that agree very closely. Large values (cm level) indicate poorer fitting solutions that are more suspect. This option provides direct user control over the maximum allowable RMS for an ARTK fix to be considered a pass."

- **Require Fixed Ambiguities**
  "If using a high precision IMU and when surveying in urban conditions with some challenging GNSS data, this option may be useful in achieving the best possible results. This option is not recommended for most systems (MEMS or tactical grade IMUs) as any GNSS updates (even one derived from float ambiguities) are generally beneficial in observing IMU sensor errors."

- **SD Tolerance**
  "If the position update returned by the GNSS processor is larger than this value, it will not be passed to the IMU filter. By default a large threshold is used as Inertial Explorer relies on variance factor testing to determine whether a GNSS position update should be applied or not"

- **GNSS Quality Number**
  "The GNSS processing engine assigns a quality number to each processed epoch between the values of 1 to 6, 1 being the best. By default Inertial Explorer does not use the GNSS quality number in pre-filtering as instead it relies on GNSS variance factor testing in determining whether a GNSS position update should be accepted. If you wish to enable a lower prefiltering tolerance, enter it here."

Table B.4: Quality number description

Quality	Color	Description	3D Accuracy (m)
1	Green	Fixed Integer	0.00 - 0.15
2	Cyan	Converged float or noisy fixed integer	0.05 - 0.40
3	Blue	Converging float	0.20 - 1.00
4	Purple	Converging float	0.50 - 2.00
5	Magenta	DGPS	1.00 - 5.00
6	Red	DGPS	2.00 - 10.00
Unprocessed	Grey	Has not been processed	N/A

B.2.3. Recommended Trajectory Processing Flow

An updated flow(chart) is recommended for the processing of the RILA trajectory solution:

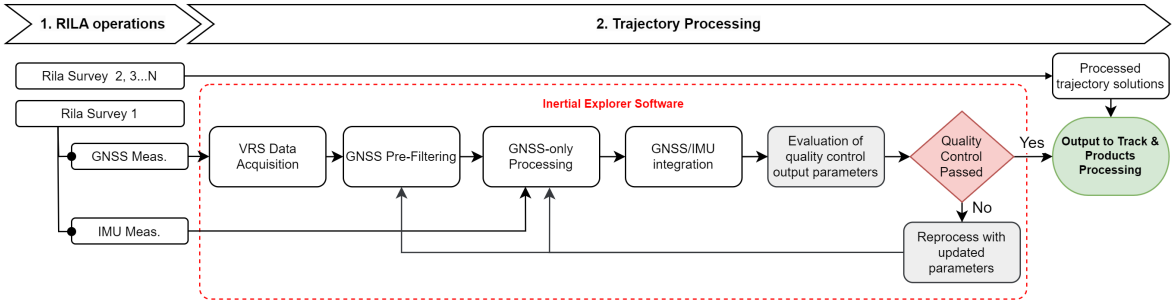

Figure B.1: Recommended RILA trajectory processing flowchart

B.3. RILA Track Processing

Flowchart of the RILA track processing process

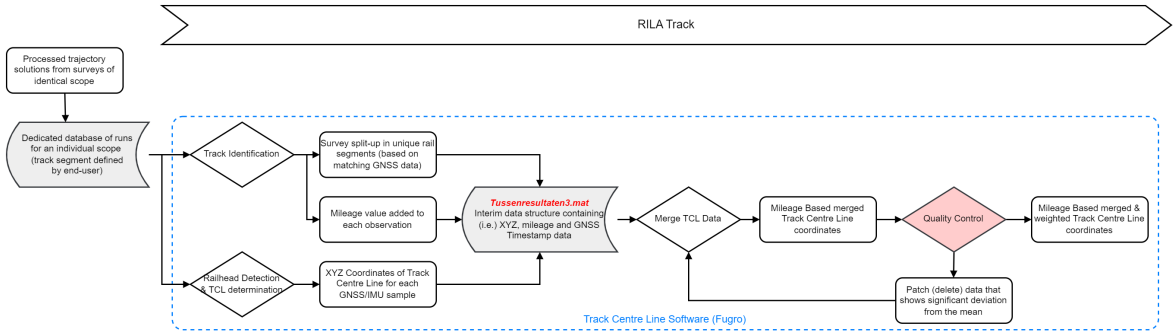

Figure B.2: Flow Chart of RILA track processing

This page was intentionally left blank.

C

Data Analysis Algorithm

C.1. Description of the Data Analysis Algorithm

The output of a processed RILA survey using Inertial Explorer, 'RILA trajectory processing' (see Figure 3.3), is a continuous time-based string of coordinates containing a days-worth of surveying. Furthermore, all output provided by the software, such as the QC metrics, are provided on the same time-based axis. All the runs over the same track segment are therefore chronologically sorted in the Smoothed Best Estimate Trajectory (SBET) solution. This can clearly be observed from the velocity profile in Figure C.1. The four runs in the survey can clearly be identified. It can even be deducted that the measurement unit has travelled two times in forward direction over the track (runs 1 & 3), and two times in the opposite direction (runs 2 & 4), hence the 'inverted' metrics.

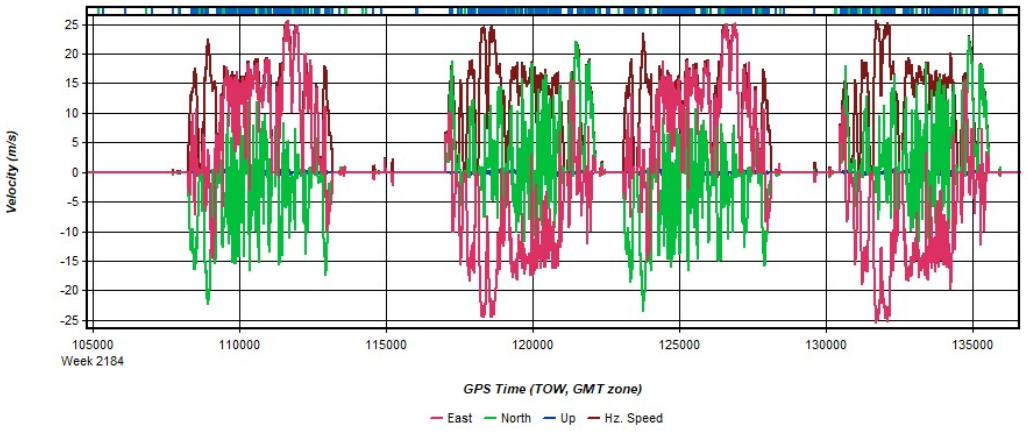

Figure C.1: Velocity profile in North, East and Up direction together with the combined horizontal speed of an arbitrary survey consisting of four runs

However, to apply the research methodology proposed in section 3.4, and compare the trajectories and the quality metrics of the different runs at a certain geographical track location, the time-based trajectory output needs to be converted to a *mileage* based output. Although 'mileage' implies a distance in miles, in this report, the definition is used to indicate the distance along a track in kilometres.

The conversion of the time-based output of the IMU trajectory to the mileage-based trajectory of the Track Centre Line is performed in the Matlab-based RILA track processing software, *RILA-suite*[1]. In short, the software identifies unique track segments and assigns a *trackID* based on the observed trajectory and existing railroad maps in each part of the survey track. In this step, for example, railway track switches are identified, adjacent parallel tracks are distinguished and other unique railway track

[1] A schematic overview of the process can be found in Appendix B

elements are established. Most importantly, however, the software can identify based on matching GNSS coordinates when the system travels over the same track segment. Next, the software assigns a mileage value to all the trajectory epochs that match the mileage of the track segment (*trackID*) at which the observation is located. This makes sure that measurements with the same mileage value (within the same scope), are taken at the exact same distance along the track, although there can be variation in the cross track direction. This information for a survey scope (all runs over the same track segment) is then stored in a Matlab data structure called `tussenresultaten3.mat`.

C.1.1. Algorithm Setup

The aim of the `Python`-based data analysis algorithm constructed for this research is to project the time-based trajectory (QC) output of Inertial Explorer onto the mileage-based axis constructed by the *RILA-suite* software. In order to do so, the algorithm consists of approximately six steps: (1) Collect all relevant data, (2) Match GNSS timestamps provided by inertial explorer onto the mileage data, (3) Construct a class instance that allows for comparison of all runs along a track segment, (4) Compute trajectory accuracy metrics and (5) Plot and present results. A simplified flowchart of the data analysis algorithm is given in Figure C.2[2].

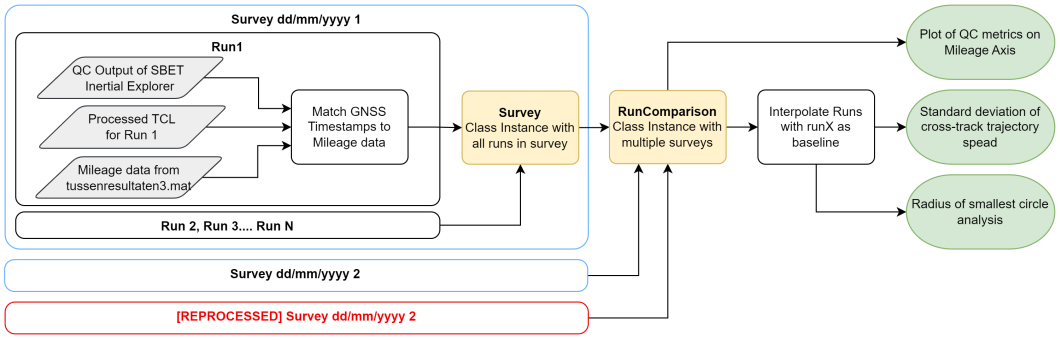

Figure C.2: Velocity profile in North, East and Up direction together with the combined horizontal speed of an arbitrary survey consisting of four runs

1. Data collection

First of all, from the `tussenresultaten3.mat` file, a conversion table is derived linking GNSS timestamps to the mileage values and TCL coordinates assigned by the RILA-track processing software. This data is available per 'run' and loaded into a `Python` data structure. Next, the time-based trajectory output containing GPS timestamps, IMU trajectory coordinates and QC-metrics are loaded from a `.txt` file, sampled every 0.5 seconds, obtained from Inertial Explorer.

2. Match GNSS time & mileage

When all input data is collected, the trajectory output can be segmented into the different (established) runs. Furthermore, the mileage and TCL trajectory coordinates can be matched onto each epoch in the trajectory output. When this is completed, it is possible to plot Inertial Explorer's trajectory QC metrics on a mileage-based axis. An example of this is given in Figure C.3, where the horizontal velocity is plotted of the survey from Figure C.1.

3. Construct comparison class

Next, in sequential order, two `Python` class instances are created in order to compare the data of all runs over the survey scope. First of all, a `SingleSurveyAnalysis` class instance is created containing all the runs of a single survey. Next, a `RunComparison` class instance is created where the data of multiple surveys, or individual runs, can be added to the comparison. This is relevant because the track geometry measurements of many railway tracks are obtained over multiple days, and thus multiple surveys.

[2]An elaborate flowchart of the algorithm, together will all the datastructures, functions and relations can be found in Appendix C

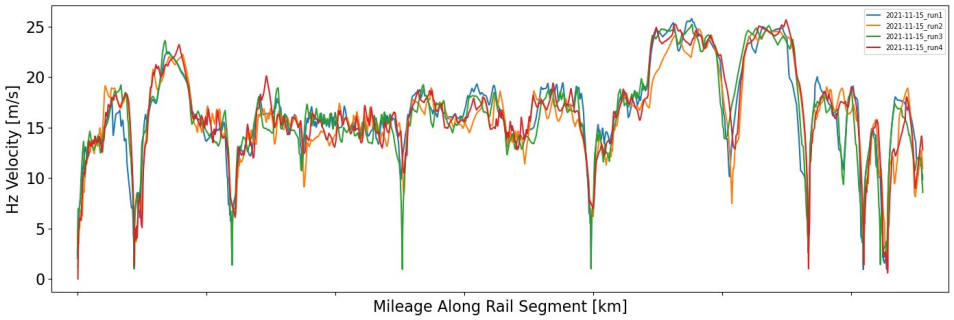

Figure C.3: The horizontal velocity profile of an arbitrary survey (from Figure C.1) consisting of four runs, plotted on the mileage axis.

4. Compute Trajectory Accuracy Metrics

The next step is to compute the accuracy metrics for the runs along a given track segment. Because the different runs start at an arbitrary position (at a railway station) and the velocity along the track is not identical (but the trajectory is sampled at a time-based interval), the observations of the different runs are situated at an irregular interval. Therefore, the trajectory solutions need to be interpolated as explained in section 3.3. To do so, the first run[3] is selected as the baseline and is used to obtain (linearly) interpolated at the same along-track location of the trajectory. This allows for the evaluation of the cross-track trajectory spread. The calculation of the trajectory accuracy metrics has been extensively discussed in section 3.3.

5. Plot & present results

After the quality metrics are computed, all information is present in the `runComparison` class instance to plot all the results. Furthermore, output data tables on the trajectory accuracy metrics are available as well as logs of all the steps performed in the algorithm.

C.1.2. Verification

To verify that the data analysis algorithm is working correctly, every step in the algorithm is extensively verified. Mostly, this has been done by performing unit tests on the different functions and implementations have been performed. Furthermore, sanity checks have been performed by plotting the data obtained in the different data structures. A good example of the importance of such unit tests combined with sanity checks is given in Figure C.4.

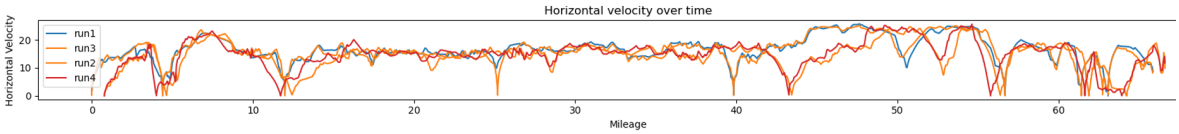

Figure C.4: The horizontal velocity profile of an arbitrary survey performed for a sanity check for the GPS Time and Mileage matching algorithm

In the process of matching the mileage data onto the QC metrics, although the software passed the unit checks, as one can observe from Figure C.4, a clear (mileage) mismatch in the velocity profile of `run1` & `run3` and that of `run2` & `run4` was present. This was caused by the use of an incorrect data structure linking mileage values and GNSS timestamps obtained from the `tussenresultaten3.mat`. Another good example is the verification of the interpolation algorithm. In Figure C.5, the original samples along an arbitrary track segment are presented in Figure C.5a. Furthermore, the properly interpolated observations are presented in Figure C.5c and the results of an incorrect, earlier version of the algorithm in Figure C.5b. As one can observe, after the interpolation in Figure C.5b, there was still some along-track deviation in the observations. To solve the problem, an interpolation correction algorithm was implemented, where the along track distance between the first iteration of the interpolated was used

[3]The first run is used because it has, by nature of the way that the RILA track data is stored, the most consistent mileage data

as correction value in the second iteration of the interpolation. This 'shifts' the points along their respective along-track linear interpolation line to find the coordinates of the trajectories in the same cross-track plane - i.e. correct interpolation.

(a) Original sampled trajectory data **(b)** Verification: Incorrect interpolation **(c)** Verification: Correct interpolation

Figure C.5: Verification results of the interpolation algorithm

All cases tested in this report have been verified using the methods displayed in Figure C.5. Furthermore, all the datasets have been analysed for anomalies that could not have been caused by the observations of the measurement system, such as gaps in the dataset and misalginment of the runs.

C.2. Extended Data Analysis Algorithm Flowchart

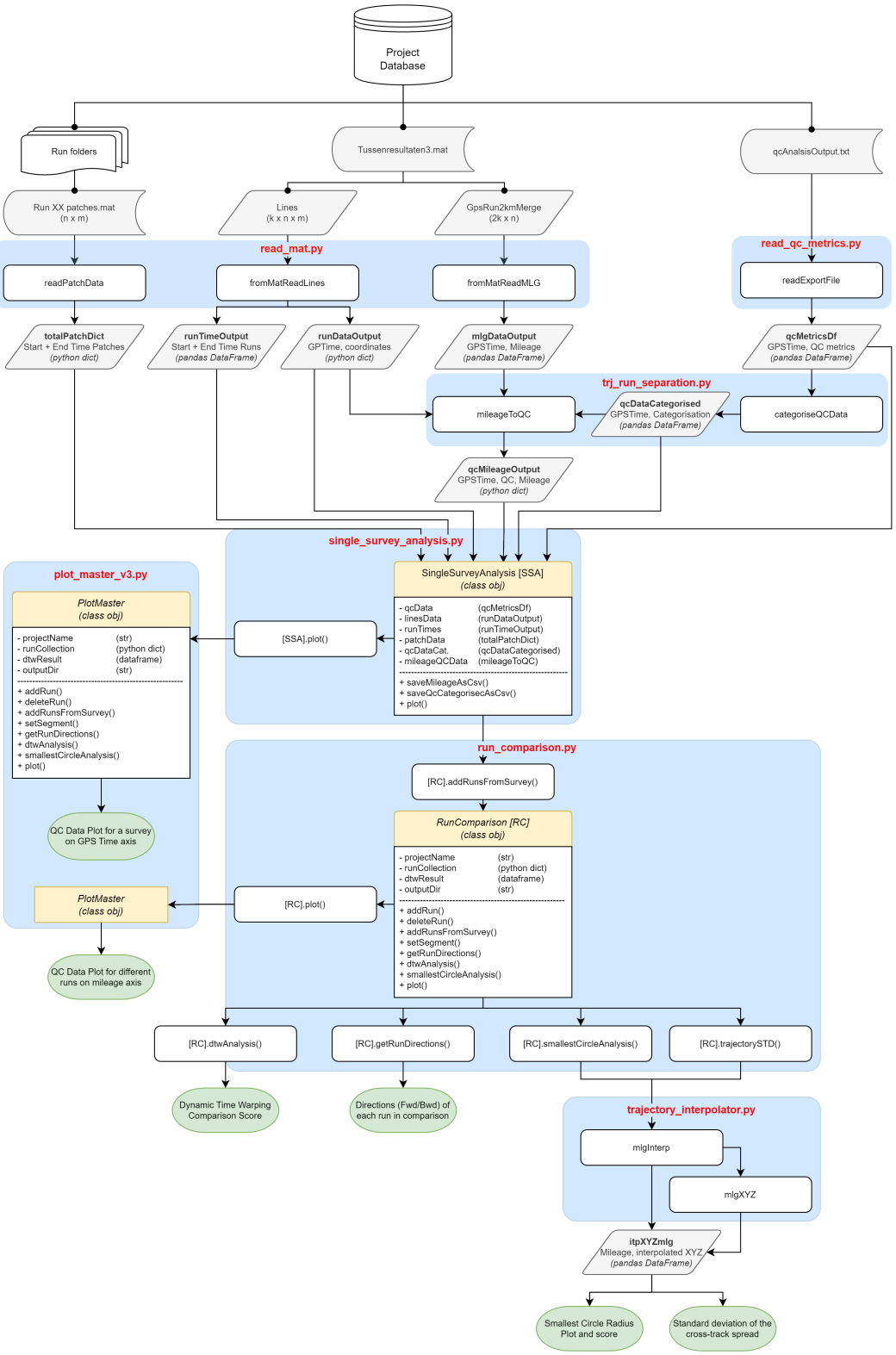

Figure C.6: Comprehensive flowchart of the data analysis algorithm constructed for this report

This page was intentionally left blank.

D

Validation Cases

In this appendix, more context to the validation cases, presented in this report, is provided. For the given validation cases, both a situational overview of the track (segment), and the Inertial Explorer SBET quality metrics are provided.

D.1. Case Study

Validation 3: km 20.5 - 23.5

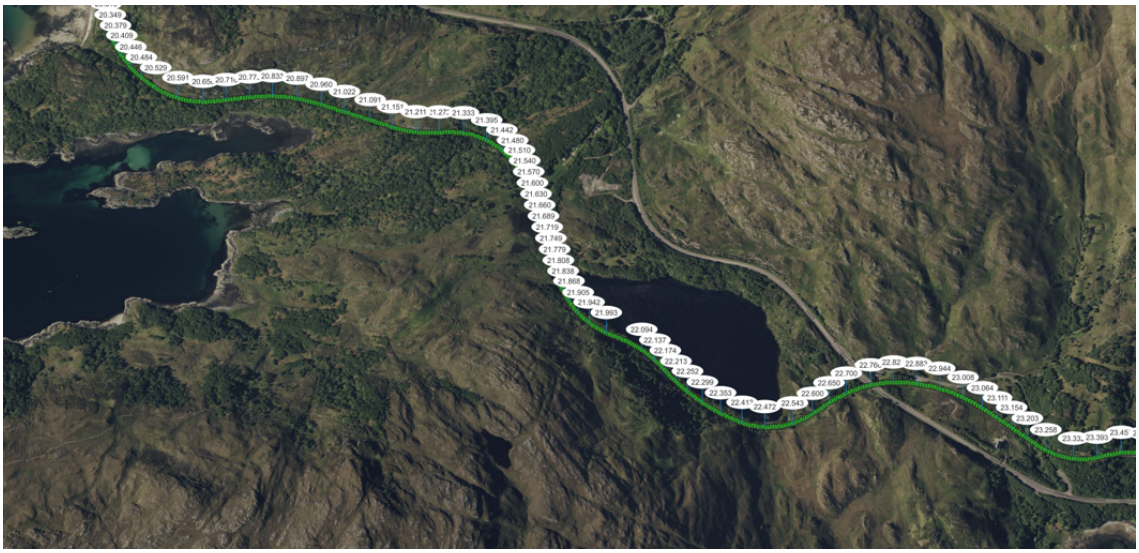

Figure D.1: Situational overview of validation case 3

Validation 1: km 59.8 - 60.8

Figure D.2: Situational overview of validation case 1

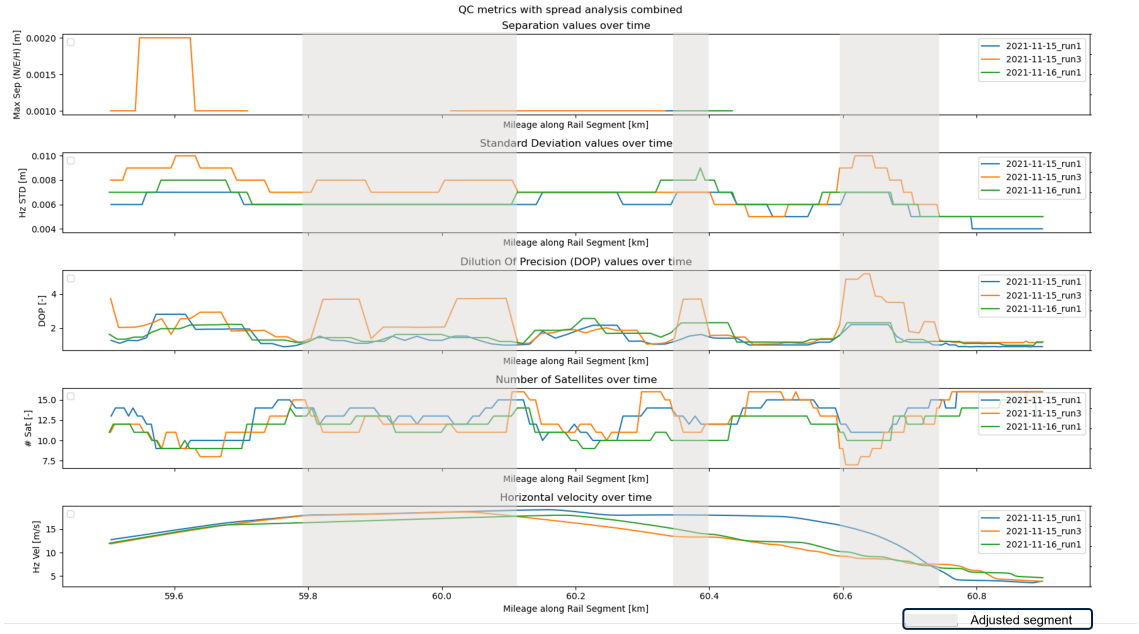

Figure D.3: SBET QC metrics of trajectory at track segment of validation case 1

Validation 2: km 40.0 - 41.2

Figure D.4: Situational overview of validation case 2

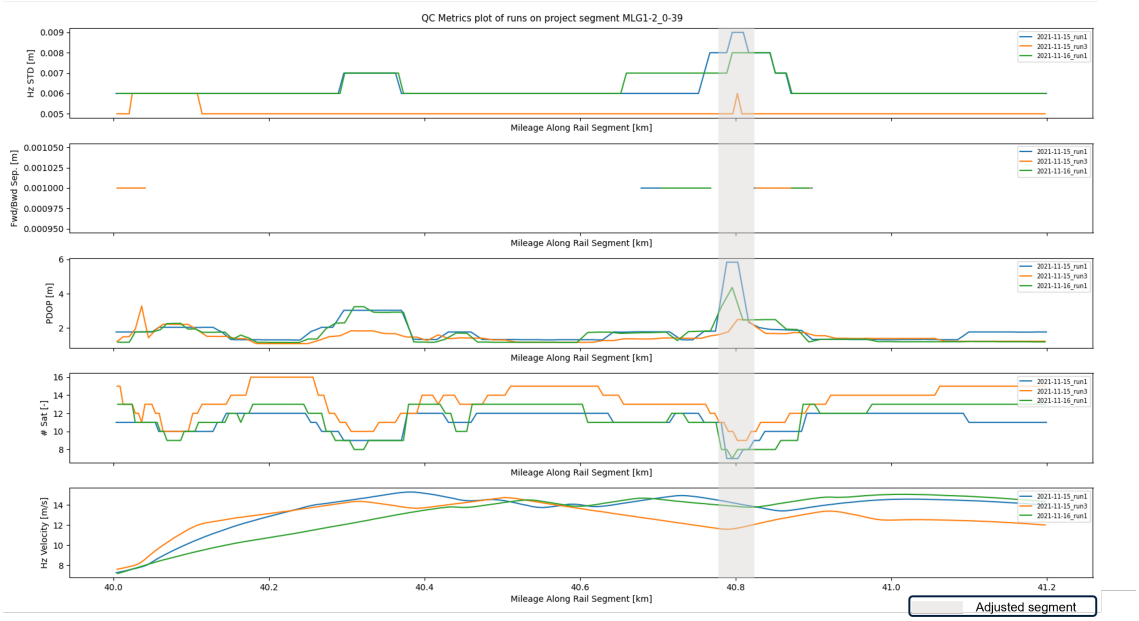

Figure D.5: SBET QC metrics of trajectory at track segment of validation case 2

D.2. PDOP Analysis

D.2.1. Manual PDOP Computation

The results of the manual PDOP computation of the critical epoch of `2021-11-15_run1`.

Table D.1: Results of the manual PDOP computation analysis at the critical epoch of `2021-11-15_run1`, GPSTime = 112014s

Sat in Analysis: G01, G03, G17, G19, G22, R03, R04, R19		
Metric	**Value**	**Unit**
GPSTime	112014	s
Mileage	55.033	km
Δt to nearest ephemeris	6:54	m:ss
NR of Sats (NS)	8	-
PDOP Observed	3.21	-
PDOP Computed	5.17	-
ΔPDOP	1.96	-
Sensitivity Analysis		
Excluded Satellite(s)	**Computed PDOP**	**NR of Sats**
All GLONASS	57.69	5
All GPS	3.18	3
G01	2.56	7
G02	2.75	7
G17	2.52	7
G19	2.58	7
G22	2.76	7
R03	3.04	7
R04	2.56	7
R19	2.74	7